AN ELASTIC CHARACTERIZATION OF THE MUSCLE CELL MEMBRANE AND ITS STRUCTURAL INTERPRETATION

by

R. Wayne Fields

A THESIS

Presented to the Department of Physiology
and the Graduate Division of the University of Oregon Medical School
in partial fulfillment of
the requirements for the degree of
Doctor of Philosophy

April 1969

APPROVED: [redacted]

(Professor in Charge of Thesis)

[redacted]

(Chairman, Graduate Council)

ACKNOWLEDGMENTS

Several individuals provided outstanding assistance during the formulation and execution of this thesis. To Drs. J. M. Brookhart and B. B. Ross I wish to express my gratitude for consultation regarding physiological and technical aspects of the study. My sincere appreciation is also extended to Dr. C. E. Smith of Oregon State University for patiently molding my concepts of the mathematical theory of elasticity, and along with Drs. J. J. Faber and B. B. Ross in directing the analysis and presentation of the data to its present form.

Although Dr. Faber has been previously acknowledged, justice cannot be done to the enormous amount of assistance and guidance that he contributed to this work. His excellent command of scientific knowledge and methodology has served inexhaustibly as aid and inspiration. Our association has been truly enjoyable and has provided great personal reward.

Lastly, I wish to offer a humble token of inexpressible thanks to my wife, Lorraine. Her undying confidence and encouragement have soothed the frustrations and given meaning to the accomplishments.

TABLE OF CONTENTS

LIST OF ILLUSTRATIONS

LIST OF TABLES

INTRODUCTION

Sarcolemma Mechanics in Perspective

The presence of muscular tissue in multicellular members of the animal kingdom is one of the prime characteristics distinguishing this group as a distinctive entity. This amazing tissue appears to have been an early evolutionary development. Perhaps because of some peculiar complexity of the mechanism of muscle function, once originated, this structure has been changed but little while whole phyla have appeared and disappeared (1). The highly organized, multinucleate cells making up skeletal muscles are believed to develop embryologically from the differentiation of single myoblasts, by the fusion of separate myoblasts, or through a combination of both processes (2). The cytoplasm of this giant cell is then organized in such a way that a general property of all cytoplasm, namely contractility, is accentuated (3).

Striated skeletal muscles are composed of long cylindrical cells surrounded by a tough elastic membrane. Generated tension is transmitted usually to the bony skeleton through tendinous connective tissue, and functions to provide support and movement (4). Individual cells run predominantly in parallel and are organized into discrete muscles by connective tissue investments. The unit muscle is invaded by blood vessels and afferent and efferent nerves, and

contains in addition various receptor end organs. Particular representatives of the efferent nerve fibers innervate muscle fibers (cells), and possess the ability to control certain aspects of fiber metabolism (5).

Single muscle fibers are highly ordered in their own right showing both longitudinal and transverse organization (5). Longitudinally, the fiber is seen to be a bundle of columns designated as myofibrils, with sarcoplasm and cytoplasmic structures typical of all cells lying between the columns. Each myofibril is in turn a bundle of long rigid protein filaments, the myofilaments, running parallel to the fiber axis. The myofilaments are not continuous, but rather are composed of two interdigitating sets sequentially arranged. This arrangement results in the striated pattern of lateral organization characteristic of this tissue and from which it derives its name. Additional structures exist in the form of the longitudinal and transverse tubule systems investing the myofibrillar columns in regular array.

When contracting muscle is examined from a physiological standpoint, its behavior can be described in terms of a model consisting of a contractile element (CE) functioning as a force generator arranged in series with a series elastic component (SEC). The SEC is functionally but not necessarily structurally distinct from the CE. When muscle is at rest the CE is assumed to be highly extensible,

and passive resistance to muscle stretch is attributed to a parallel elastic component (PEC) connected in parallel with both the CE and SEC (6, 7). The SEC has been characterized as having an exponential stress-strain curve concave to the stress axis (8), while the PEC shows more complicated characteristics but is also concave to the stress axis (9).

The anatomical structures responsible for the behavior manifest in these model components is unknown, but is historically conceded to be tendon for the SEC and the sarcolemma and connective tissue for the PEC (10). The CE is thought to be ultrastructurally represented by overlap of the myosin and actin myofilament sets (11). Data on the PEC characterization for single muscle fibers shows a stress-strain curve also concave to the stress axis (12), although the behavior of whole muscle is not equal to the sum of individual fiber responses (13).

A wealth of information has also accumulated concerning ultrastructural and physiological correlations of muscle behavior at the level of individual fibers. An enormous amount of circumstantial evidence has arisen in support of the sliding filament hypothesis of muscle function (11) originally proposed in 1954 (14, 15). This model envisions active muscle as generating force in regions of myofilament overlap, while in passive muscle the interdigitating filaments are free to slide past one another. The sliding filament

hypothesis is the most popular model of muscle function at the sacromere level. However, many other models exist that can also explain the known information. As an example, Garamvölgyi (16, 17) proposes a model whereby the CE is localized to coiling filaments in the Z line, whereas another model proposes the shortening results from lateral action of short range molecular forces (18, 19).

The information to date begins to form a coherent picture at a superficial level, although much controversy still rages. Obviously, the fiber as a tension generator during activity and as an elastic element at rest must have elements continuously connected throughout its length to transmit these forces. The complete understanding of single fiber mechanics requires the precise evaluation of the contribution of all relevant fiber components during rest and activity. It will be shown that attempts to carry out such analyses have so far been somewhat imprecise and inconclusive, the major problem being the separation of cellular components for independent characterization. Certainly, the sarcolemma is one key structure offering mechanical continuity throughout the fiber length. It is also the most accessible component, and under certain circumstances it can be mechanically sampled independently of other cell contents as described in later sections of this review.

The present work is concerned with characterizing the mechanical properties of the sarcolemma. In prelude to discussing the

experimental procedures and results, however, it is necessary to review the pertinent literature.

Ultrastructure of the Sarcolemma

The concept of a membrane existing as a distinct structure surrounding individual muscle cells was originated by Schwann (20). He describes this element as being very transparent, structureless, and definitely not a fibrous material derived from the surrounding connective tissue. It was seen as a very narrow and sharply defined border around each secondary muscle cell, the ultimate product of primary cell fusion during embryologic development. Schwann claims it was difficult to be sure the membrane was not an optical artifact in mammalian fibers. In insect muscle, however, he observed in retraction zone regions, produced by separation of the intracellular muscle substance (see figure 7, page 46), a definite membrane connecting the two halves of material. This situation is cited as evidence clearly demonstrating the existence of a membrane surrounding individual muscle fibers.

Bowman (21) confirmed Schwann's findings that the membrane is not of connective tissue origin. Rather it is "a tubular sheath of the most exquisite delicacy, investing every fasciculus (fiber) from end to end, and isolating its fibrillae (myofibrils) from all the surrounding structures." Bowman applied the name sarcolemma to this

membranous structure, and considered it to be distinct from the connective tissue fibers which could be seen lying on its outer aspect. Confusion has since arisen as to what should be called sarcolemma and has prevailed through modern times (22). For reasons presented later in the discussion, the term sarcolemma will be used henceforth to designate in addition to the structureless sheath of Schwann and Bowman some intimately associated overlying connective tissue layers tending to remain with the fiber after dissection.

This general picture of the sarcolemma remained essentially unchanged for nearly a century. Further characterization of the connective tissue of the muscle, however, led to its description in terms of three components. These components were titled the epimysium, perimysium, and endomysium in the order of decreasing level of organization controlled. The epimysium envelops the whole muscle organizing it into a unit structure. The muscle is subdivided into bundles of muscle fibers by the perimysium, while the endomysium comprises connective tissue within fiber bundles and more or less closely associated with individual fibers (23). Modern concepts of the sarcolemma include in this structure connective tissue intimately associated with the clear continuous sheath (24). These connective tissue layers are also portions of the endomysium (25).

More recent studies of sarcolemma structure with the light microscope have contributed additional observations. Using

microdissection techniques, Nagel (26) found the sarcolemma to be a tough elastic membrane surrounding the whole muscle fiber. In addition he claimed that the thick "structureless" membrane of Schwann and Bowman had embedded in it interlacing collagenous birefringent fibers. This viewpoint was also held by Bairati (27). Using silver stains the latter author observed a fine network of fibrils around the periphery of the sarcolemma, with a glassy smooth matrix containing fibrils as the continuous phase of the tube wall.

The presence of fibrils embedded in the continuous phase reported by Nagel and Bairati was controversial. Thus Bremer and Weatherford (28) find the inner continuous phase to be a structureless membrane closely applied to the surrounding connective tissue layer, as does Barer (18, 22). The former authors found the continuous plase to be a viscous elastic sheath, which can be pulled away from the underlying myofibrils but returns almostto its original position when released. The two-component model consisting of connective tissue overlying a continuous phase is also verified by Gutman and Young (29) and Long (30). These authors caution the interpretation of light microscope observations, however, and stress the very important point that what is called sarcolemma in cross-sectional viewing can be subject to artifactual misinterpretation.

Electron microsope observations pertinent to sarcolemma structure began appearing in 1948. Reed and Rudall (31) and

Draper and Hodge (3) found in support of the two component model that the continuous membrane phase could be discerned as a distinct structure from an overlying fibrillar matrix. The inner membrane aspect (figure 1-A) shows adherent strands of remaining sarcoplasmic reticulum in irregular patterns upon which are imposed more regular circumferential markings at the level of myofibril Z-bands (31, 32). The outer aspect of the membrane (figure 1-B) exhibits discrete fibrils lying on an undulating continuous phase having depressions apparently coincident with Z-lines (31). Electron micrographs revealing cross sectional detail suggest the same general model (33).

Draper and Hodge felt in concurrence with Nagel and Bairati that the continuous membrane phase may be the plasma membrane and embedded fibrils intimately associated into a specialized kind of surface structure. This possibility is also considered by Reed and Rudall, but is opposed in the report of an independent electron microscope study of Rozsa et al. (34). The latter authors feel that the two components are intimately associated but that no fibril components are embedded in the continuous phase. The fibrils of the outer layer possess striations with a 640 Å periodicity suggesting that they are collagen filaments (31). Dense maculae or spots 400 - 1000 Å in diameter seen at irregular intervals on the inner aspect of membrane surface preparations (31, 35) may correspond to the

Figure 1. Electron micrographs of the inner (A) and outer (B) aspects of the sarcolemma. A, specimen from a leg muscle of the toad, Bufo marinus, from formalin fixed and blended muscle. Z-band remnants (Zbr) are seen as faint light-colored tracts in regular array running perpendicular to the fiber axis. From Draper & Hodge, Australian J. Exp. Biol. and Med. Sci., 1949. 27, 465-503. (3) B, the outer membrane aspect shows fine fibrils lying on a surface that undulates in association with the muscle fiber striation pattern. Fibrils are of comparatively uniform diameter and are banded like connective tissue collagen. Many fibrils can be seen running parallel to one another at a large angle to the fiber axis (perpendicular to the troughs of the undulations). The preparation is from frog or toad leg muscle. From Reed & Rudall, Biochim. Biophys. Acta, 1948. 2, 19-26. (31)

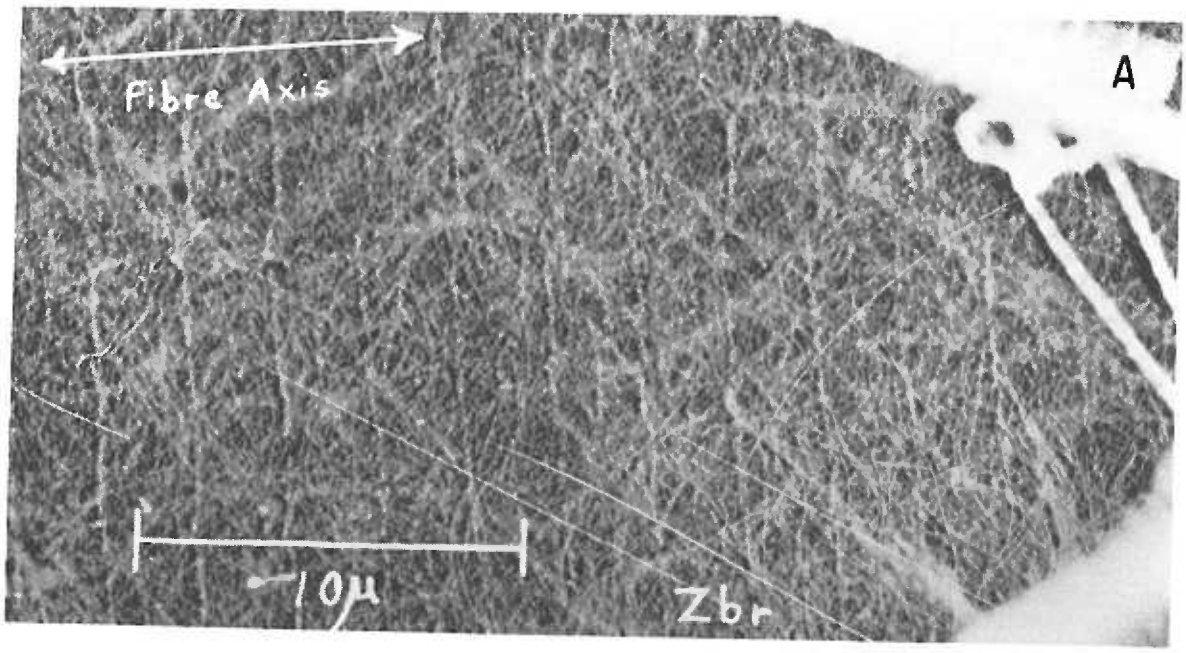
Fibre Axis
A
10μ
Zbr

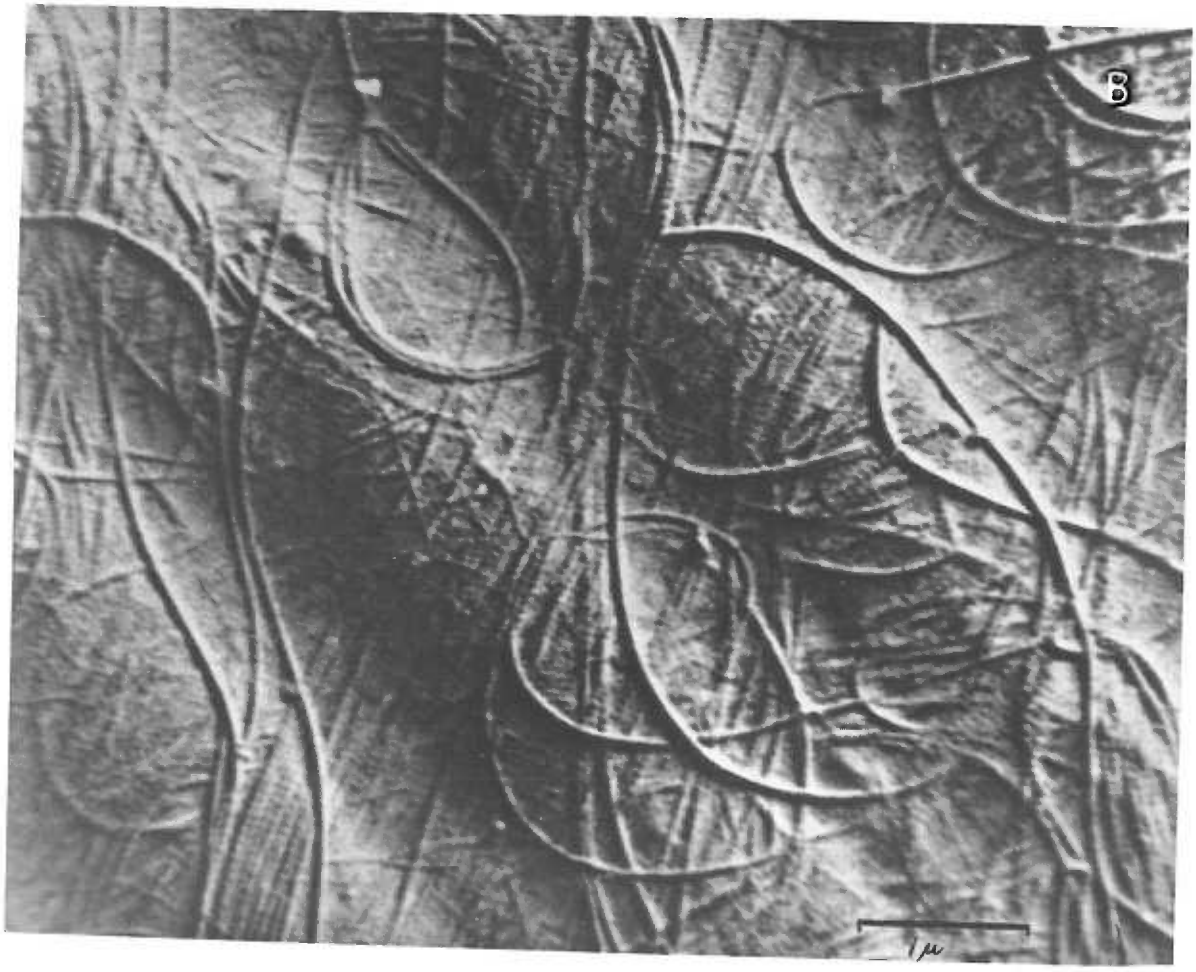
B
1μ

dense oval bodies seen by Robertson (36) adjacent to the cytoplasmic border in membrane cross-sections.

Draper and Hodge (3) have also looked at membrane surface ultrastructure in samples of folded sacrolemma fragments, confirming the marked difference between the inner and outer surface configurations. It was also noted that in both the fibrils and the membrane outer surface there appears to be some organization suggesting a helical alignment around the whole fiber. The collagen filaments appeared to be arranged in two helices wound in opposite directions in stocking fashion, with general directional axes at about 45 and 135 degrees to the fiber axis. This general arrangement of the collagen suggested to these authors that this may be the biological device by means of which is obtained an elastic membrane giving structural support to the fiber and yet capable of transmitting tension to the tendon. Collagen arranged in parallel bundles as in tendon is relatively inextensible.

The majority of the workers reviewed to this point used frog or toad leg muscles, although data representative of various mammalian species is also presented. No systematic species differences were noted. The question as to whether the continuous membrane phase contains embedded fibrils is still debatable from this information, but more current workers, to be discussed presently, have expressed the belief that all fibril components are structurally distinct

from the continuous phase of the membrane.

Two additional complexities of general sarcolemma structure were introduced by Robertson (36) in 1956 and are illustrated from the work of Mauro and Adams (24) in figure 2. Robertson obtained electron micrographs disclosing sarcolemma cross-sectional detail from striated muscle of the chameleon lizard Anolis carolinensis. A "membrane complex" was revealed consisting of two dense layers separated by a light, uniform core of 200 - 300 Å width. The inner dark laminae of this complex is a sharply defined dense zone coincident with the cytoplasmic interface. The outer dark laminae was of variable thickness and density, being 100 - 300 Å in width.

On the outer aspect of the membrane complex, Robertson's electron micrographs show more or less loosely packed and irregular round or oval dense profiles 250 - 350 Å in diameter. They have a longitudinal repeat period of about 700 Å suggesting they are collagen fibrils. In addition, a second class of fibrils can be seen interspersed among the collagen (see figure 2). These second fibrils are very delicate in nature as their diameter is well under 100 Å, and they are arranged in an apparently random fashion. It is emphasized that the large collagen fibrils cannot be a component of the outermost dark laminae of the membrane complex because their diameter is much too large. The small fibril component could be a membrane component from diameter considerations but no such

Figure 2. Electron micrograph illustrating four components of sarcolemma cross-section. The surface "membrane complex" of Robertson is seen as the combination of an inner structure (pm) identified as the plasma membrane from other evidence, and an outer structure (a) of unknown nature designed as the amorphous layer. These continuous membrane components underlie a network of fibrils composed of a large diameter component (c), probably collagen, and an unidentified small diameter component (f). Some fibrils appear grouped as cables (cc). From Mauro & Adams, J. Biophys. Biochem. Cytol., 1961. 10, 177-185. (24)

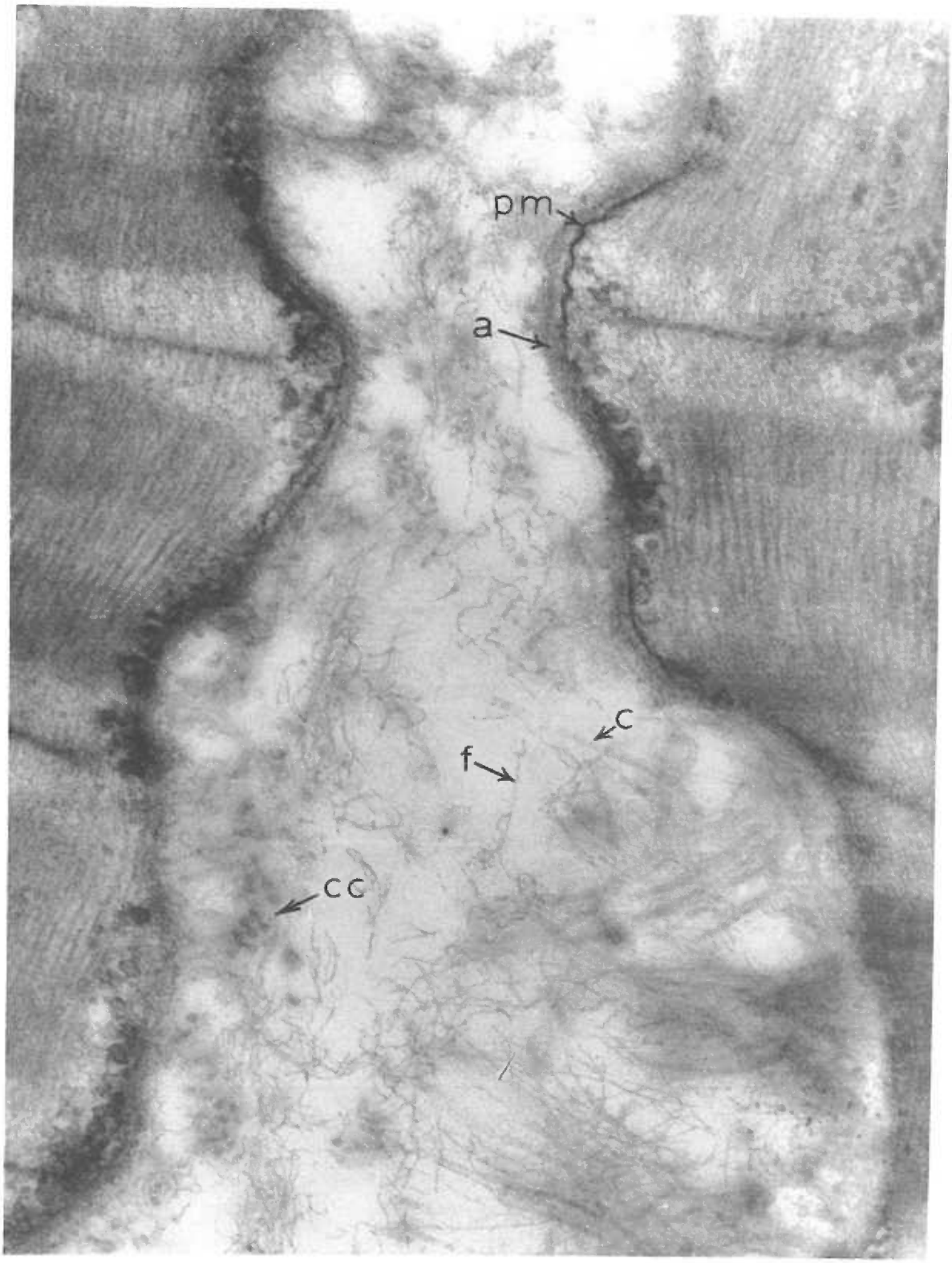
pm
a
c
f
cc

evidence is found. The chemical nature of the fine fibril component is unknown.

The dark inner laminae of Robertson's membrane complex is also revealed to be a three component structure showing dark laminae surrounding a light 40 Å central core. This inner three component structure is seen to lie coincident with the sarcoplasmic border in the muscle fiber. It is also analogous to a characteristic structure seen at the cytoplasmic interface in a wide variety of other cell types (37). The implication is that such a structure is common to many biological membranes including the muscle fiber. It is also of the proper thickness to be equivalent to the "physiologic plasma membrane" derived from physical, transport, and electrical studies. Robertson therefore feels the inner dark line of the membrane complex can be identified as the plasma membrane, whereas the outer light and dark areas represent a second continuous phase component of extracellular nature functioning physiologically as a basement membrane. The latter is called the amorphous layer and is considered to be a structure distinct from the plasma membrane.

The structural distinction of the plasma membrane and the amorphous layer is supported by further evidence, as they show differential electron staining properties (38). In permanganate preparations, which generally show cellular and mitochondrial membranes in good contrast, the amorphous layer is barely visible. The

of pleats parallel to the fiber axis, which, if unfolded, would fit a fiber or more nearly normal size. The outer two filament components of the sarcolemma remained distinctly outside the amorphous layer pleats, but continued to be closely associated. It is clear that the plasma membrane and the amorphous layer are distinct structural entities.

Very recently, some pertinent evidence relating to the surface configurations of the continuous phase and the fibril mat has appeared. Figures 3-A, B, and C show the surface ultrastructure of a single frog semitendinosus fiber revealed at successively higher magnifications in the scanning electron microscope. The fiber had been pretreated with a bacterial collagenase before fixation and shadow casting. Several prominent circumferential features can be seen, consistent with the banding patterns found in regular electron micrographs by previous workers, and probably a consequence of the continuous phase of the membrane conforming to the dry mass distribution of underlying tissue. The markings of the surfaces of relaxed and contracted fibers showed differences in accord with the sliding filament theory of muscle contraction.

Figure 3-D illustrates a muscle fiber untreated with collagenase, characterized by conspicuous longitudinally organized fibrous bundles, presumably collagen, covering the undulating muscle cell surface. The bundles are interlaced with a random network of finer

Figure 3. Scanning electron micrographs of the muscle fiber surface. The preparation is from the frog semitendinosus muscle. Fibers fixed with glutaraldehyde and dehydrated through serial concentrations of acetone. A, B, and C show successive magnifications of fibers from which external collagen has been removed by treatment with a bacterial collagenase. D, muscle fiber untreated with collagenase, showing prominent fibrous bundles covering the cell surface. From Boyde & Williams, J. Physiol. (London), 1968. 10-11P (41)

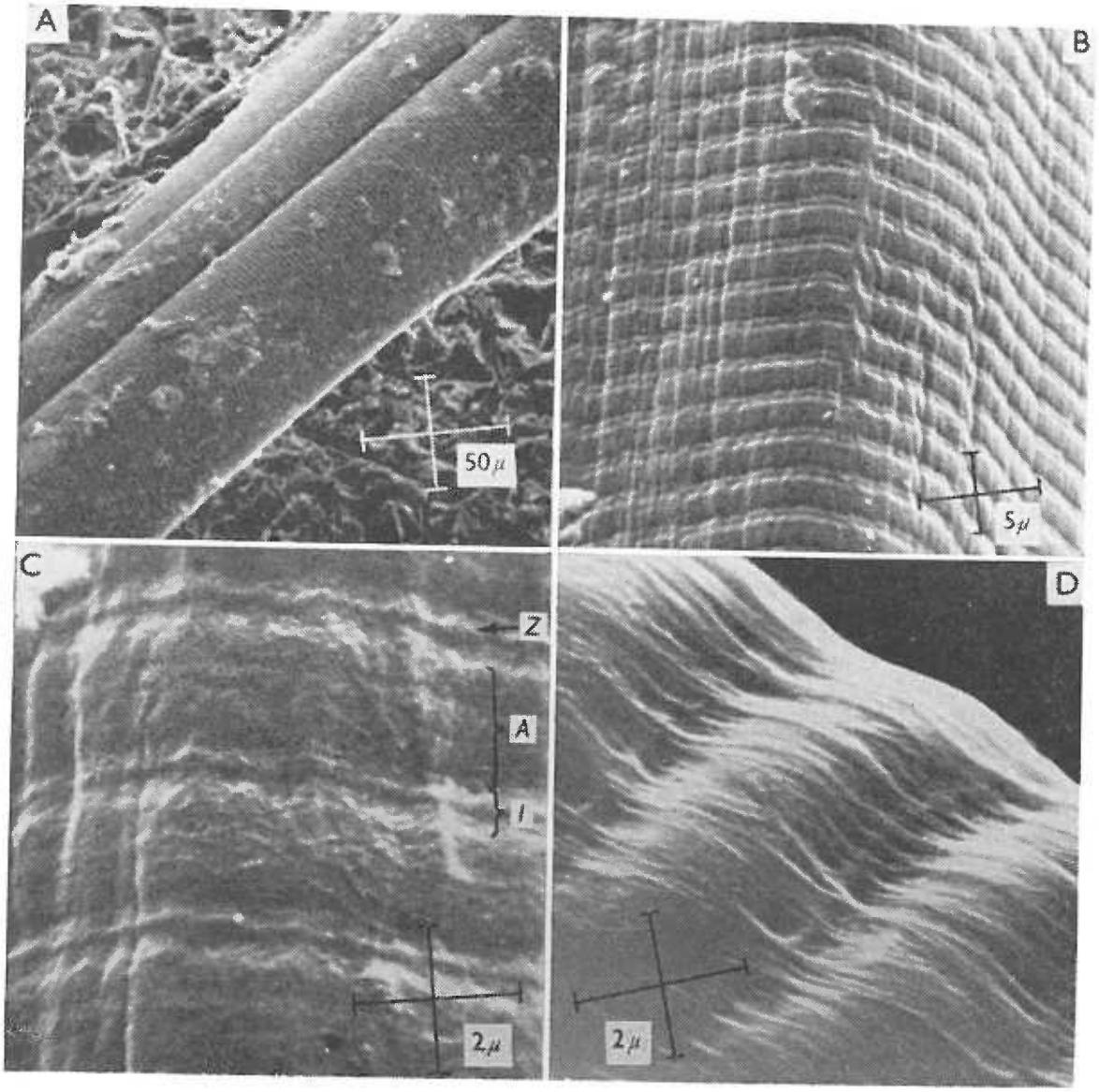
A
50 μ
B
5 μ
C
Z
A
I
2 μ
D
2 μ

fibers. Thus it appears that the surface structure as illustrated by Reed and Rudall (figure 1-B), although demonstrating undulations, may have misrepresented the fibril components as being irregularly distributed due to bundle disruption during preparation.

We therefore have come to view the sarcolemma as a very complex structure. It is now pictured as having four components in cross-section. On the outer aspect lie two interspersed fibril components, a group of large diameter fibrils possessing striations reminiscent of collagen, and a second class of small diameter fibrils of unknown nature. The surface ultrastructure shows prominent fibril bundles arranged either parallel or at a small angle to the fiber axis, interconnected by additional fibril components. These fibril layers overlie the undulating continuous membrane complex of Robertson, which is composed of an outer amorphous layer 300-600Å thick of unknown nature and function, and an inner plasma membrane of 75-100Å width (24). The membrane complex or continuous phase seen in electron micrographs of sarcolemmal cross-sections probably corresponds to the structureless clear sheath seen in views perpendicular to the fiber surface by Schwann and Bowman. The inner aspect of this continuous phase shows remnants of sarcoplasmic reticulum and circumferential markings at the level of Z-lines. It will be shown later that the sarcolemma in cross-section also appears to be scalloped in contour parallel to the fiber axis,

with dips at the level of Z-lines and possibly also at the M-line level. This behavior is also suggested by the undulations noted in studies of surface configuration.

The Muscle Fiber-Tendon Junction

The discussion of sarcolemma ultrastructure to this point has centered on central regions of the muscle fiber. This treatment was primarily concerned with the sarcolemma as a structural entity. However, ultrastructural information can also contribute to understanding of the role this membrane plays in muscle mechanics, because any tension postulated to be carried by the sarcolemma or other cellular structures and transmitted to tendon must also be borne through the region of fiber-tendon transition. Details regarding the structural features of this interface are therefore obligatory to functional interpretation of mechanical stresses borne by various fiber components.

The historical literature reveals a great controversy concerning fiber attachment ultrastructure. Two theories are prevalent. The Continuity Theory held that direct connections exist between the fibrillae inside the fiber and fibrillae of the tendon, the strength of the union depending on this continuity. In contrast, the Sarcolemma Theory asserted that the sarcolemma forms an uninterrupted limiting membrane between the substance of the muscle fiber and tendon

fibrillae (30).

The historical arguments and findings are thoroughly reviewed by Carr (42), who was a proponent of the Continuity school of thought in the early twentieth century. This author claimed the demonstration of continuity between the myofibrils and tendon fibrils in photomicrographs of sections of fixed fetal pig skeletal muscle. No evidence was found for sarcolemma intersection with the long axis of the fiber at any point in the region of its transition to tendon. Similar conclusions were reached by Butcher (43), following observations on fixed embryological specimens of skeletal muscle and tendon from albino rat fetuses.

In contrast, more recent studies with the light microscope lend support to the Sarcolemma Theory. From stained sections of the fiber attachment region of skeletal muscle fibers in the adult monkey, Goss (44) described a layer of reticular fibrils enveloping the end of the muscle fiber and lying between the fiber terminal and the tendon proper. He furthermore shows reticular projections of this layer which invaginate the terminal cell membrane. He emphasized the significance of the Bielschowsky silver staining method employed in selectively staining these argyrophilic fibers which he claims are not clearly depicted by usual staining procedures. Myofibrillae were confined to the substance of the muscle fiber and in no case did they give evidence of being continuous with fibrils outside

the enveloping terminal sarcolemma.

A similar investigation was reported by Long (30) in which several stains were simultaneously applied to serial sections of the triceps surae of fetal and post partum rats. The special staining technique results in argyrophilic reticular fibers being stained black, myofilbrillae and other sarcous elements red, and the collagenous fibers of tendon green. She found that the myofibrils terminate on the inner aspect of the continous terminal sarcolemma, while reticular fibers of the attachment region envelop the terminal fiber to continue as sarcolemmal and endomysial reticulum proximally and are continuous with the tendons distally. No evidence was found for continuity between myofibrillae and tendon fibrillae. Therefore the recent results of Goss and Long both support the Sarcolemma Theory. It is interesting to note that Speidel (45) also found the sarcolemma to be continuous around the terminal muscle fiber and furthermore shows that the terminal sarcomere ends with a Z-line.

Electron microscopic data on the attachment region appeared in 1954 (46). Porter records investigations on young zebra fish indicating sarcolemma continuity around the terminal muscle fiber in support of the recent light microscopic observations (30, 44). The sarcomere banding of myofibrils is seen to stop a micron or so short of the terminal sarcolemma. Tapering strands of unknown nature traverse this intervening sarcoplasmic space between the

myofibril termination and the terminal membrane, appearing to be non-contractile continuations of the myofibrils. These fibrils then insert into the sarcolemma. Tendon fibrils appear to insert in the sarcolemma opposite these attachments of the myofibril extensions forming a continuance or extrapolation of them. Barer (22) also concluded that the sarcolemma was continuous around the fiber end from microdissection studies, and that tendon fibrils inserted into the terminal membrane.

The data of Porter suggests an interesting alternative to the two-theory dichotomy. His results imply that the major contentions of both the Sarcolemma and Continuity Theories may be correct. The viewpoint of the former theory that the sarcolemma is continuous around the fiber terminal is verified, as is the assertion of the Continuity school that the muscle and tendon fibrillae are continuous or at least directly opposed across a continuous sarcolemma. The conclusion from the available literature must be, therefore, that the known ultrastructure of the muscle fiber-tendon attachment region does not preclude substantial tension transmission by either muscle substance myofibrillae or the sarcolemma to the tendons.

Sarcolemma Connections to Intracellular Structures

One last consideration remains regarding sarcolemma ultrastructure. Functional interpretation of membrane mechanics

requires knowledge about structures that may mediate mechanical interactions between the sarcolemma and intracellular structures. Connections are known to exist via the transverse tubule system (47), although there is no reason to believe they serve a mechanical function. The discussion will center upon the existence and nature of connections not associated with the tubule systems of the fiber, but rather morphologically associated with the Z- and M-lines of the sarcomere. Such information is logically related to the circumferential bands at the level of the Z-line noted on the inner aspect of the sarcolemma (31, 32, 35).

According to Garamvölgyi (48), it was originally suggested by Dwight in 1873 that connections to the sarcolemma may exist in the Z-line region. This proposal triggered an enormous controversy reaching into the present century centered around the nature and/or existence of Krause's Grundmembrane. This structure was supposed to be a rigid disc-like structure seen in the microscope as the Z-line, being continuous across the entire fiber cross-section and rigidly anchored to the sarcolemma. The historical work is thoroughly treated in the reviews of Jordan (23) and Fenn (49). The results of work up to the review of Fenn show a continuance of the controversy. For this reason and because the historical work is treated elsewhere, the present discussion is confined to more modern treatments.

A wealth of recent workers have concluded that although connections do exist between the Z-structure and the sarcolemma, these structures are relatively weak and easily overcome (3, 18, 22, 33, 50, 51). A wide variety of techniques were employed in these studies including microdissection, various extraction procedures, and preparation of electron micrographs using cells from many species and in various cell states. Conflicting opinions are still manifest, though, as Walls (52) and Edwards et al. (53) feel that the proposed connections do not exist, whereas Podolsky (54) thinks the connections exist and are strong.

Recently, a Hungarian school of workers piloted by Ernst has produced an abundance of information on muscle function in general and on the topic of sarcolemma connections in particular. They first demonstrated the existence of interfibrillar bridges or connections between myofibrils and from this system to the sarcolemma using microdissection techniques (55, 56). They describe a Z-system consisting of discs occupying the cross-sections of individual myofibrils interconnected to each other and the sarcolemma by thin fibril networks. Members of the Hungarian school subsequently described the isolation by extraction of single Z-discs from individual myofibrils (57, 58), and later of large Z-networks consisting of many Z-discs still connected by surviving interfibrillar bridges (59). This Z-network model was later confirmed in electron microscope

studies (60), exemplified in figure 4. The Hungarian school employed insect flight muscle in most of their studies.

There appears to be in addition to periodic Z-discs in single myofibrils, a second less dense class of discs alternating with the former and localized to the region of the M-line (61). These M-discs were demonstrated in electron micrographs of single myofibrils after extraction, which clearly showed a string of discs every other one of which was identified as a Z-disc. The consensus of opinion offered by the Hungarian school is that the Z-network interconnecting myofibrils and sarcolemma and possibly a similar system at the M-line level provide the physical basis for some degree of sarcomere alignment between adjacent myofibrils, but is not arranged properly to function as a rigid transverse connection across the entire fiber cross-section.

An additional line of evidence bearing on sarcolemma connections shows a repeated festooned pattern of the sarcolemma in longitudinal cross-section (figure 5). The scalloped sarcolemma outline was first noted by Carr (42), having dips coincident with Z-lines. This observation was made with the light microscope on fetal pig diaphragm muscle fixed in situ during maintained contraction. Jordan (23) also noticed a scalloped membrane outline in fixed tissue, and concurred with Carr in feeling such a pattern may signify sarcolemmal connections to underlying structures.

Figure 4. Electron micrographs of inter-Z bridges (A) between two myofibrils and (B) between the sarcolemma and an adjacent myofibril. The preparation involved insect flight muscles fixed in a buffered 1% solution of osmium tetroxide for one hour, followed by embedding in Araldite and thin sectioning; stained by an alcoholic solution of phosphotungstic acid. A, bridges between adjacent myofibrils are thought to be absolutely distinct from the sarcoplasmic reticulum, because of the direct continuity of the bridge and the Z-discs (Z) and the similar stability of bridges and discs in response to various chemical agents. (mi), mitochondrion. B, the cell membrane (cm) appears thickened as a dense triangular body at the attachment site (att) of a bridge (Zbr) connecting the sarcolemma and an adjacent myofibrillar Z-disc (Z). M-line (M) of the sarcomere banding pattern is also indicated. Both A and B from Garamvölgyi, J. Ultrastructure Res., 1965. 13, 435-443. (48)

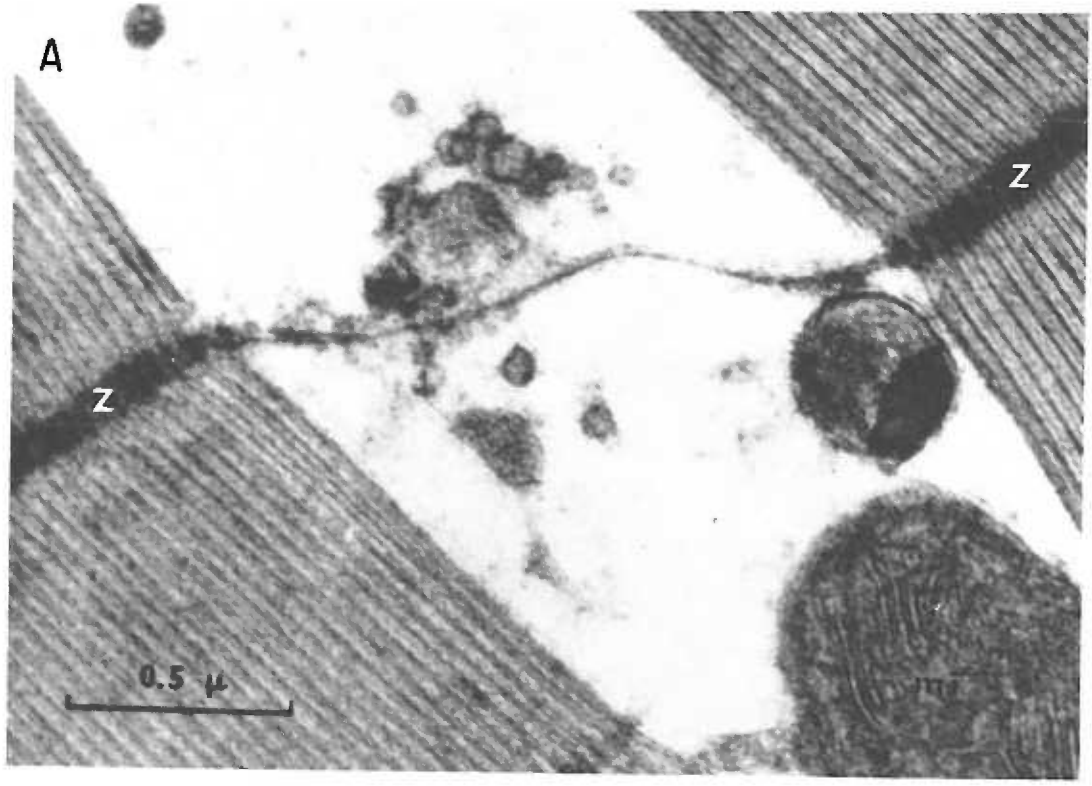
A
Z
Z
0.5 μ

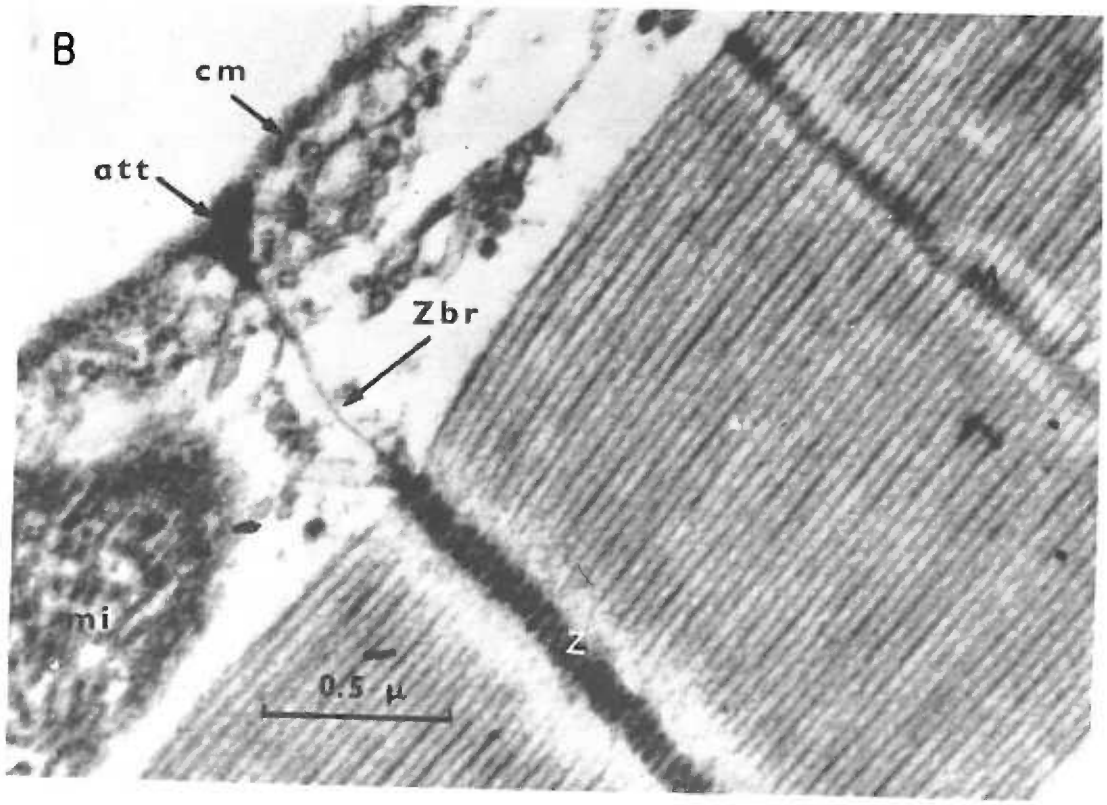
B
cm
att
Zbr
mi
Z
0.5 μ

Figure 5. A, photomicrograph and B, electron micrograph illustrating membrane festooning. A, specimen is from expt. #68 in the present work. Single frog semitendinosus fiber suspended in Ringer's solution. Note scalloped cell outline on left aspect, emphasized by festooning of the diffraction bands. The festooning seen through the light microscope should be interpreted with caution, as the contour details are below the resolution of the microscope. 1045X. B, electron micrograph illustrating membrane festooning. The scalloped contour is not well defined, but the sarcolemma (S) appears loose and dips are apparent near the Z-lines. Z, A, M, I label the typical cross banding of the sarcomeres. (fc), "fenestrated collar", portion of the sarcoplasmic reticulum at the level of the M-line; T, triads are formed by the transverse tubule centrally and terminal cisternae of the sarcoplasmic reticulum laterally; L, lipid. Sarcomere length approximately 2.4μ. Frog semitendinosus muscle. From Street, Sheridan & Ramsey, Med. Col. Virginia Quart., 1966. 2, 90-99. (59)

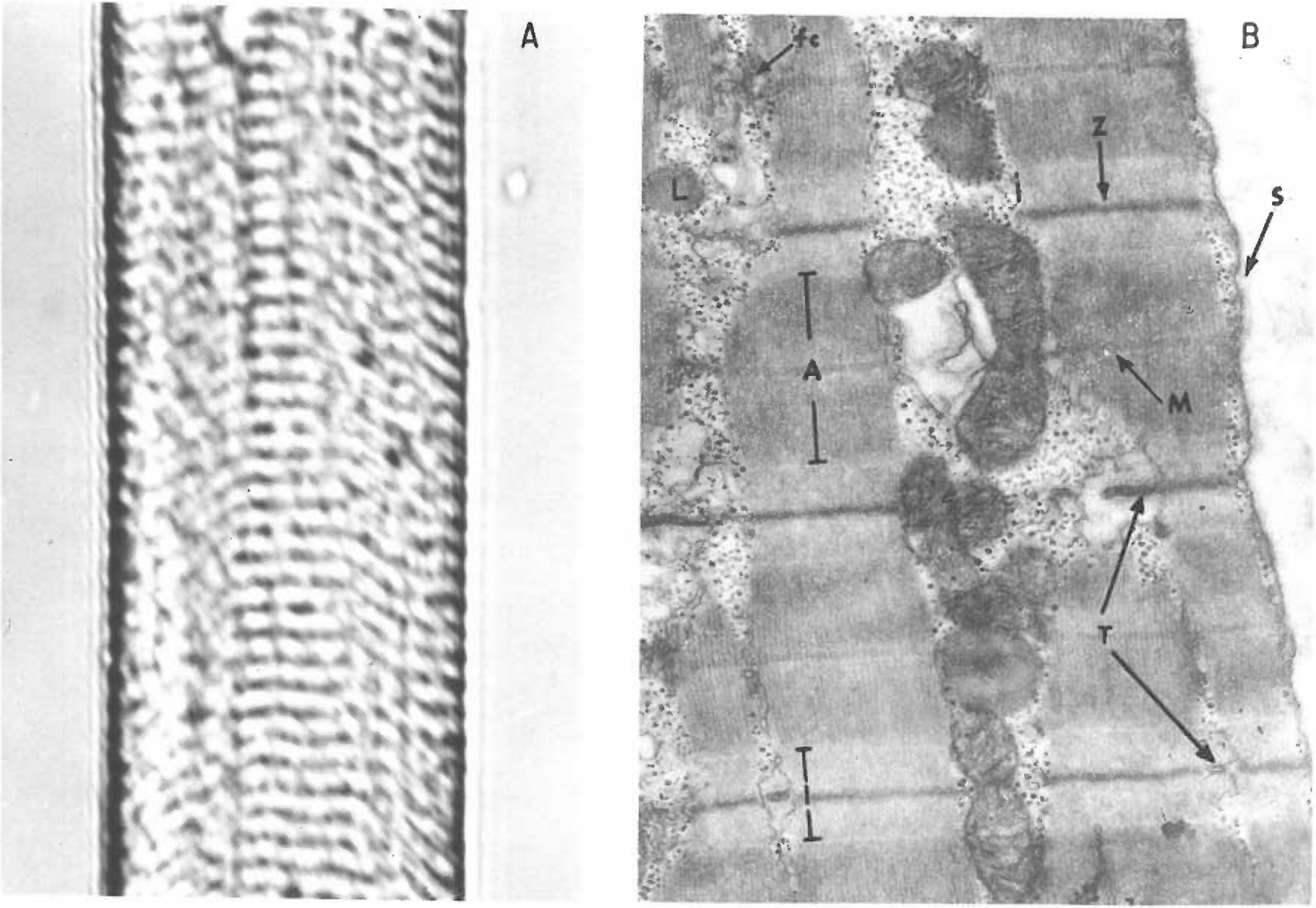
A
B
fc
Z
L
I
S
A
M
T

This pattern and alignment was confirmed by early electron micrographs (31, 36, 62, 63). Data of this nature may represent the ultrastructural basis for the proposal of Martin (64), who evoked membrane folding as a hypothesis to explain the constancy of conduction velocity in curarized frog sartorius fibers at lengths 67-120% of resting length. He calculated that if the membrane were a cylindrical tube, the decrements in fiber radius and membrane thickness with stretch over this range should result in membrane resistance and capacitance changes leading to a 50% increase in conduction velocity over the length range investigated. Electrical parameters would be unaffected if the membrane merely unfolded. Unfortunately, his calculations are not presented. Furthermore, the membrane folds do not appear deep enough to allow such extensive stretch without introducing membrane stress, although it is possible that longitudinal membrane folds exist and also unravel with fiber lengthening.

Electron micrographs reported by Street et al. (47), reproduced in figure 5-B, verify scalloping having depressions coincident with Z-lines. The preparation involved frog semitendinosus and sartorius fibers fixed at various lengths during contraction. In addition, the authors confirm a previous observation by Dorn (65) that sarcolemma depressions also appear to occur at the level of the M-line. They renew the suggestion originally made by Jordan (23) that

this may signify M-connections to the sarcolemma serving to aid Z-connections in maintaining alignment.

In light of present evidence, it seems reasonable to tentatively conclude that interfibrillar fibrous connections exist at the Z-line level serving as non-rigid connections interlacing the myofibrils and extending to the sarcolemma (60). The sarcolemmal attachment of such connections are to a thickened circumferential ring observed on the inner aspect of the membrane at this level (60), coincident with depressions or scallops in the longitudinal sarcolemma outline (47). Recent evidence also suggests that connnections may exist at the level of the M-line (47). It is important to note, however, that the structural significance of membrane festooning is unknown, and such a contour may not signify sarcolemma connections.

The Mechanics of Single Muscle Fibers at Rest

The previous section dealing with membrane ultrastructure emphasizes the great complexity of this structure and its poorly understood relationships with other cellular elements. Structural information is used in conjunction with morphological and physiological correlations during various functional activities of the cell to derive mechanisms of function. The discussion of single fiber mechanics in the present section is therefore complimentary to the preceding one for mechanistic interpretations.

One of the most fundamental characteristics of muscle is its length-tension behavior. There has been a long history of such studies on whole muscle beginning with Weber (66) in 1846. The first length-tension characterization of single fibers was carried out much more recently by Sichel (67). Short central segments of single frog sartorius muscle fibers were marked with carbon particles, and were found to obey Hooke's Law when elongated. Defining fiber stress as the force per unit cross-sectional area and strain as the relative elongation referred to a particular reference length, the fact that central fiber segments obeyed Hooke's Law signifies that the stress-strain relationship was linear. Unfortunately Sichel does not describe his determination of the reference length, but presumably it represents the length at which the fiber first begins to exert passive tension upon stretch as is customary. Furthermore, his data only cover relative elongations over the range 1.00-1.12. With these facts in mind, he finds the ratio of stress to strain, the longitudinal modulus of elasticity of the fiber segment, to be 2.5×10^6 dynes/cm^2.

The classic 1940 paper of Ramsey and Street (25) describes their length-tension characterization of whole frog semitendinosus single fibers. It is significant in that a much greater range of elongations is investigated. These workers found a non-linear stress-strain relationship concave to the stress axis for relative

elongations as great as 2.00. The results, however, do not significantly differ from those of Sichel over the range of relative elongations between 1.00 and 1.12. The reference length was carefully defined as that length at which maximum isometric tension was developed, and was called the "resting length" of the fiber. At the resting length so defined, the passive tension was less than 1 mg, and it was empirically noted that this was the length at which the fiber just became taut during stretch. Elongations were carried out very slowly to allow for viscous equilibration.

Particular values on the length-tension curve vary among individual fibers. One obvious reason offered was that the fibers varied in diameter. A typical example showed arbirary force values of 0.0, 0.4, 2.3, and 8.0 during slow elongation at respective relative elongations of 1.00, 1.25, 1.50, and 1.75. The range of forces found at an elongation of 1.75 was 20-130 mg for six fibers, with an average of 50 mg distorted by one high value. Thus there is much interfiber variability. Slow elongation was described as a 5% increase of length in not less than four minutes. Marked hysteresis is present as slow release from the elongated state results in force values of 0.0, 0.2, 1.0, and 8.0 at the same elongations quoted for stretch.

The laboratory of Buchthal and co-workers in Copenhagen has published an enormous amount of data related to the behavior of

single muscle fibers. A force-extension characterization of single frog anterior tibial muscle fibers carried out by Sten-Knudsen (68) is shown in figure 6. The agreement with the data of Ramsey and Street for the average force required to induce comparable elongations is good, considering species and methodological differences. The "reference length" defined by Sten-Knudsen refers to the fiber equilibrated to a load of approximately 0.8 mg, and differs somewhat from the value of length under a 5 dyne load which is customary for the Buchthal laboratory (13, 69-72). The latter workers agree with the general fiber behavior found by Ramsey and Street and by Sten-Knudsen as does Carlsen et al. (73).

Ramsey (74) feels that very slow elongation of single fibers is necessary for reproducible results, as he finds rapid stretches give inconsistent values. The effect is attributed to variations in the amount of connective tissue remaining at various positions along the fiber, rapid stretch resulting in disproportionate elongation of fiber segments in inverse proportion to the amount of remaining endomysium. The Buchthal school carries out stretches rapidly with subsequent time allowance for tension adjustment (75). Following this procedure, Sten-Knudsen (68) found that 1 mm segments of single frog tibialis anterior fibers in various relative positions along the cylinder axis elongated proportionately. The general agreement in the results obtained by these two schools on intact fibers (68, 76)

Figure 6. Force-extension diagram of isolated anterior tibial muscle fibers of the frog (A) at rest and (B) during isometric tetanic contraction. Ordinate, relative force (dynes/dynes), defined as the external load borne by the fiber as a fraction of the force at the point where the additional force during activity is zero (intersection of A and B curves). Abscissa, extension ratio (cm/cm), defined as the fiber length divided by the "equilibrium" length of the fiber (the fiber length when the external fiber force was 0.8 ± 0.2 dynes). Curves A and B represent the average values found for nine experiments, conducted at 0°C on fibers from Rana esculenta and Rana temporaria. The vertical bars indicate the standard error of the mean for the nine experiments. From Sten-Knudsen, Acta Physiol. Scand., 1953. 28, Suppl. 104, 1-240. (68)

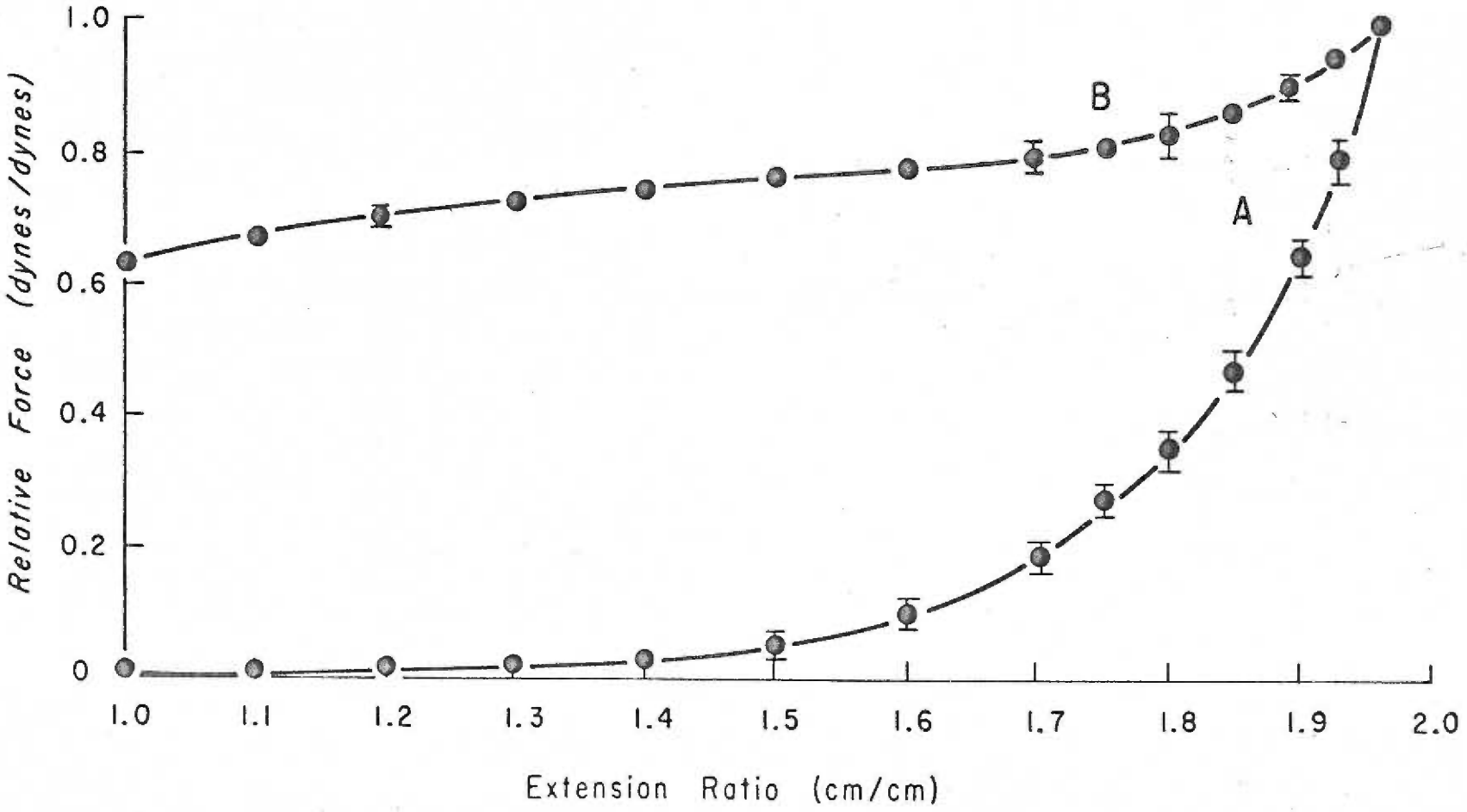
1.0
0.8
0.6
0.4
0.2
0
Relative Force (dynes/dynes)
B
A
1.0
1.1
1.2
1.3
1.4
1.5
1.6
1.7
1.8
1.9
2.0
Extension Ratio (cm/cm)

implies that in intact fiber investigations either slow stretch with immediately measurement or rapid stretch followed by measurement delay to allow for tension adjustment leads to similar results. However, the disagreement in data from these two schools on fibers containing retraction zones discussed in the next section may be due to such methodological differences (68).

Two additional experimental approaches have been applied by the Buchthal school to attempt mechanical resolution of fiber components. One approach involves studying the dynamic behavior of single fibers, in which mechanical parameters are noted during quick stretch or release (transient experiments) and rapid, small, periodic length changes (vibration experiments). In a second approach depending on the anisotropicity of muscle, the mechanical characterization was carried out accompanying static and dynamic torsional disturbances.

Transient experiments led to the conclusion that sudden step changes in load result in length and tension changes consisting of two components, an instantaneous pure elastic effect, and a prolonged effect beginning with an initially high velocity that gradually disappears (69, 77). The prolonged creep and stress relaxation of the fiber proceed exponentially with time and last several minutes (77). In agreement with the results of vibration experiments (76, 78), the stiffness, i.e., the ratio between the decreases in tension and

length due to quick release, increased proportionately with the load on the muscle (72).

Vibration experiments revealed that small periodic oscillations result in length changes that lag behind changes in load (77). This phase difference can be considered to consist of two components, an elastic one and a viscous one. The elastic stiffness of the fiber increases linearly with load, whereas the viscous component rises more slowly. An osmotically induced 20% decrease in cell water content leads to a three-fold increase in both the elastic and the viscous stiffness, while a 70% increase in fiber water gives no measurable change. These results indicate the structural elements of the fiber are in a state of maximum hydration at the normal osmotic concentration. It also indirectly suggests that the muscle substance contributes to passive stiffness.

Since the muscle fiber is mechanically anisotropic, forces of interaction are different in various directions (69). A correlation of longitudinal and transverse measurements may therefore be expected to contribute to understanding of the minute structural elements responsible for fiber behavior (68). Resistance to twist can be described in terms of general mechanical moduli just as can longitudinal stiffness. Sten-Knudsen found that the torsional stiffness of single tibialis anterior fibers is independent of deformation amplitude and vibrational frequency up to 10 cps. Frequencies above

10 cps showed torsional stiffness increasing with frequency, the value at 50 cps being 2.6 times that at 10 cps. With increasing load, the torsional stiffness increases in a parabolic fashion.

Sten-Knudsen also measured ratios of torsional to longitudinal stiffness and found them to be 7-30 times less than would be expected if the fiber behaved as a pure isotropic body (68). Comparing fiber response with an ideally anisotropic model consisting of parallel chains without entanglements shows the ratio to be 10-40 times greater in muscle. These findings imply that transverse forces of interaction must be present to account for the torsional stiffness of the resting fiber. Such interactions would arise if the minute structural elements are cross-linked to form a three-dimensional network (68, 75, 79).

In 1954 Natori (80) introduced a new technique allowing an additional accumulation of information regarding mechanical contributions of fiber structures. Employing delicate microdissection procedures, the sarcolemma was removed from large expanses of single toad fibers. The resulting skinned-fiber preparation is in many ways the converse of membrane tube studies discussed in the following section, as each is an attempt at isolating the sarcolemma or the muscle substance for independent characterization. Length-tension characterizations revealed that fiber compliances were the same with and without the sarcolemma for lengths up to 140% of rest

length. At greater elongations, the compliance of regions enclosed by membrane was less than unenclosed segments. These results represent additional evidence supplementing dynamic and torsional investigations in suggesting that the muscle substance contributes to passive rigidity. Analogous experiments carried out recently by Podolsky (54) are in general agreement.

Skinning a muscle fiber of its sarcolemma is a drastic procedure. Undoubtedly more than membrane is removed or damaged. The plasma membrane responsible for the maintenance of different intracellular and extracellular environments is no longer present, thereby exposing the sarcoplasm and myofibrils to foreign media. Protoplasmic exposure to high calcium and magnesium concentrations, which exist in the extracellular fluid, can cause rigid gelation (81), while the fiber sarcoplasm is considered to be normally a semifluid (82). Obviously, extensibility comparisons between skinned and normal fiber regions are jeopardized by these considerations, although the resultant conclusions concur qualitatively with many further lines of evidence.

Gonzales-Serratos (83) recently described some elegant experiments suggesting, in agreement with data from the Buchthal school (68, 72, 79), that the myofilaments are cross-linked in the resting fiber. Single frog semitendinosus fibers were isolated and embedded in gelatin. Resting fiber lengths can then be altered in the

direction of decreasing lengths by mechanical compression of the gelatin block. As the fiber is shortened in this manner, a reduction of sarcomere lengths was noted. The overall fiber remained straight, but the myofibrils became wavy. Subsequent stimulation resulted in a reversible straightening of the myofibrils.

A similar conclusion was reached by Grimm and Whitehorn (84) from studies on isolated rat papillary muscle. Proteolytic enzyme addition reduced passive and active tension equally. Actomyosin extraction reduced resting tensions, while myosin extraction did not. This suggests that actin is more directly involved in the maintenance of resting tensions. Recent observations of Parsons and Porter (85) on contracting muscle fibers in cultured cells imply, furthermore, that the force restoring the resting length of the sarcomere comes from the contractile elements themselves and not from external elasticity. Individual myofibrils were seen to seek a kinked configuration following relaxation if the overall fiber was fixed in a configuration shorter than rest length. Thus a wealth of independent evidence assigns a significant role to the muscle substance as a contributor to resting fiber elastic behavior.

Mechanics of Fibers Containing Retraction Zones

The phenomenon of muscle fiber retraction zones was briefly mentioned in an earlier section. The fact that a region of membrane

free of solid intracellular material results from retraction zone formation (see figure 7, page 46) was recognized by several workers as an opportunity to explore the mechanical properties of isolated sarcolemma. The basic experimental design employed, with minor variations, has been to compare relative elongations of empty tube regions with intact segments of the same fiber. Comparison of the two types of regions regarding their extensibilities is then used to assess the proportion of the load in the resting fiber borne by the sarcolemma. This extrapolation assumes that the same radial stresses are active in both intact and tube segments, that the membrane in the tube portion has not had its mechanical properties altered by damage or by a change in environment, and that the tube region contains a fluid, i.e., a material incapable of bearing shearing stresses, so that all force is carried by the membrane.

Sichel's studies on the mechanical properties of central segments of single frog sartorius fibers have been discussed (67). The qualitative conclusion is also expressed that length changes of tube and intact fiber regions markedly favor the former during stretch, indicating that although the sarcolemma exhibits appreciable elasticity, it is but a fraction of the total fiber elastance. Unfortunately, this statement is not supported by data, the detailed analysis of this phenomenon being reported in a later paper (86). Using a similar procedure to his previous experiments, Sichel finds that the

elongation of tube regions was on the average 2.2 times that of intact fiber regions, the range being 1.1-4.2. The lowest values were observed in tube regions where the coagulum had not separated cleanly from the sarcolemma. It is concluded that the intact fiber should resist extension by more than twice the sarcolemma alone.

The elegant paper of Ramsey and Street (25) appeared in the year preceding Sichel's second report. This work and subsequent discussions by these authors (74, 87, 88) thoroughly treats their data and viewpoints on tube region manipulations and the implications regarding cell mechanics. The basic tube region experiment was conducted on whole frog single semitendinosus fibers with the variation that the relative elongations of tube regions were compared to length changes of the whole fiber. As for intact fibers, length alterations were induced slowly (74). Two lines of evidence were offered implying that the sarcolemma carries the entire brunt of passive loads. Injured tube regions were found to lengthen in approximately the same proportion as the intact fiber during stretch. Secondly, the resting tension of an injured fiber is precisely the same, at the same lengths, as that of the same fiber before injury. Thus these facts were contradicted by the later data of Sichel (86).

The methodology of Ramsey and Street is an important consideration. Fiber tensions were recorded by optical magnification of the deflection of a relatively stiff quartz cantilever attached to the

fiber tendon. The limiting factor in data acquisition was felt to be the linear measurement of the magnified lever excursion. For a load of 100 mg, the magnified excursion was approximately 10 cm and was read to an estimated 0.5 mm. At high loads (more than 100 mg) the accuracy was therefore at least within 1%, but for small loads of say 5 mg the error could be as much as 1 mg, or 20%. Within these limitations, these workers found that the resting tension was entirely due to the sarcolemma, since any contribution by the muscle substance could not have been greater than 1 mg at any degree of stretch (88).

The Buchthal school of workers has carried out extensive investigations on retraction zone tube regions. They have used the basic experimental design essentially as described in that comparisons of relative elongations were made between tube regions and intact segments of the same fiber. Contributions by this school began in 1942 (69), when the results of Ramsey and Street (25) were objected to on the grounds that the sarcolemma in tube regions appeared to be in a disproportionate state of elongation. The stress fields in intact and tube region membranes are therefore different and hence comparisons of relative elongation are cautioned. The Buchthal discussion was in conjunction with mechanical studies on single frog semitendinosus fibers. It was these objections offered by Buchthal et al. in 1942 that led to the Ramsey paper of 1947 (88)

offering a defense for their reasoning and in turn concluding the reasoning of the opposition was unsound.

A thorough experimental treatment of tube region elongations appeared from the Buchthal laboratory in 1951 (70). The conclusion was reached, with reservations, that the sarcolemma does not contribute to the elastic modulus of the cell until the intact fiber has been stretched to about 1.5 times the "equilibrium length". The conclusion should be somewhat reserved in that evidence is also presented suggesting that the sarcolemma in tube regions is either in an incomparable state of tension or is plastically deformed, thereby negating comparisons. Intact single frog semitendinosus fibers were isolated, and injury was subsequently induced by gentle mechanical compression.

Breaking stresses and strains were also determined. Casella noted that stretching a damaged fiber always results in rupture within an empty tube segment. The breaking stresses and strains were on the average 38 and 34% less in injured versus normal fibers respectively. Breaking forces of intact fibers at 20°C were on the average 4350 mg and occurred at a mean strain of 3.39 cm/cm. Further experiments compared fiber equilibrium length determinations before and after artificial mechanical injury with subsequent formation of retraction zones. The equilibrium length of the fiber increased an average of 25% after retraction zone formation. The

change in equilibrium length varied with the extent of injury and was noted to be as much as 60%. This data leads Casella to conclude after Buchthal et al. (69) that the sarcolemma in tube regions is in a stress state incomparable with normal regions in the same fiber. It is important to realize that Casella induced injury in normal fibers stretched to 140% of equilibrium length, while Ramsey and Street (25) do not state conditions at the time of injury but it apparently was at much lower stresses (75). Casella finds furthermore that during extension of injured fibers, the tube region elongates relatively more than intact regions. Within the retraction zone proper, there is equal relative elongation in the tube region, the clots at each end of the tube, and in the segments of disorganized muscle substance on either side.

The methodology employed by Casella is typical of the Buchthal school. Thus stretches were carried out rapidly with subsequent time allowance for tension adjustment to the new length. The data of Mauro and Sten-Knudsen (71) indicates that length-tension curves of injured frog semitendinosus fibers rapidly produced and sequentially repeated indicate marked non-reproducibility. The extension arm of the first curve actually lies above the same for the intact fibers, and enormous hysteresis is manifest in the overall loop. Subsequent loop determinations shift along the strain axis, show reduced hysteresis, and eventually approach the curves shown by

Casella. Mauro et al. induced injury at lower fiber elongations, indicating that the methods of injury inducement and stretch are critical parameters. This consideration is undoubtedly significant in explaining discrepancies between various workers. Casella also noted that stretch of an injured fiber containing tube regions results in the appearance over time of new retraction zones, adding additional interpretive complexities.

The main objective in tube region studies has been the elucidation of the relative roles of muscle substance proper and sarcolemma in bearing passive loads. Since a major obstacle is the separation of components for independent analysis, Buchthal and Weis-Fogh carried out additional experiments on insect flight and abdominal muscles, which are peculiar because they possess merely a meshy remnant of sarcolemma (13).

Injured insect cells exhibited behavior markedly different from frog fibers. Insect fibers underwent a decrease in equilibrium length upon injury, while the tube diameter equaled its original value in the intact fiber. Most fibers show equilibrium length increases (70) and tube radial reduction (25, 70). The diameter of the cross-striated content increased, suggesting this peculiar behavior may be due to non-specific swelling. Upon stretch, fiber rupture always occurred in tube regions. In some instances, stretch of uninjured abdominal muscles gave normal resistance to stretch until the

muscle substance broke leaving an empty tube region. The force immediately decreased toward zero, and upon subsequent stretch, the preparation thereafter followed length-tension curves typical of injured fibers (13). This evidence, along with the lower breaking stress of tube regions, is claimed as a demonstration that the main resistance to passive stretch must be assigned to the striated muscle substance (10, 13, 72).

This concludes the available information relating to intact and tube region comparisons of fiber mechanical properties. Obviously the sarcolemma as a material has considerable structural strength. The evidence is inconclusive, however, in either quantitatively characterizing the sarcolemma in terms of parametric moduli or in evaluating the role of this membrane in fiber mechanics. Of the three major assumptions involved in such experiments, only one has been supported by data. This involved the apparent mechanical comparability of tube and normal segment membranes (24). Evidence is presented implying the incomparability of tube to normal regions because of differential membrane stress states (69, 70), negating a second assumption. No evidence or discussion of the third assumption as to whether or not the tube region contains a true fluid substance is offered in the literature.

Occurrence and Morphology of Retraction Zones

The classic treatise of Schwann (20) in which he proposes the cell theory of biological organization has been mentioned. This monumental manuscript also alludes to a peculiar phenomenon observed in insect muscle, in which the muscle substance of individual fibers was seen to be separated but held in juxtaposition by the remaining cell membrane. Such cellular regions, which are now designated as retraction zones (figure 7), are of great importance to the present treatment because of their involvement in the literature and because their use is employed in the present investigation.

Historically, many authors have noted conspicuous clots accompanying degeneration in injured skeletal muscle fibers. Bowman (21) clearly illustrates them in his classic paper of 1840 for the muscle fibers of boa, man, skate, and frog. Zenker's monograph on the degeneration of human skeletal muscle accompanying typhoid fever calls attention to waxy formations included within some degenerating fibers (89). The most characteristic feature of this type of skeletal muscle disorganization, which has come to be known as Zenker's waxy degeneration, is the phenomenon of muscle clotting. Muscle clotting, or the formation of retraction clots, is followed in many instances by subsequent retraction zone formation (45).

Following Zenker, many investigators have studied muscle

Figure 7. Photomicrographs of retraction zones, (A) unstained, and (B, C) stained for emphasis of connective tissue. A, fresh single muscle cell from the tibialis anticus of the frog, illuminated by a combination of transmitted and reflected light. A few minutes before taking the photograph the cell was gently damaged by mechanical compression, resulting in the eventual formation seen here. The muscle cell contents have divided, retracted, and formed two clots seen at each end of a region of sarcolemma tube. 340X. B, low power photomicrograph of a retraction zone stained for connective tissue by Laidlaw's silver impregnation method. Retraction zone geometry is distorted because the fiber became twisted during preparation. 320X. C, oil immersion photomicrograph of the central portion of the retraction zone seen in B, illustrating the fibrils associated with the sarcolemma. 1200X. A, B, and C from Mauro & Adams, J. Biophys. Biochem. Cytol., 1961. 10, 177-185. (24)

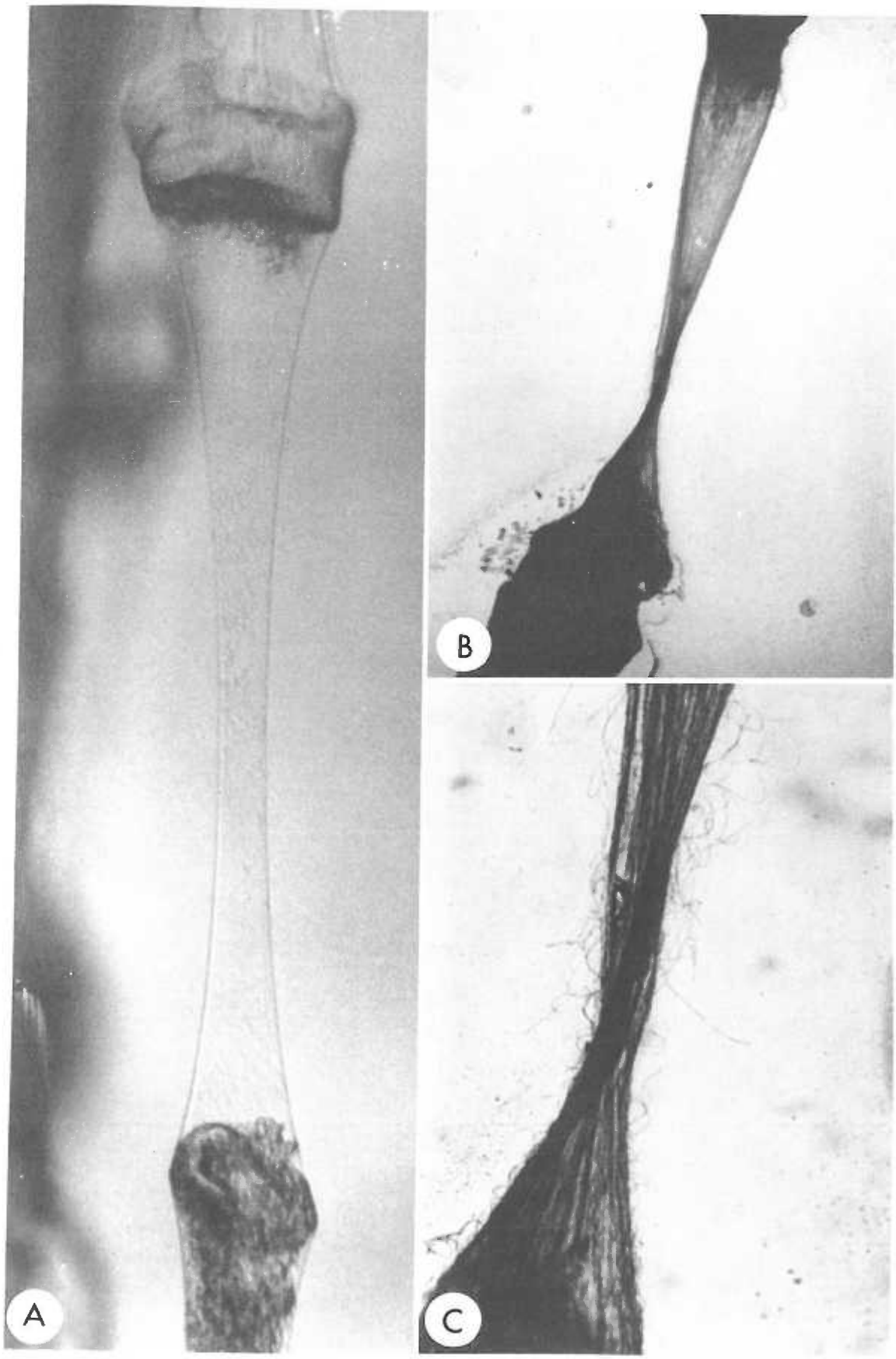
A
B
C

fiber disruption of the waxy type. Cohnheim (90) showed that cutting off the blood supply to the tongues of frogs by ligating blood vessels was followed in the course of two days by Zenker's waxy degeneration of some tongue muscle fibers. Waxy degeneration of voluntary muscle is also seen in association with pneumonia (91, 92), and it becomes apparent that the phenomena of retraction clotting and retraction zone formation are of an importance far exceeding their attraction from curiosity and morphological peculiarities advantageous for muscle cell membrane investigations. Artificial insults can also produce such characteristic disorganizations, as slight injury with a dissecting needle (93), contracture induced by tetanus toxin (94), tenotomy (95), and caffeine administration (96) have been noted to induce similar formations.

Nageotte (97) observed that two kinds of irregular, deeply staining, transverse zones of extreme contraction may be produced in fibers. In one type "congelation" occurs in the zones of extreme shortening so that the contraction is irreversible. Such formations are equivalent to muscle clots. In the other type congelation does not occur, and the zones of extreme contraction slowly relax until normal conditions are again restored. The clotting phenomenon seems to be a result of properties of the contractile material itself that become apparent as a non-specific response to various insults.

The wide occurrence and previous lack of a thorough

investigation of clotting and retraction zone formation led Speidel (45, 98) to attempt an alleviation of this deficiency. He succeeded admirably as these works stand by themselves as authorities on the subject. In the first paper, Speidel (98) shows from work on in vivo fibers of living tadpoles that the origin and growth of a retraction clot can be precisely correlated with the progressive transformation of individual sarcomeres, during both partial and total disorganization of the cross-striated muscle substance. Such data points to the intracellular origin of material forming the clot, and therefore the dependence of clot formation on properties of the muscle substance. Also, the entire sequence of regulation and repair of individual fibers in which retraction clots or zones had been induced was directly observed in the living animal. Fiber regeneration was seen to proceed by an initial establishment of longitudinal traction and the appearance of cross-striations. The fiber then grows in diameter by 200-300% or more, with the elastic sarcolemma accommodating itself to the larger size.

Speidel's investigations (45, 98) sampled frog tadpoles and various representatives of arthropod and mammalian species. As noted by other workers the phenomena described were found to follow a wide variety of insults including electrical injury, starvation or malnutrition, solutions of alcohol, sodium chloride, many other chemical agents, hot water, and mechanical injury. A whole

spectrum of clot formations from very fine discs to large clumps with retraction zone formation may follow the injury, the type of clot depending on the nature and severity of injury, the past history of the fiber, and its developmental stage. Clotting is consistently oriented in a transverse direction to the fiber axis, eventually enveloping the whole fiber cross-section as it grows. Individual clots also accumulate muscle substance from neighboring sarcomeres as do the clots found in retraction zones.

Casella (70) offers a vivid description of damage development following mechanical compression of the fiber in a localized area. At the moment of compression a strong local contraction could be observed at the point of injury, which transformed into an opaque irregular clot over a period of a few minutes. As time progressed, the clotted fiber contents retracted progressively, leaving a tube of empty sarcolemma at both sides of the center-clot which had formed at the point of injury. Also, regions at the perimeter of damage along the fiber gradually would lose their cross-striations, and retract more and more until the fiber was divided into a portion with intact cross-striation and unchanged diameter, regions consisting of clots with irregular diameters, segments occupied by empty sarcolemma tubes with reduced diameters and, finally, areas situated between normal and clotted regions characterized by an unchanged diameter and by granular disintegration of the cross-striation. The

spread of disorganization occurred at a declining rate and was essentially complete within an hour, although additional spread could be induced by stretching the fiber. The morphology associated with various forms of damage has been beautifully illustrated by Thoma (93).

A consideration of importance in addition to retraction zone morphology is that of sarcolemma ultrastructure in this region. The membrane has obviously not been completely disrupted mechanically, as it is still capable of transmitting significant loads (70). But the ultimate objective is knowledge of sarcolemma in intact cell regions, and it is therefore mandatory to know the comparability of normal and tube region membranes.

Pertinent electron microscopic data exists on this point (24). The plasma membrane and amorphous layer were seen to be still closely associated, although the integrity of the plasma membrane layer varied from appearing to be superficially intact through various degrees of disintegration. In some instances only remnants were present, leaving the amorphous layer as the only intact member of the continuous membrane phase. The two fibril layers appeared normal in ultrastructure. Regarding physiological activity, repeated attempts to demonstrate EMF and electronic responses have met with failure (24), although on occasion contractile activation can cross over empty tube regions (19, 45).

In spite of the lack of physiological activity, the empty tube region of retraction clots does seem to provide a reasonable model of normal cell membrane as regards structures thought to be involved in the mechanical properties. The mechanical properties of the sarcolemma are usually attributed to the two outermost fibril layers (19, 24). The measurements of the breaking stress of tube region membrane by Casella (70) showed that the scatter of such determinations was small. If marked disruption generally occurred in sarcolemma mechanical components during retraction zone formation, a wide range of values for breaking stress would be expected. Casella's evidence suggests, in contrast, that the tube region membrane is mechanically intact. Furthermore, a lack of significant mechanical contributions by the plasma membrane is implied.

Theoretical Construct

The general morphology of retraction zones was described in the previous section. This unique system provides an opportunity for characterization of the mechanical properties of the sarcolemma based upon a mathematical model involving a thin shelled cylinder under internal pressure. The literature does not offer evidence indicating that zone contents are truly fluid in nature. However, experimental data reported later in the present treatment confirm this assumption of previous workers. It is therefore appropriate to

introduce at this time a theoretical description of relevant model systems.

Consider a thin cylindrical elastic shell containing and surrounded by fluids under pressure (figure 8). We require that all sections of shell material taken perpendicular to the cylinder axis have the same thickness and elastic properties, i. e., that the cylinder is homogeneous. However, for generality we do not require that the material be isotropic, which implies that the elastic constants in various directions through an element of shell material do not have to be identical. We define P as the trans-shell pressure gradient, being the internal minus external pressure, and stipulate in addition that this gradient must be greater than zero. The segment of the cylinder under investigation is considered to be far removed from the actual ends of the cylinder so that end effects may be neglected. Static fluid systems are specified so that the pressure gradient across the shell wall is everywhere constant.

The following derivation is adapted from Burton (99). The internal and external pressures act everywhere at right angles to the wall of the cylinder. A unit length of tube has a surface area, A, of πD, where D is the diameter. The net force, F, tending to expand a unit length of cylinder in the radial direction is then given by

$$F = PA = \pi DP.$$

The force holding this expanding force in equilibrium per unit length

Figure 8. Diagramatic representation of the physics of a cylinder under internal pressure. The indicated equations are derived in the text. Symbols: A, area (cm^2); D, cylinder diameter (cm); R, cylinder radius (cm); P, excess internal hydrostatic pressure ($dynes/cm^2$); F, force (dynes); T_s, circumferential tension (dynes/cm); T_p, component of longitudinal tension (dynes/cm) due to pressure P. A, equilibration of forces in the circumferential direction. A cylindrical segment of unit length has an area πD and therefore is subjected to a pressure force πDP. This force is held in check by T_s. B, equilibration of forces in the longitudinal direction. The pressure force exerted longitudinally is equal to PA, where A is the cross-sectional area of the cylinder. The longitudinal pressure force is balanced by T_p.

A

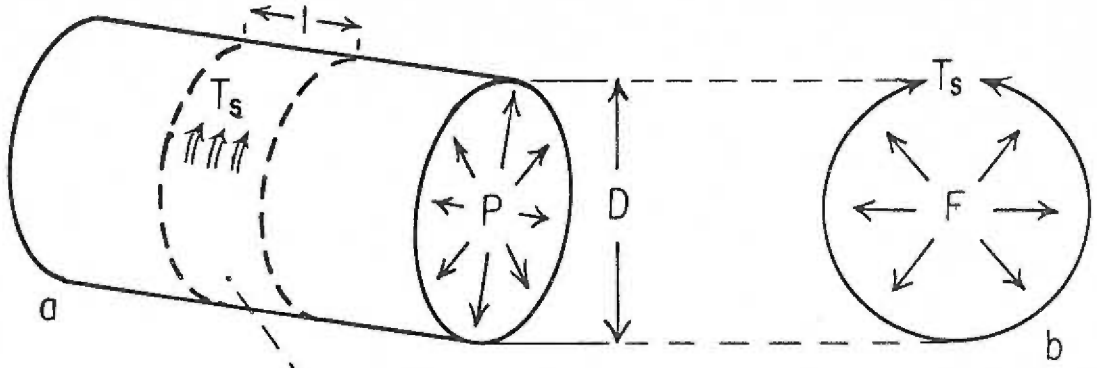

$A = \pi D \cdot l = \pi D$

$F = PA = \pi DP$

$T_s = PD/2$

B

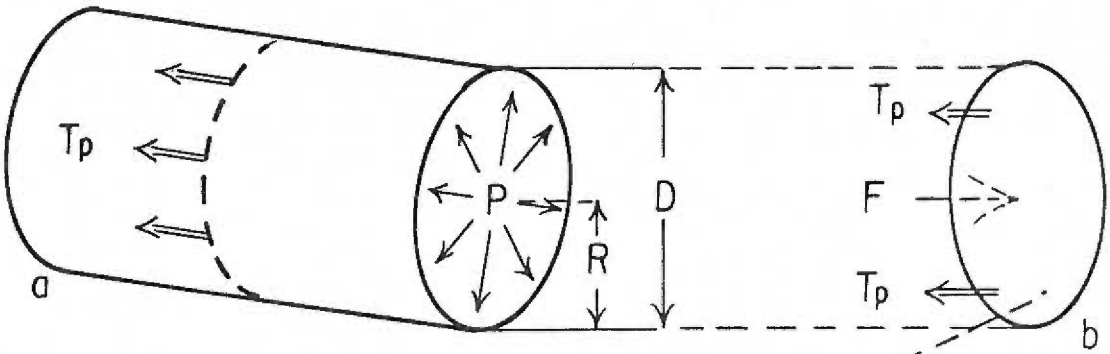

$A = \pi R^2$

$F = PA = \pi R^2 P$

$T_p = PD/4$

of the tube is the circumferential tension in the wall T_s.

By equating the expanding and restraining forces, a relationship is determined between the trans-shell pressure gradient P and the circumferential tension T_s. To do this the principle of virtual work is applied to the present system with the realization that T_s can be expressed either as force per unit length or as energy per unit area. The principle of virtual work states that if a small displacement is made from the equilibrium position, as increasing the tube radius from R to R + dR, the work done must be equal to the change in shell energy that would result. In such an expansion, the pressure will do work equal to 2 RPdR per unit length of tube resulting in an increase in shell energy of $2\pi T_s dR$ over this segment. Equating and making the substitution D/2 for R, we have

$$2\pi RPdR = 2\pi T_s dR,$$

$$T_s = PD/2$$

For equilibrium then, the circumferential tension must always equal one-half the product of the trans-shell pressure and the diameter.

In addition to the circumferential tension, there must also be a longitudinal tension in the wall of a cylindrical shell if it is to be in equilibrium with the trans-shell pressure. The total resultant of all pressure forces acting on the end of a central segment of a cylinder

is equivalent to the force that would be exerted on a plane partition at right angles to the cylinder axis and closing off one end. This force would be $\pi R^2 P$. If T_p is the longitudinal force in the wall per unit circumferential length, the restraining force over the wall cross-section is $2\pi R T_p$. Again equating expanding and restraining forces and substituting D/2 for R,

$$\pi R^2 P = 2\pi R T_p,$$

$$T_p = PD/4.$$

Comparison of the equations for T_s and T_p shows that for the particular case of cylindrical geometry the circumferential tension always equals twice the longitudinal tension in a tube subjected to internal pressure forces only. If the cylinder is also subjected to external loads along its axis, the resulting tension (force per unit circumference) in the cylinder wall adds to the pressure component T_p.

The above derivations are very simple and completely disregard any considerations of the properties of the material making up the wall of the cylinder. The same relationships can be derived beginning from the assumption that the shell material exhibits linear "stress-strain" characteristics. That is to say, the shell material is considered as the prime entity which reacts to external forces via internal stresses (force per unit cross-sectional area) and strains

(change of length per unit reference length). Such an analysis not only predicts the pressure-tension relationships described above, but also relates these quantities to the parametric elastic moduli describing the behavior of the shell material. Furthermore, additional information arises regarding end effects and geometrical changes under various load situations important to the present model. Such relationships appear from solution of the differential equations of the system, which requires the introduction of important boundary conditions. The assumptions and predictions of the theory of thin elastic shells as presented by Kraus (100) will therefore be discussed in detail below. The derivation of the equations describing the system will be omitted in the light of their meticulous treatment by this author and their great complexity.

In the three dimensional theory of elasticity, the fundamental equations occur in three broad categories. These categories consist of equations of motion obtained from a balance of the forces acting on some fundamental element of the medium, strain-displacement relations found from a strictly geometrical consideration of the process of deformation, and lastly the constitutive law of elasticity (Hooke's Law) which is introduced to provide a relationship between the stresses and strains in the elastic medium. The solutions of problems in three dimensional elasticity theory involve vast complications which have been overcome in only a few special cases.

One such special case involves elastic shells that are "thin", being analogous to practical situations in which the ratio of radius of curvature to shell thickness is 10 or more. The introduction of several simplifying assumptions including the requirement that the shell be thin has led to a subdiscipline within the theory of elasticity known as the theory of thin elastic shells. Predictions and assumptions of this latter theory for thin elastic cylindrical shells under internal pressure will now be reviewed.

The most basic assumption in thin shell elastic analysis is that the shell is thin. The actual implications of this assumption are specified more specifically in two additional restrictions. Normals to a reference surface chosen within the shell are required to remain normal to it and undergo no change in length during deformation. The assumption of the preservation of the normal implies that all of the strain components in the direction of the normal to the reference surface vanish. This further implies that there is no shear stress interactions between the normal and the plane of reference. A second assumption justified by the shell being thin is the neglect of normal stresses, since these forces have a negligible lever arm through which to act. The theory also depends on shell deflections remaining small so that all derivations and calculations can be referred to the original configuration of the shell, and, together with Hooke's Law, assures that the resulting theory will be a linear

elastic one. The shell substance is assumed to be homogeneous but is allowed to be orthotropic.

It will be noticed from the above discussion that only small deflections with linear stress-strain behavior are allowed. The sarcolemma does not meet either aspect of this assumption as will be shown later. Fortunately this fact does not negate qualitative predictions of material behavior from thin elastic shell theory. It implies, however, that quantitative estimates of certain boundary condition behavior are cautioned and parametric moduli cannot be generally specified as constants but must rather be qualified to the stress-strain-history state of the cylinder wall.

The pressure-tension relationships predicted by both thin shell theory and static considerations are relatively simple. However, they are also of limited validity, being true only when considering segments of cylinders far removed from boundaries or concentrated load points. The objective of the present analysis is to model retraction zones of single muscle fibers so that pressure-deformation data can be effectively evaluated. Obviously, retraction zone morphology as previously described is far from being representative of true cylindrical geometry. As a general rule, retraction zones show a curved longitudinal contour, although in especially long zones the central region is seen to be cylindrical for long distances while being curved only near the ends (see Results section). It will presently be

shown that this phenomenon is typical of thin elastic cylindrical shells under internal pressure if bending resistances are included in evaluating shell behavior and if edge loads are present at the ends. This is a reasonable model of retraction zones as the clots which form at either end of the empty tube segment are of much larger diameter than normal fiber regions implying that significant radial stresses are present at these points. The additional considerations of bending resistance and edge loading do not change the equations presented above in any way except in shell regions approaching boundaries or points of concentrated loads.

Applying the above considerations to the differential equations describing shell elastic stress and strain relations leads to some very pertinent results. The net effect of adding boundary conditions and edge loadings in addition to pressure-dependent relationships is to introduce distortions of the previously presented equations as retraction zone ends are approached. Such distortions are common to all shells regardless of the nature of the shell material. The finite range of shell regions near ends where such distortions are present is a function of particular system parameters. Thus for a homogeneous orthotropic thin elastic cylinder under internal pressure with end effects manifest, a decay length can be defined which represents the distance from a particular end at which end effect disturbances have fallen to about 4% of their maximum value. Specifically, this

decay length L_c is given by the expression

$$L_c = \pi \left[\frac{a^2 h^2}{3(1 - \nu_{xs}\nu_{sx})} \cdot \frac{E_x}{E_s} \right]^{1/4}$$

where . . .

L_c = decay length (cm),

a = cylinder radius (cm),

h = shell thickness (cm),

ν_{xs} = Poisson's ratio relating the effect on longitudinal strain of circumferential stress (cm/cm),

ν_{sx} = Poisson's ratio relating the effect on circumferential strain of longitudinal stress (cm/cm),

E_x = elastic modulus in the longitudinal direction (dynes/cm^2),

E_s = elastic modulus in the circumferential direction (dynes/cm^2)

for the above model. Thus, it is seen that the decay length is a function of the radius, thickness, and elastic properties of the cylinder. It must be remembered that in considering retraction zones we are not justified in applying equations such as this quantitatively. However, the qualitative prediction of the presence of end effects and the resulting distortion of purely pressure dependent behavior is not impaired.

For the present analysis, it is therefore necessary to establish criteria for the use of retraction zones. Depending on the membrane elastic parameters and retraction zone length, it is possible that

boundary conditions from the two zone ends may overlap in central membrane areas. The evaluation of pressure-dependent data free from end effect distortions implies the use of retraction zones long enough to contain central cylindrical regions responding purely to internal pressure in the circumferential direction. Boundary effects are signaled by geometrical disturbances, most obviously by an increase in diameter. Thus a reasonable criteria would be to use only those zones which possess definite cylindrical central segments, with all geometrical measurements being restricted to this central region. Such zones are less common than ones possessing finite longitudinal curvature throughout their length, but do exist as shown in the Results section.

Experimental Design

The preceding section describes the predictions generated from a mathematical model system anticipating retraction zone morphology. The theoretical development is of a very general nature indeed as a minimum of assumptions were introduced. Although the shell material is required to be homogeneous so that similar stresses in different membrane elements results in similar strains, the shell material is allowed to have different elastic properties in various directions, and is considered dependent upon boundary conditions and arbitrary loadings through wall bending

resistances as well as normal elastic properties. General retraction zone behavior appears to closely follow qualitative predictions of the model, and by analogy it may be argued that parameters found to be of importance in the model are also active in the sarcolemma. Through morphological studies, many important internal forces and torsional interactions of the membrane can therefore be qualitatively assessed.

Pertinent quantitative information is also accessible, although the number of experimental parameters that can be quantitated during forced distortions of retraction zone membrane are limited. It is very fortunate that the derivations of characteristic equations governing shell behavior lead to surprisingly simple results for certain special cases. Thus if length and diameter changes can be correlated with determinations of the trans-membrane pressure difference and the external load borne by muscle fiber in central cylindrical segments of long retraction zones, this limited data provides a powerful tool for assessing mechanical properties of the membrane. These length, diameter, pressure and force measurements provide sufficient data to characterize the force-extension relationships of the shell material independently in both the longitudinal and circumferential directions. The characterization completely describes the behavior of the shell material within the stress limits investigated, provided the cylindrical geometry is maintained.

The empty tube regions of muscle fiber retraction zones thus offer an excellent system for mechanical investigations on the sarcolemma, provided the criteria for avoiding end effect distortions are honored.

To provide the proper data for membrane characterization, therefore, length and diameter measurements must be correlated with internal zone pressure under conditions in which external longitudinal loads can be quantitated and under controlled conditions of environmental pH, temperature, and medium substrate content. To insure freedom from restraints imposed by neighboring cells, single muscle fibers are used, and to enable maximum correlation with previous work the frog semitendinosus is the muscle of choice. Internal hydrostatic pressure in the zone can be controlled by inserting a micropipette, the lumen of which is thereby made continuous with the empty tube region interior and pressure generating, recording, and calibrating equipment. Since high optical magnifications are required for pipette insertion and geometrical measurements, the experimental chamber employed must be adapted for attachment to a microscope stage to allow high power viewing and chamber positioning. Direct mechanical measurements should be supplemented with morphological studies of retraction zone behavior to see if membrane properties are compatible with the model system.

Several important aspects of the proposed experiment should be examined in control experiments. It is reasonable to assume that

under increased internal pressure retraction zones may leak, thereby jeopardizing pressure recordings. Some estimate of the magnitude of leakage and its effect on pressure quantitation should be attempted. Further experimental controls should include tests of preparation reliability and studies indicating whether or not retraction zone membrane is a reasonable mechanical model of the sarcolemma in normal fibers.

Certain features of data interpretation have been mentioned. The main experimental objective was the determination of particular mechanical properties of the sarcolemma in retraction zones. It will be shown that the observed mechanical properties can be most logically explained in terms of a fibrous network, composed of individual elements having a specific force-extension relationship and geometrical arrangement. The implications of the proposed structural hypothesis regarding the known functional properties of single muscle fibers will be discussed.

MATERIALS AND METHODS

Acquisition and Housing of Frogs

Summer frogs (Rana pipiens), three to four inches in body length, were obtained from a local biological outlet and used throughout the study. The animals were native to Sinaloa, Mexico, where environmental temperatures of 50-100°F prevail. They were therefore not refrigerated but rather housed at room temperature in the laboratory, retained in a plastic tub with a wire mesh lid. The housing tub was inclined to allow the animals a choice among a pool of fresh water, a dry area, and a region of moist moss.

The first animal to jump in response to partial removal of the housing tub lid was selected for an experimental procedure. Not all acquired animals were used, as those deemed "unlively" or showing symptoms of the disease "red leg" were discarded.

Isolation of the Semitendinosus Muscle

The experimental animals were rendered unconscious by a sharp blow to the head, decapitated, and their spinal cords were pithed. They were then placed supine, ventral side up, in a large petri dish, where the muscle isolation procedure was performed after allowing a few minutes for random muscle contractions induced by pithing to subside.

Muscle isolation was initiated with a skin incision along the full length of the ventromedial aspect of the upper leg, followed by section of the knee attachments of the exposed Satorius, Adductor magnus, and Rectus internus major and minor muscles. These muscles were freed from underlying tissues by blunt dissection as far proximally as possible, thereby exposing the medial and lateral heads of the Semitendinosus. The medial head of the Semitendinosus was then removed from the animal by sequentially cutting the proximal tendon, associated connective, nervous and circulatory tissue as the muscle was reflected distally and, finally by section of the distal tendon insertion and the lateral head of the Semitendinosus. The isolated muscle was thoroughly washed with Ringer's solution (Table I) and placed in Ringer's for storage in the refrigerator.

The Semitendinosus muscles from both legs were isolated to provide a spare muscle for fiber isolation. During the muscle isolation procedure, Ringer's solution was applied frequently to exposed tissues to prevent drying. The same Ringer's medium was used for all preparatory, storage, and experimental procedures, and was identical to that employed by Ramsey and Street (25) augmented with 100 mg% glucose. The isolated muscle was stored overnight at 2-4°C before an experiment.

TABLE I

Modified Ringer's solution composition (after Ramsey, et al., with glucose added).

NaCl	6.5 grams/liter
KCl	0.20 grams/liter
NaH_2PO_4	0.23 grams/liter
Na_2HPO_4	0.87 grams/liter
$CaCl_2$	0.20 grams/liter
Glucose	1.00 grams/liter
Na^+	130.5 mEq/liter
K^+	2.7 mEq/liter
Ca^{++}	2.8 mEq/liter
	136.0 mEq/liter
Cl^-	121.0 mEq/liter
$H_2PO_4^-$	1.9 mEq/liter
$HPO_4^=$	12.2 mEq/liter
	136.0 mEq/liter
pH	7.3

Isolation of Single Muscle Fibers

Individual fibers were isolated from the muscle in a small chamber (figure 9-A) containing provisions for fiber mount and temperature control of the Ringer's medium. Coils embedded below the dissection chamber were connected to a system maintaining a rapid circulation of ice water (figure 9-B), permitting the temperature in the isolation compartment to be maintained at 3-4°C. The cold temperature prevented an undue rate of fiber deterioration that otherwise occurred, probably in response to metabolites released by damaged tissue.

After activation of the temperature control system, one muscle was removed from refrigerated storage and mounted in the dissection chamber in such a way that small fiber bundles were exposed for isolation. The muscle was fixed at an extremely slack length by pinning the tendons, carefully pulled apart under lateral traction, and held as a thin rectangular sheet by appropriate placement of dissecting pins. In this manner the tendon, which takes the form of a sheet as it enters the muscle normally, was retained in a lateral orientation. This procedure greatly facilitated fiber exposure, as individual fiber terminations were thereby extended over a wide lateral plane, rather than in their accustomed oblique and staggered fashion for some distance along the muscle axis.

Figure 9. A, Photograph of the dissection chamber. Petri dish (a), serving as the chamber proper, is embedded in dental acrylic (b) contained in a metal film case (c). The petri dish rests on coils embedded in the dental acrylic (not shown), permitting temperature control of chamber contents. The preparation is mounted on an elevated plate (d), perforated to allow fluid circulation and access of mounting pins to the underlying silastic rubber layer (e) in the bottom of the chamber. Three irregular holes cut from the silastic layer allow more efficient heat exchange with coils. Small cup (f) is used for transport of an isolated fiber to the experimental chamber.

B, Photograph of the dissection apparatus. The dissection chamber is connected through tubing to a stainless steel reservoir. The reservoir rests in a plastic tub, which is packed with ice during an experiment. Water contained in the reservoir is thereby maintained at 0°C, and is circulated through the experimental chamber encasement by a Bronwill Constant Temperature Circulator, extending into the reservoir from external mounts. Microdissection is aided by a Bausch & Lomb dissecting microscope, model SKVB-73.

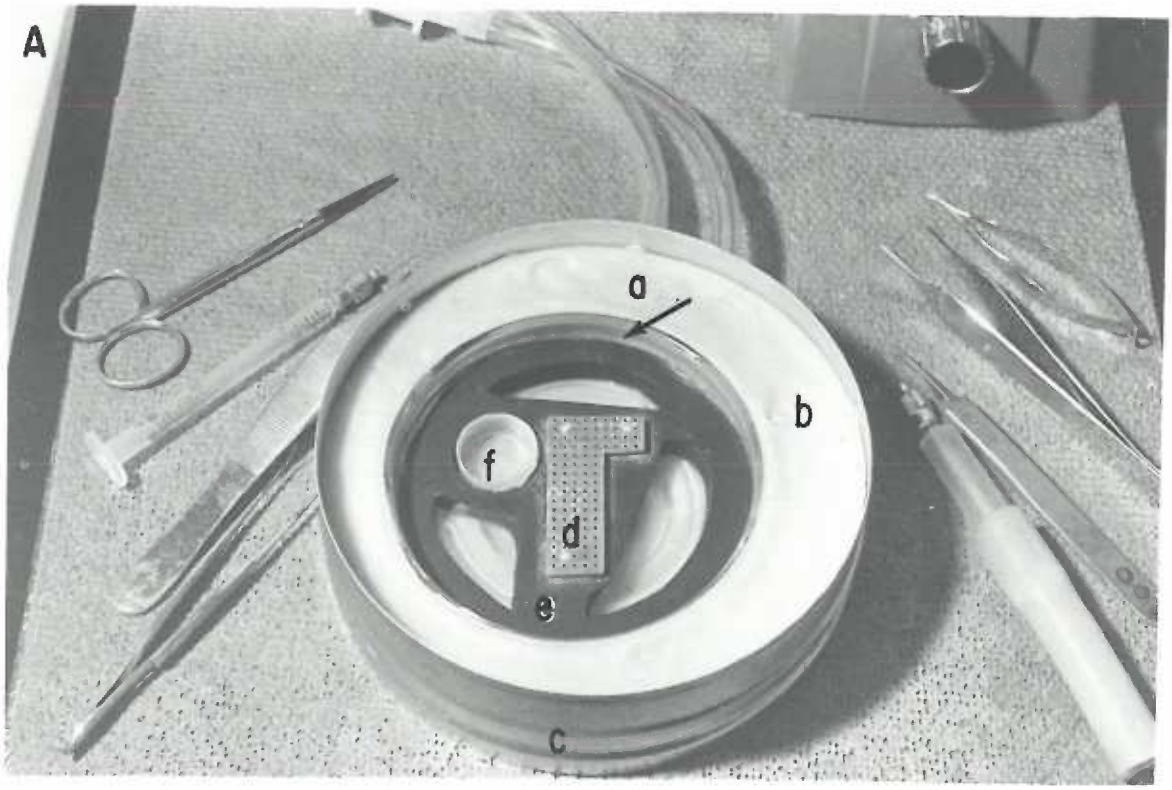
A
a
b
c
d
e
f

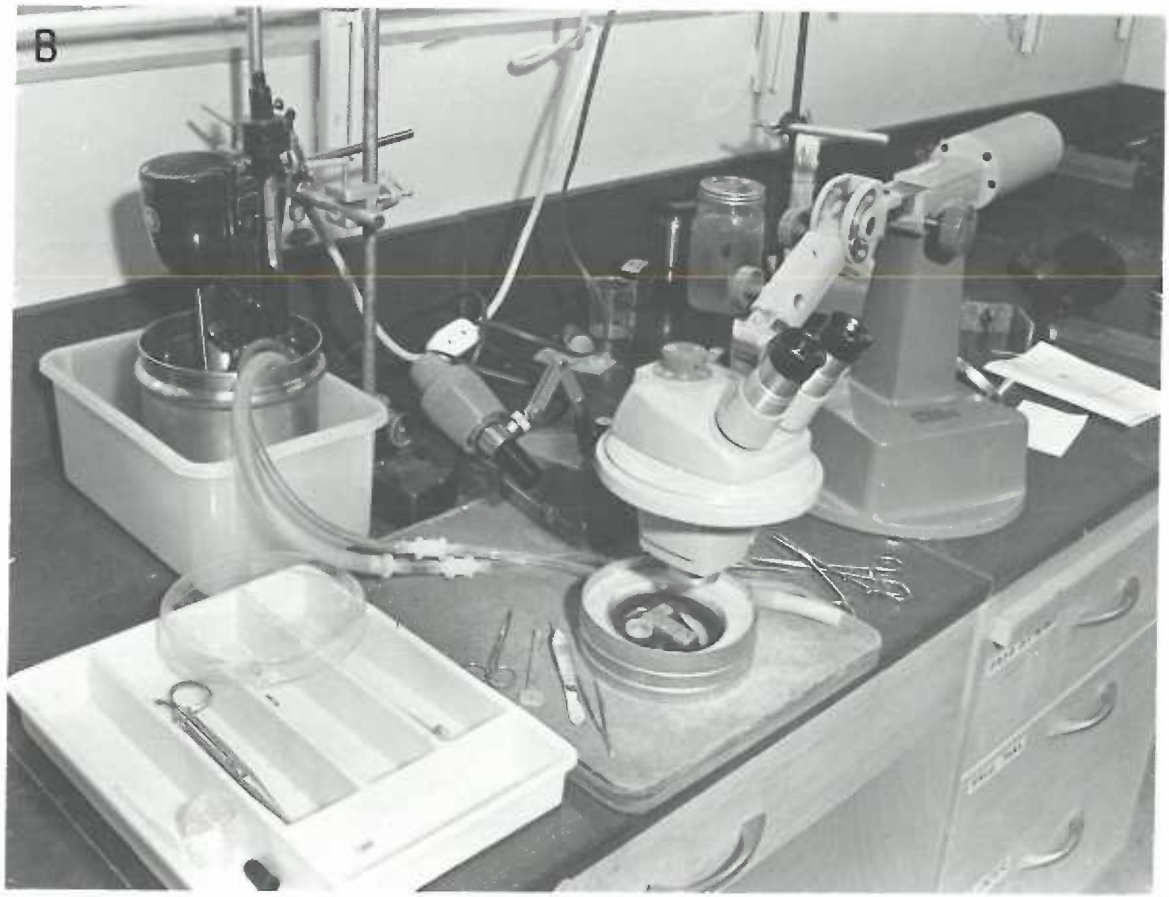
B

Further dissection was accomplished with the aid of a dissecting microscope at 20-40X magnification. Single fiber isolation was initiated by clamping the tendon sheet on the side opposite to the attachment of a small selected bundle of fibers, followed by freeing of this tendon area and the attached fibers from their neighboring tendon and bundles. The retained bundle was freed from other bundles for approximately half its length to the region of nerve entry. The exposed fibers were cut midway between tendon and nerve with longitudinal traction applied to progressively reduce bundle cross-section. It was not found necessary to dissect the severed fibers from those remaining, because the divided fiber became free of the major portion of the remaining bundle. Fiber sectioning was continued until one fiber remained. The broken fibers were cleaned from both the tendon and nerve ends of the fiber with dissecting scissors, and the original bundle was cut just past the nerve. A bundle of cut fibers, firmly interconnected with connective tissue associated with the nerve, was thereby retained at the nerve end of the fiber segment to serve as the mounting terminal on the fiber end opposite the tendon.

This procedure allowed a long segment of a single fiber to be isolated very rapidly (5-10 minutes) without the necessity of contacting the final fiber with dissection instruments. Occasionally, it was found necessary to tease apart small bundles of 2-5 fibers for short distances to allow entry of the dissecting scissors. Small syringe

Figure 10. A, Photograph of the experimental chamber. Coordinate and descriptive axes are indicated, relative to the orientation of the chamber on the microscope in the experimental situation. The chamber proper (a) is an L-shaped compartment, 1.2 cm deep, with provisions for inflow and outflow of fluid (clamped tubes). Each of the two stainless steel wires (b) and (c) extending into the chamber is connected to an independent micrometer drive, indicated as (d) and (e) respectively. The left (front) extension arm (b) also contains a strain gage element (f) lying in the x-y plane. The associated wiring runs to a connector mounted on the binding post.
B, Photograph of the experimental chamber mounted on the microscope. The experimental chamber (a) locks into a chamber holder (b) replacing the microscope stage slide clamp, permitting control of chamber position with the stage controls (c) and (d) relative to the objective lens (e). The strain gage (f) is connected via wiring to a cable socket (g) mounted on the same binding post as the micrometer drives. (h) and (i) are the fiber support arms. Coordinate and descriptive axes are indicated.

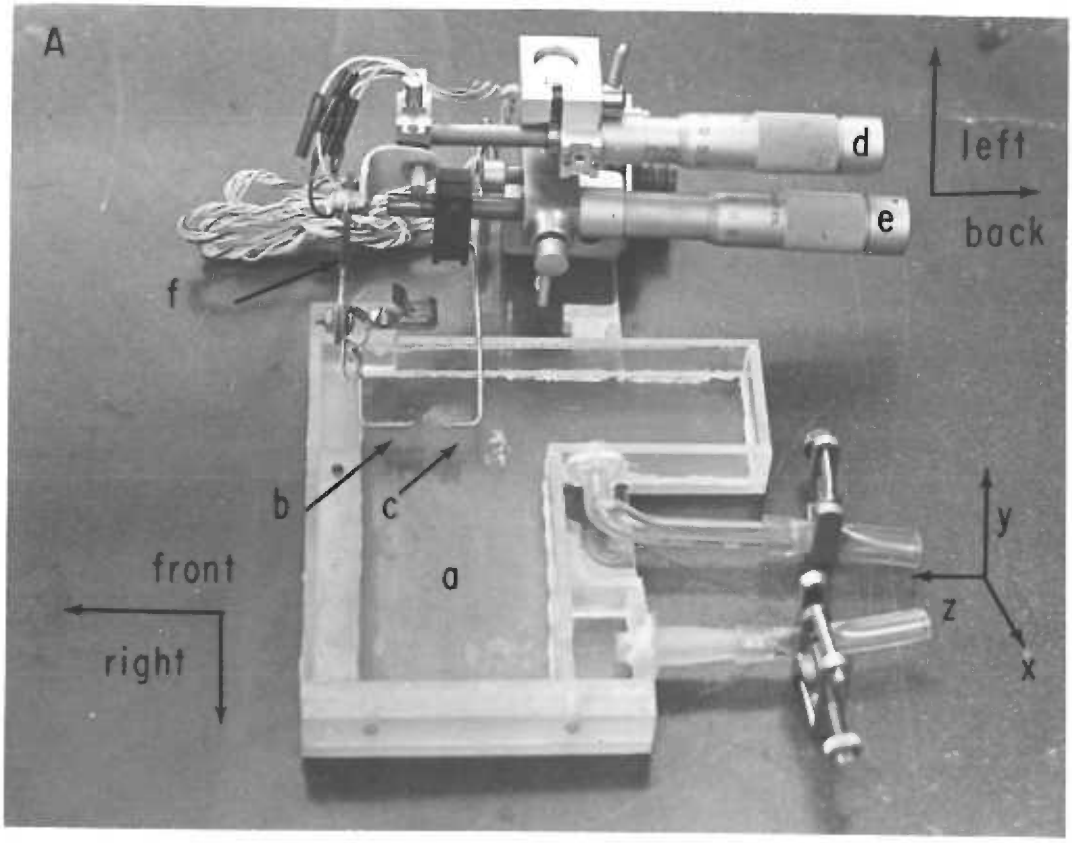
A
d
e
f
b
c
a
left
back
front
right
y
z
x

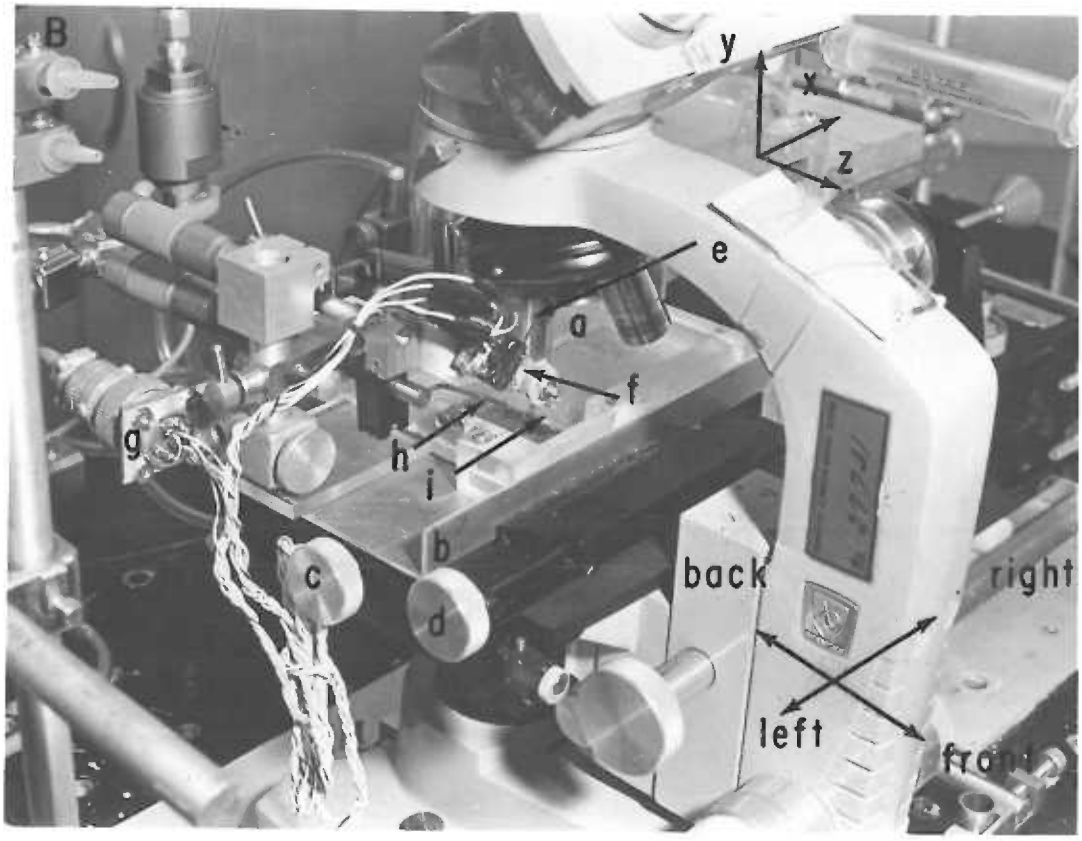
B
y
x
z
e
a
f
g
h
i
b
c
d
back
right
left
front

Figure 11. Fiber mounting apparatus in the experimental chamber. Minute rubber bands (a) clamp the terminal tufts (b) of an isolated fiber segment (c) to the stainless steel extension arms (d). The position of the mounted fiber as it is situated during the conduct of an experiment is indicated with respect to the chamber baseplate, surface of the fluid (e), micrometer drive assemblies, the objective lens (f), and the coordinate and descriptive axes.

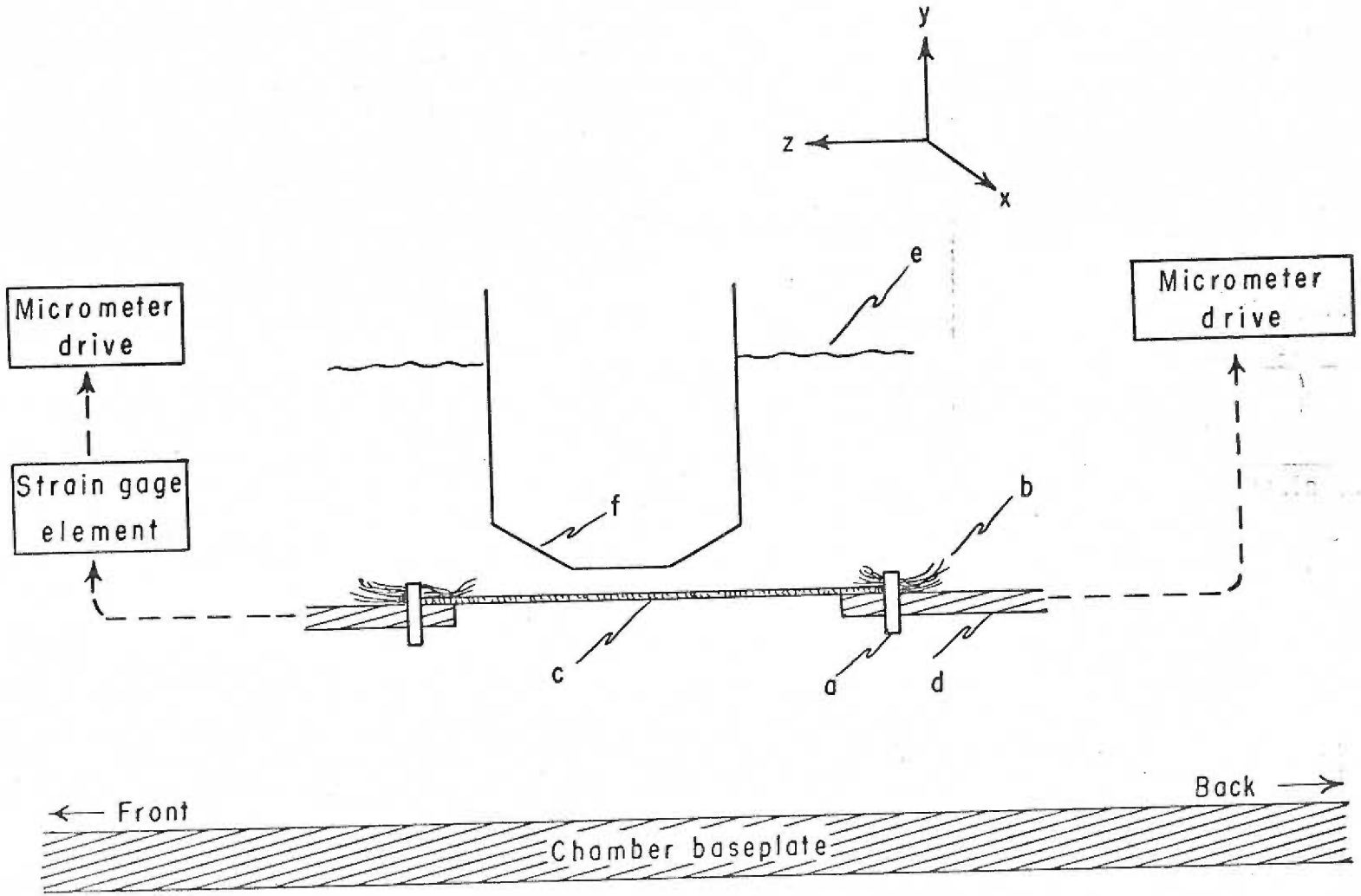
y
z
x
Micrometer drive
Strain gage element
Micrometer drive
e
f
b
c
a
d
Back
Front
Chamber baseplate

These directional definitions are indicated diagrammatically in photographs of the chamber alone (figure 10-A) or mounted on the microscope (figures 10-B, 12), and in the diagram of the mounted fiber (figure 11). The experimental chamber (figure 10-A) is oriented on the microscope such that the two micrometer drives are to the left of the chamber proper when viewed by the experimenter sitting in front of the microscope (figures 10-B, 12), and control movement in the front-to-back direction (parallel to the z axis). The fiber is mounted near the left side of the chamber, midway between the chamber baseplate and the surface of the solution. The chamber, when mounted on the microscope, can be positioned with the stage controls so that the fiber axis intersects the vertical optical axis of the microscope, the latter being parallel to the y coordinate axis. The large expanse of open chamber to the right of the fiber provides space for a micropipette to be horizontally oriented parallel to the x axis, and therefore perpendicular to both the fiber and the optical axis of the microscope.

The experimental chamber was locked into a special holder in place of the microscope stage slide clamp, allowing control of fiber position relative to the objective lens along all three coordinate axes. The objective employed was a Cooke-Baker 40X air lens (NA 0.7) which had been waterproofed for use in Ringer's solution by applying calking material to all glued junctions. Access of substage

Figure 12. Photograph of experimental apparatus. Note the indicated co-ordinate and descriptive axes. A Leitz micromanipulator (a) controls pipette position via an extension arm (b) extending into the experimental chamber (c). All equipment rests on a plate (d) covering a concrete weighing table (e). The microscope rides on a small platform supported by roller bearings (f) and moved by a rack-and-pinion device (g) along the z axis. The pressure generating syringe with the bolt drive removed (h) and the pressure transducer (i) can be seen in the background.

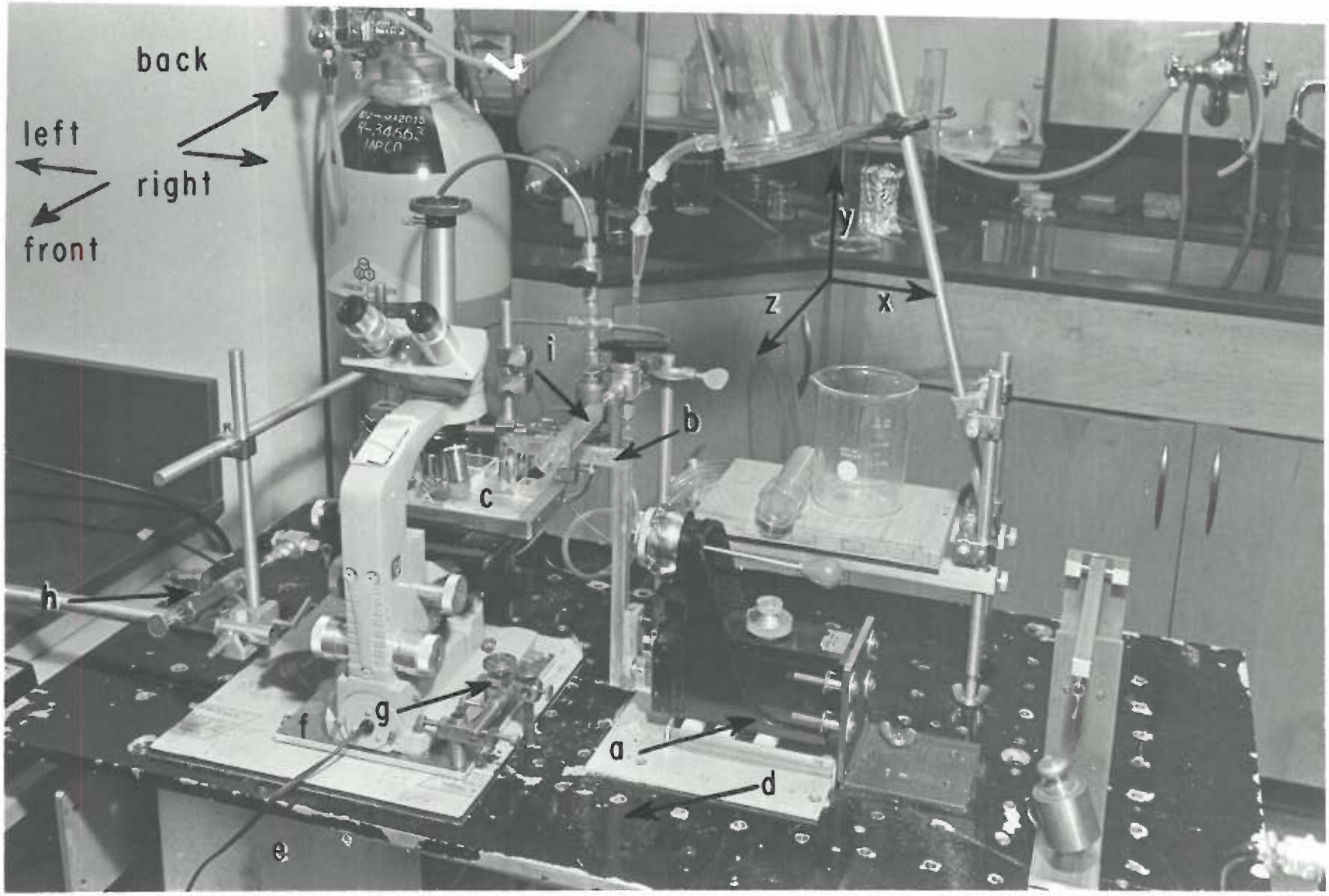
back
left
right
front
y
z
x
i
b
c
h
f
g
a
d
e

illumination to the preparation was provided through a hole cut in the chamber holder and by virtue of the transparency of the plexiglass baseplate of the chamber.

Mention was made above to the fact that a micropipette, oriented parallel to the x axis, could be brought into the open expanse of chamber to the right of the fiber. The position of the pipette was controlled by use of a Leitz micromanipulator (figure 12) lying on its side. This particular manipulator was selected for its extremely fine movement in one direction, and had to be laid on its side to orient this fine movement perpendicular to the fiber axis. Operation of the unit in this position required fixation of the manipulator base relative to the benchtop and support of its movable outer housing by teflon rollers. The manipulator also provided coarse control of pipette position along the y axis, but had no provision for motion parallel to the z coordinate. The latter degree of freedom was gained by placing the microscope on a platform supported by roller bearings and propelled along the z axis by a rack-and-pinion device.

The microscope and micromanipulator rested on a large metal plate fastened through a layer of viscous putty to a concrete weighing table (figure 12). The resulting complex proved to be relatively resistant to building vibrations and consequent independent mechanical reactions of experimental components encountered with earlier arrangements.

Induction of Fiber Damage

Usually, no morphologic derangements were apparent in the isolated fiber segments. After preliminary examination and measurements, acceptable fiber segments were damaged in a mild and controlled fashion by compression between two micropipette barrels in an attempt to induce the formation of retraction zones. The procedure was accomplished with the fiber mounted in the experimental chamber on the microscope. One micropipette was usually fixed in the Leitz micromanipulator while the second was held by hand.

The site of damage along the fiber segment could be preselected by the following procedure. The entire length of fiber segment was examined and a site selected. A micropipette under micromanipulator control was then brought into the field of view and positioned such that it lay under the fiber at exactly the position selected for damage. The objective lens was swung out of the way, and with the unaided eye the micropipette was raised with the micromanipulator until the fiber was slightly elevated. A second micropipette held by hand was then carefully laid against the first, gently compressing the fiber. Both pipettes were rapidly removed and the objective lens swung back into the optical axis. The site of damage could then be observed in the field of view. The apparent nature of retraction zone formation is presented in a later section.

Force Measurements

The force borne by the fiber during experimental manipulations was recorded by a sensitive strain gage, installed as a component of one of the fiber support arms (figure 10-A). The force transducer was connected to a Grass (model 5) polygraph. General drift of the recording system was minimized by a warm-up period of 24 hours. A consistent linear drift of baseline, not of polygraph origin, was also noted during the conduct of experiments. Prior to carrying out the experiment, the micrometer drive assembly containing the strain gage element was removed from the chamber and transported to another portion of the laboratory where force calibration was accomplished (procedure described below). Following calibration, the unit was returned to the experimental chamber. It was felt that the linear baseline drift of the force recording was related to this prior change in environment of the strain gage element. It may have been due to a thermal effect of long time constant, possibly the result of uneven heating of different sides of the transducer by the microscope lamp. Force measurements were therefore corrected for a linear drift of baseline during the experimental period by noting the terminal discrepancy, usually about 4 mg after 2 hours.

The force transducer was calibrated by applying known forces along the axis of the terminal portion of the support arm of which the

strain gage was a part, thereby duplicating the experimental situation. It was inconvenient to carry out this procedure in the experimental chamber. Rather, the micrometer drive assembly containing the strain gage was removed from the chamber, mounted in a separate portion of the laboratory, and reoriented so that the terminal segment of the support arm was vertical and pointing downward. The force transducer was calibrated by hanging known weights from the site where the muscle fiber was clamped experimentally.

A calibration curve for the force measurement system is presented in figure 13, demonstrating that the system is linear to within better than 1% of full scale over the range 0-500 mg. This is of sufficient range to cover the experimental values, and to insure that the small gravitational effects introduced by the difference in strain gage orientations during experimental and calibration periods could not affect the accuracy of the calibration.

Pressure Control and Measurement

The hydrostatic pressure inside of retraction zones was controlled by the pressure in a closed external system communicating with the zone interior through the lumen of a micropipette. The pressure system is schematically depicted in figure 14, and can be seen basically to consist of four sidearms joined at a common point. The functions of pressure generation, measurement, calibration and

Figure 13. Calibration curve of the force recording system. Abscissa is force applied to the fiber mounting clamp and ordinate is mm pen deflection (sensitivity 0.1 mv/cm) on the polygraph paper. Each plotted point is the mean of at least three readings, the scatter of which was included in the dot outline.

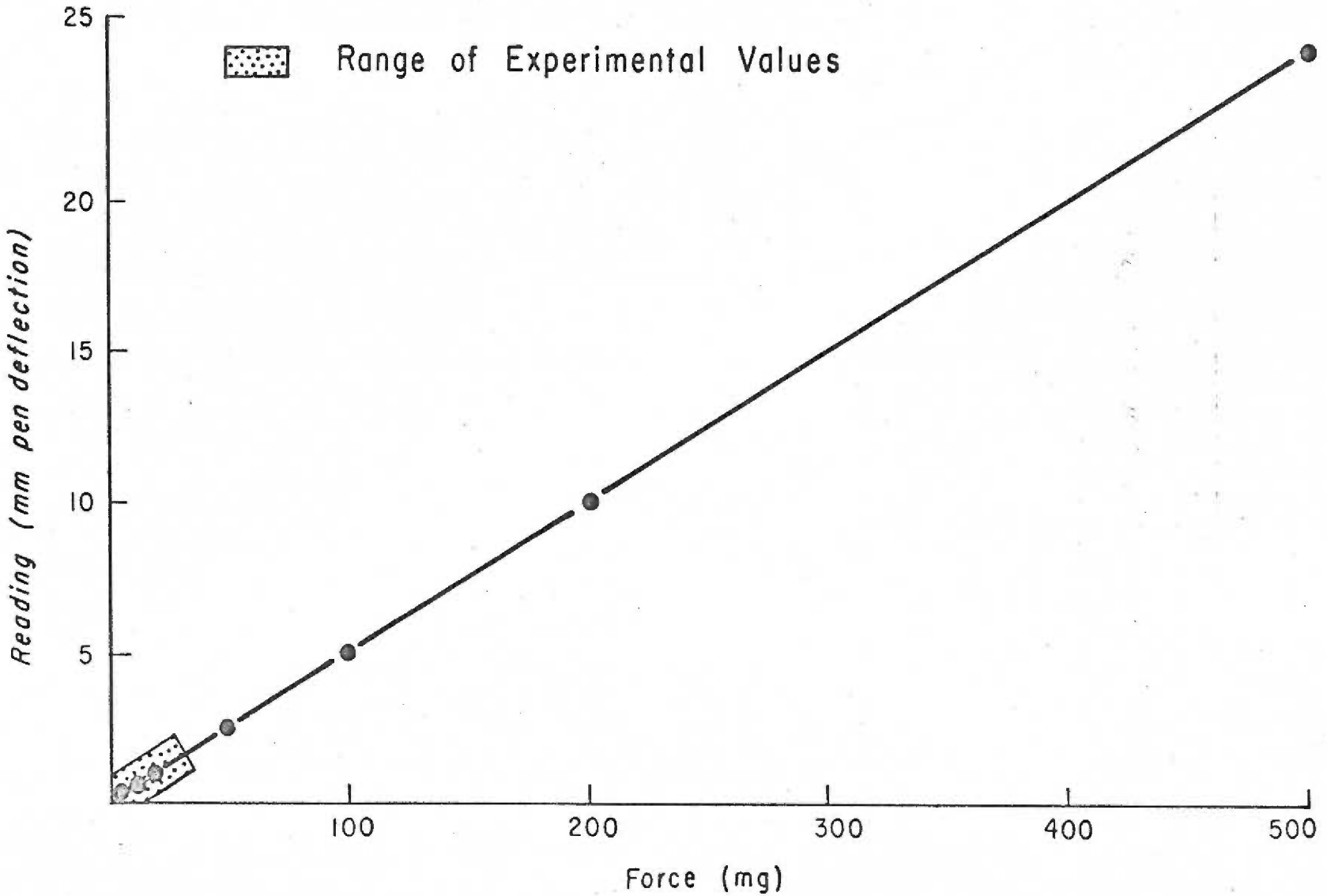
Range of Experimental Values
Reading (mm pen deflection)
25
20
15
10
5
100
200
300
400
500
Force (mg)

Figure 14. Schematic diagram of the pressure system. A, the pressure generation arm, showing a rigidly mounted syringe (a) whose plunger (b) is driven by a bolt drive (c). Bubble (d) is introduced for system compliance. B, pressure calibration arm, connected to main system through valve (e). Pressure in the main system, acting through the plunger of a tuberculine syringe (f), applies torques to weights (g) suspended from a pivot (h). (See Appendix I). C, pressure transmission arm, showing flexible length of polyethylene tubing (i) connecting main system to pipette (j). Pipette is held by spring clamp (k) and positioned with a micromanipulator (l) relative to the preparation (m). D, pressure recording system, showing the pressure accessory (n), diaphragm (o), and universal transduction cell (p). The signal output of the transduction cell is recorded using a Grass model 5 polygraph (q), which produces a permanent chart record (r).

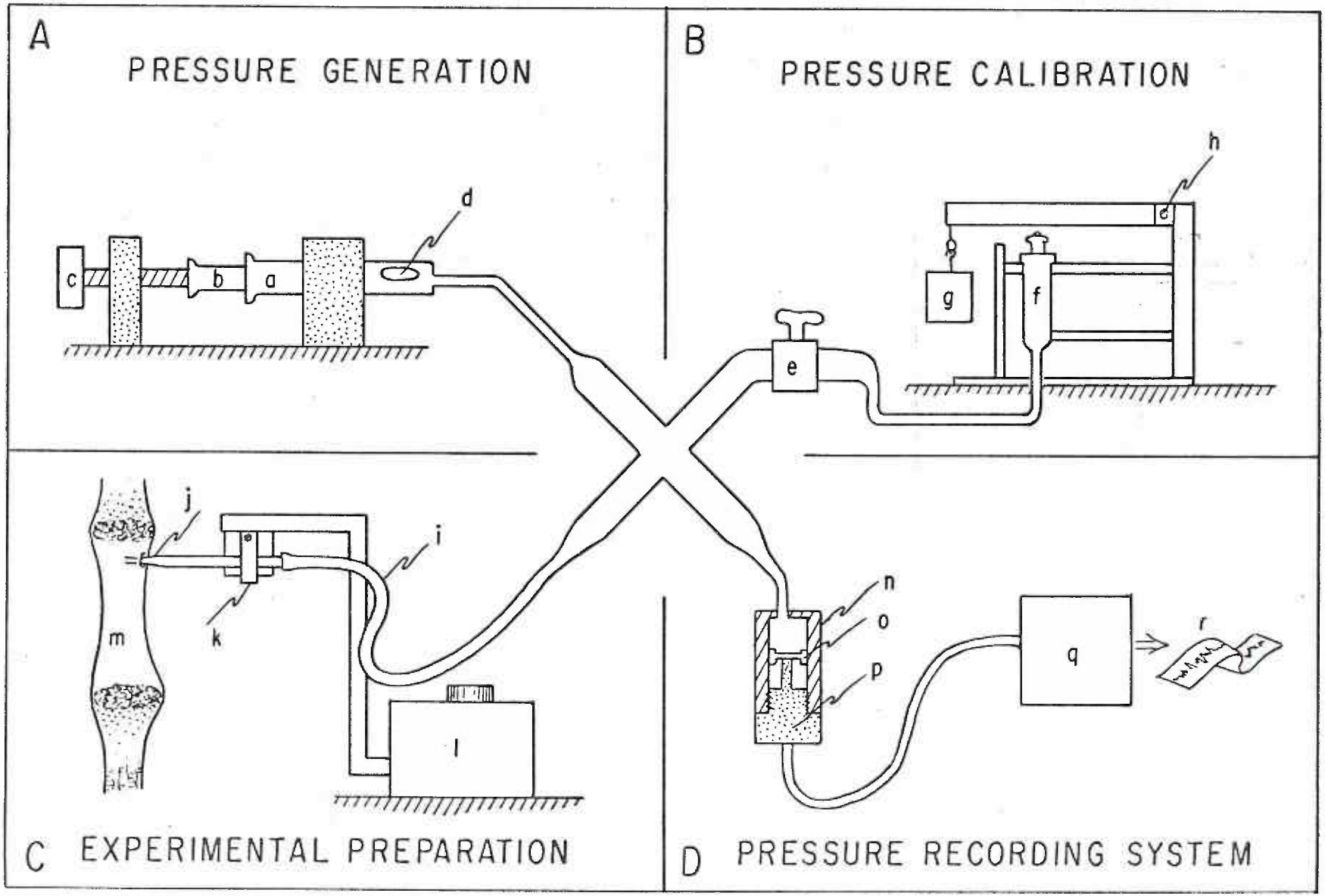
A
PRESSURE GENERATION
B
PRESSURE CALIBRATION
a
b
c
d
e
f
g
h
i
j
k
l
m
n
o
p
q
r
C EXPERIMENTAL PREPARATION
D PRESSURE RECORDING SYSTEM

transmission to the retraction zone are relegated to different arms. The pressure system is composed for the most part of components capable of withstanding high pressures. All lines were 1/4" O. D. copper tubing, connecting high pressure Whitey valves serving as control points, and syringes adapted for pressure or fluid volume control. All unions were made with Swagelok tube fittings, excepting those to syringes which required specially designed junctions. Such a rugged system was necessary due to the high pressures (10^4 mmHg) required to deform retraction zones over a significant range of diameters. The only flexible element was a 6" length of polyethylene tubing (Intramedic, PE 240), 0.095" in outside diameter, required to connect the micropipette to the pressure system.

The pressure system contained two oiled syringes, one in the generation arm and one in the calibration arm. In the generation arm (figure 14-A), the syringe barrel was rigidly mounted, and system pressure was controlled by varying plunger penetration (see figure 12). Pressure system compliance was determined by the size of a small air bubble introduced into the syringe. For calibration, a valve normally isolating the calibrating arm was opened, allowing pressure in the main system to act on a syringe plunger of known cross-section to lift standard weights (figure 14-B). This special calibrating device was required because the unusually high pressures made the use of a mercury manometer (30 feet tall) impractical.

The construction and theory of operation of the calibrating device are discussed in Appendix I.

The pressure measurement arm (figure 14-D) terminated in a Statham UGP4 pressure accessory containing a UGP4 - 200 diaphragm (limit 10^4 mm Hg). Diaphragm distortion was sensed by a Statham UC3 universal transduction cell to which the pressure accessory was adapted. This pressure monitoring system had a working range comparable to that employed experimentally. The signal output was recorded using another channel of the Grass model 5 polygraph employed in force measurements.

Figure 15 is the calibration curve of the calibrating device and recording system combination. It can be seen that the behavior is linear within a scatter of approximately 3% of the maximum pressures employed experimentally.

Dimensional Measurements

Dimensional measurements such as retraction zone length or central diameter, fiber diameters, striation spacing, and membrane mark separations were made visually and recorded as eyepiece micrometer divisions. Two eyepieces of different magnifications (5X, 18X) were used simultaneously in the microscope to permit rapid measurements at differing powers. Each eyepiece contained a micrometer disc which was calibrated against a stage micrometer.

Figure 15. Calibration curve of the pressure recording system. Abscissa is pressure applied to the tranducer diaphragm and ordinate is mm pen deflection (sensitivity 20 mv/cm) on the polygraph paper. Five readings are indicated at each of the six values of pressure, with a straight line drawn through the origin and the mean of points at the highest pressure. The pressures employed experimentally covered most of the calibration range.

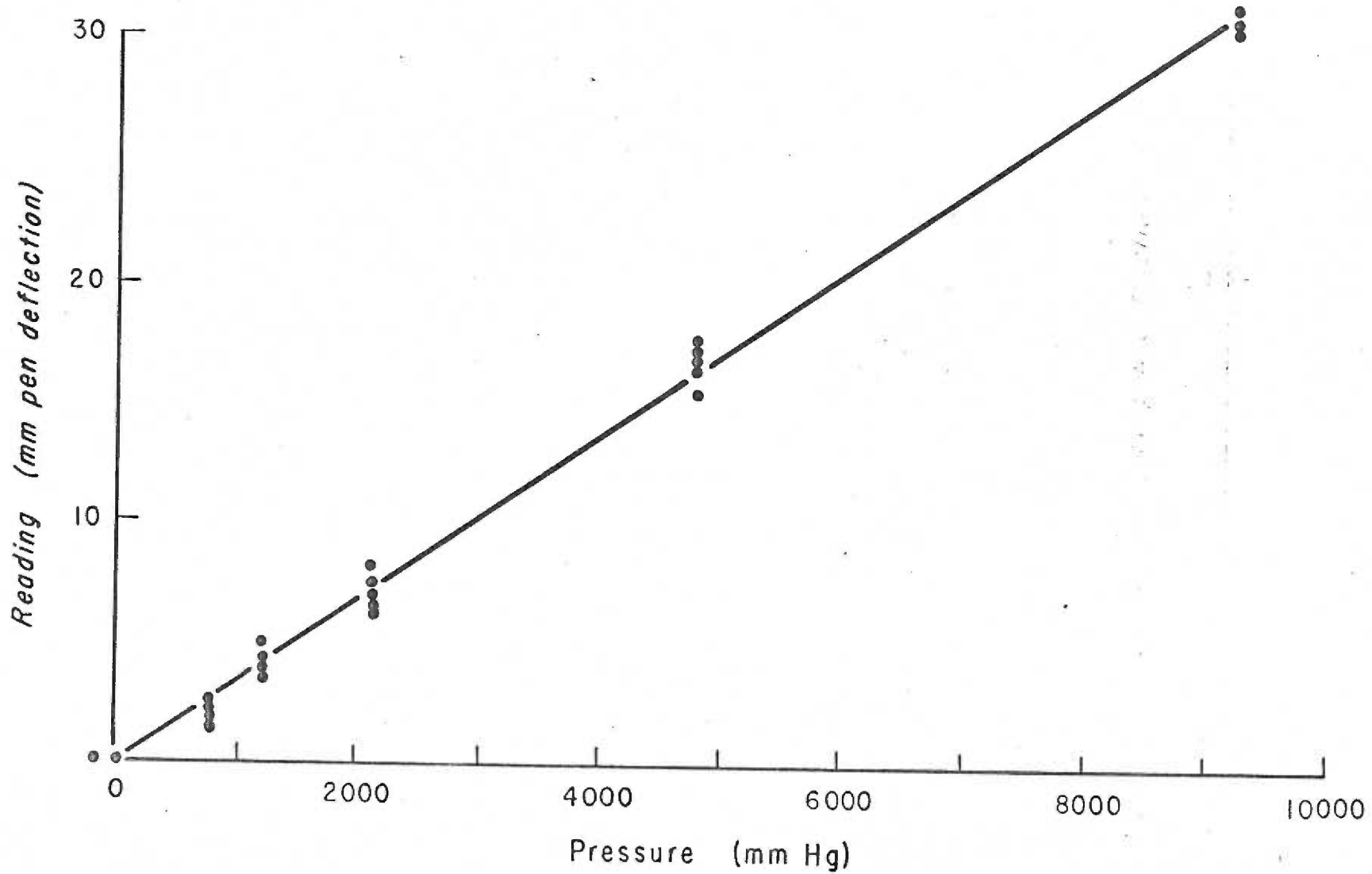
30
20
10
0
2000
4000
6000
8000
10000
Reading (mm pen deflection)
Pressure (mm Hg)

The objective and micrometer were submerged in Ringer's solution to ensure that the optical conditions were identical to those encountered during the experiments. The results showed a value of 1.93 microns/division for the 5X eyepiece optical system, and a value of 2.30 microns/division for the system employing the 18X eyepiece.

5X readings could only be estimated to 1 division ($\approx 2\mu$) with precision, whereas the 18X pathway could be read to an estimated 0.2 divisions ($\approx 0.5\mu$). Data was usually recorded to the nearest division for both optical systems, the 5X being used for mark separations, zone length, and striation spacings, and the 18X for fiber and zone diameters. On occasion, 18X data was recorded to an unjustifiable precision of 0.1 divisions.

Micropipette Manufacture

Micropipettes were pulled on an Industrial Science Associates, Inc. micropipette puller model MI from thoroughly cleaned and dried Kimax 1.6 - 1.8 mm outside diameter capillary tubing. It was empircally found desirable to use micropipettes having outside tip diameters of 0.5-2.0μ with a very long gentle taper. These were difficult to manufacture directly, and more commonly pipettes of much smaller diameter were pulled and then broken off at the desired diameter by gently brushing the tip with a frayed cotton swab. Tip

size and shape were verified under the microscope at720X magnification.

Satisfactory pipettes were mounted on special holders, placed in a transport rack, and subsequently submerged in a "filling chamber" containing 95% ethanol (figure 16:A-C). The filling chamber was then placed in a vacuum jar, and the ethanol subjected to vacuum boiling for 1-2 hours to cause pipette filling and removal of bubbles. This process was aided by periodically releasing the vacuum, thereby stressing the bubble attachment sites with rapid shape changes.

The pipettes must contain Ringer's solution for experimental use, although they were initially filled with ethanol to allow more effective removal of bubbles. The alcohol was displaced by an exchange process, accomplished by placing the pipettes, still mounted on the holders resting in the transport rack, in a large (1 liter) container filled with Ringer's. When pipettes were intially placed in this exchange reservoir, alcohol could be seen to rapidly stream from the pipette lumen, probably as the result of specific gravity differences. The process was substantially complete in 1-2 minutes. Nevertheless, the pipettes remained in the bath for one hour, at which time they were transferred to a second container for an additional exchange period. After one hour in the second exchange chamber, the pipettes were considered to be filled exclusively with Ringer's solution.

Pipettes prepared by the common procedure described above

Figure 16. Schematic diagram of the micropipette manufacture sequence and apparatus. A, freshly pulled micropipettes (a) are mounted with rubber bands onto holders, which consist of rubber grommets (b) glued to a polished glass rod (c). B, holders ride in a transport rack through filling and exchange processes. The transport rack is constructed of an aluminum block base (d) containing holes drilled to fit the glass rods, and a vertical aluminum rod (e) serving as a handle. C, for filling, the transport rack is placed in a large beaker (f) covered by a lid (g) elevated by braces (h). When this complex is placed in a vacuum jar, fluid contained in the beaker can be subjected to subatmospheric pressures, and yet condensate cannot drip back into the solution. D, following Ringer's exchange, the pipette holders are removed from the transport rack and transferred to plastic centrifuge tubes (i) for centrifugation. The grommets (j) on the holders are shaped to result in a snug fit between holder and tube, while preventing wall contact with the pipettes. Pipettes are oriented tip down for filling and exchange, and tip up for centrifugation.

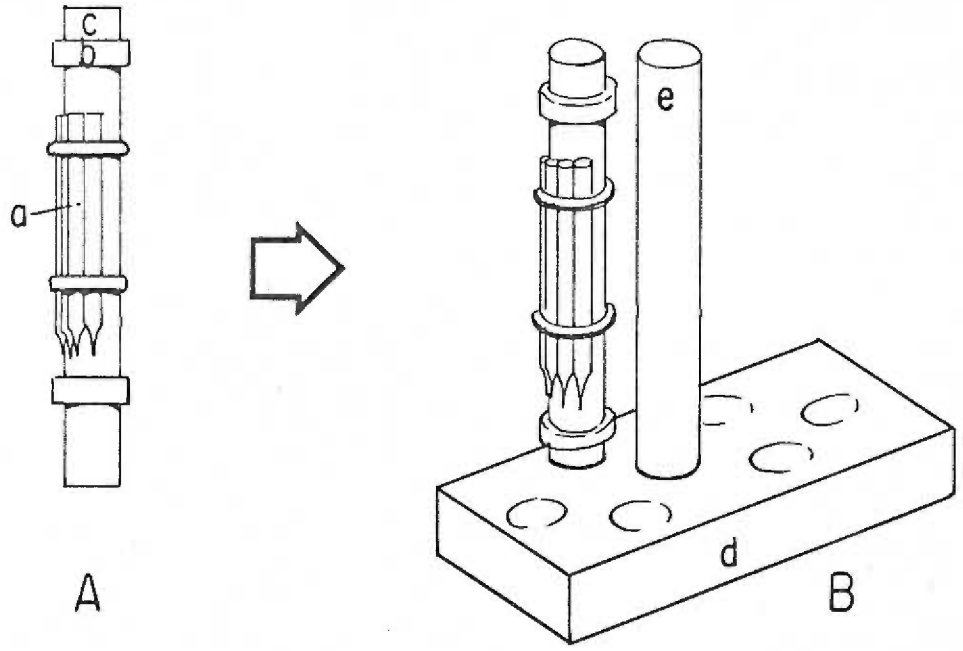
c
b
a
A
e
d
B

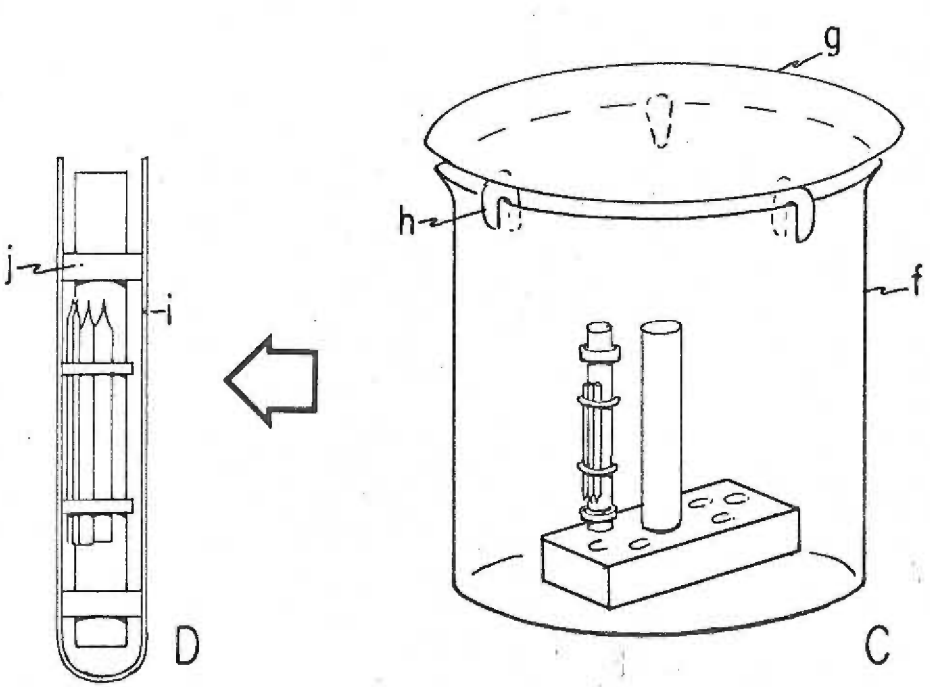
g
h
f
C
j
i
D

typically do not possess patent lumens allowing hydrostatic pressure transmission. It was found necessary to remove particulate contaminants from the pipettes and their suspension media. The alcohol and Ringer's solutions were triple filtered through Millipore filters (0.22μ pore diameter) by aspirator suction prior to filling and exchange. Furthermore, the pipettes were carried through a unique centrifugation and suction sequence following Ringer's exchange. The special holders to which the pipettes were fastened during filling and exchange were also designed to fit into plastic centrifuge tubes, (figure 16-D), in which the pipettes were centrifuged, tip up, for one hour. A small fraction of particles were of density less than one and tended to rise into the tips during centrifugation. The latter process was therefore followed by a procedure in which aspirator suction was applied to each pipette individually for a period of 20 minutes.

Pipettes having been carried through all of the above procedures were almost perfectly clean, and could be kept that way indefinitely if stored submerged in filtered Ringer's solution in a sealed container. For an experiment, a pipette was removed from a holder, attached to the PE tubing connector to the pressure system, mounted in the micromanipulator clamp, and rapidly submerged in the experimental chamber to prevent fluid evaporation from the tip. The remaining pipettes on the holder were returned to storage. The

short periods of time when the storage vessel was opened resulted in significant contamination of the pipettes remaining in storage, limiting the practical number of pipettes manufactured at one time to 10-15.

Experimental Protocol

Preliminary procedures common to all experiments. Prior to mounting a freshly isolated fiber, the force transducer was calibrated, and the micrometer drive assembly containing the transducer was fastened to the experimental chamber. The latter was then filled with Ringer's, and the isolated fiber was transferred from the dissection chamber to the experimental chamber in a small transport cup (see figure 9-A). The fiber was mounted to the micrometer drive support arms with the unaided eye. The small rubber band near the end of one arm was lifted with fine forceps, the portion of retained tendon or clump of sectioned fibers at the end of the fiber segment was inserted under the rubber band with a second pair of forceps, and the band was released (see figure 11). The procedure was repeated to clamp the remaining end of the fiber to the second support arm.

The above procedures were carried out on a counterspace next to the experimental benchtop. Once mounted, the length of the preparation was adjusted until the isolated fiber segment was just taut,

and the experimental chamber was carried to the microscope and securely fastened to the chamber holder with three screws (see figure 10-B). At this time, the objective lens was swung into place, and the fiber was located and examined along its entire length to insure morphological compatibility with the desired experiment.

Qualitative observations. Many features of fiber morphology were qualitatively observed in various experiments. Hundreds of fibers were studied to establish the general morphology of retraction zones and other forms of cell disruption resulting from fiber damage. The geometrical forms of specific segments within retraction zones were of prime interest, particularly the nature and form of retraction clots and empty tube regions (see figure 7, page 46). Retraction zone morphology was examined with emphasis on the contour assumed by the membrane, from the point of view that the sarcolemma is an elastic structure whose dimensions are determined by the interplay of intrinsic form and external forces. Detailed accounts of the processes involved in the formation and spread of damage were also noted, again with specific accent on membrane behavior. The latter observations included the correlation of membrane structure and form with the nature of the underlying cell contents, and the changes in position of specific membrane loci relative to other membrane areas and to underlying areas of disruption as damage developed. Investigations made in the experimental chamber at high

magnification were supplemented by many experiments conducted in the dissection chamber, involving morphological studies of damaged and undamaged fibers in teased muscle viewed with the dissecting microscope.

Quantitation of certain morphological features. Many experiments included measurements of the length and diameter of the empty tube region of retraction zones. These measurements were obtained from freshly formed zones following the initiation of fiber damage (see previous section) and after various experimental manipulations of the cell. The recordings were intended as an index of zone shape. Lengths were measured from points at either end of the empty tube region where the tube membrane first came into contact with the retraction clot, an average value being recorded if membrane contact with a particular clot was unsymmetrical around the fiber. The zone diameter was recorded in the central portion of the empty tube region, at the point of minimum width. Diameter and length data was recorded at rest length of the fiber, defined as the length where fiber tension would just become detectable if the cell were further elongated. This length was determined by slowly stretching the fiber until a detectable force (1 dyne) was noted, and then returning the fiber to slightly shorter lengths until the force disappeared. The diameters of several normal regions of the fiber, indicated by an intact striation pattern, were also recorded at rest

length. In addition, several experiments included a measurement of sarcomere length at a predetermined fiber force (4 dynes), determined by recording the number of sarcomeres occupying a fixed cell length.

Mechanical properties of the sarcolemma. The stress-strain behavior of retraction zone membrane was investigated in many experiments. Longitudinal and circumferential lengths of a segment of the empty tube region were noted in response to changes in the hydrostatic pressure gradient across the zone membrane, to alteration in the external force placed on the fiber, or to both stresses simultaneously. The hydrostatic pressure inside the zone was controlled through the lumen of a micropipette, and force measurements were made using the force transducer previously described. Membrane lengths in the longitudinal direction were recorded as changes in the separation of small marks on the membrane, while circumferential lengths were taken as the zone segment diameter. Readings were exclusively obtained from the central segment of empty tube region membrane in "long" retraction zones, where cylindrical geometry prevailed (see the Results section). A given datum combination of a pressure, a tension, and two membrane length measurements, found for a particular state of the membrane, will be referred to as a "pressure-deformation-tension data set", or simply a PDT data set.

Following the preliminaries typical of all experiments, PDT investigations began with the induction of fiber damage by methods previously described. A time period of one hour was then allowed for the fiber damage to develop and stabilize. Next, "long" retraction zones were formed from "short" zones (by procedures discussed in "Results"), the fiber was brought to rest length, and the selected retraction zone was penetrated with a micropipette. The site of pipette impalement was located in all instances near one end of the empty tube region, as far as possible from the central cylindrical segment where geometrical measurements were made.

PDT data sets were obtained in the following manner. With the fiber held at a particular length, the pressure inside the retraction zone was raised in a step fashion to some value, and the membrane dimensions and the external force on the fiber were recorded along with the pressure. Once the readings were acquired, the pressure was returned to zero for several seconds to allow membrane relaxation. The pressure was then raised to some new value and again correlated with membrane lengths and fiber forces. PDT data sets, for that one particular length of the fiber, were collected in this manner until repeated measurements at various zone dimensions had been acquired. This usually involved 10-20 data sets. Care was taken to randomize the order of pressure magnitudes imposed and minimize the time each pressure pulse was manifest, to

reduce any accumulation of viscous deformations of the membrane material.

The collection of PDT data sets obtained at a particular fiber length was referred to as a pressure run or simply a "run." When the initial run had been completed, the pipette was removed from the cell, the fiber was stretched to a new length, and the micropipette was reinserted, after allowing two to four minutes for the fiber tension to adjust to the new length. The relative elongation of the original or of a new cylindrical zone segment was also recorded, and a second pressure run was conducted at the new fiber length. Pressure runs and stretching episodes were continued in this manner for as many cycles as possible. However, the complex nature of apparatus and techniques associated with collecting PDT data created a situation of high vulnerability to failure, and experiments involving a large number of runs were exceptional.

Measurements of the breaking force of damaged fibers were obtained in some experiments, following other qualitative or quantitative investigations. The fiber was stretched from rest length at a slow uniform rate until the fiber broke, and the force just prior to rupture of the fiber was recorded.

Data Reduction and Analysis

Quantitative information relating to retraction zone shape, the

length and corresponding diameter of an empty tube region, was normalized with respect to the diameter of undamaged regions of the same cell showing normal cross-striations. The minimum diameter of the empty tube region (D_Z) divided by the diameter of the undamaged fiber (D_N), when both values were determined at rest length of the cell, was referred to as the "normalized zone diameter", (D_Z/D_N). The corresponding zone length measurement, designated L_Z, was referred to as the "normalized zone length", (L_Z/D_N), after a similar normalization. Collectively, the resulting dimensionless quantities, (D_Z/D_N) and (L_Z/D_N), are called "normalized zone shape variables", and were used as quantitative indices of shape in the same or different retraction zones following zone formation and after various experimental manipulations of the muscle fiber.

As described in the Introduction, a pressure-deformation-tension (PDT) data set includes sufficient information to calculate the tension (force per unit length) and strain (change of length relative to a reference length) independently for both the circumferential and longitudinal directions in the retraction zone membrane, under conditions in which the segment of empty tube membrane being considered is of cylindrical geometry.

For calculation of strains, changes of length in the longitudinal and circumferential directions were referred to the dimensions of

the unstrained zone membrane, found when the pressure gradient across the membrane and the external force borne by the fiber were both zero. Thus

$$e_s = \frac{D - D_o}{D_o} \quad \text{and} \quad e_x = \frac{L - L_o}{L_o}$$

where . . .

e_s = membrane strain in the circumferential direction (cm/cm);
e_x = membrane strain in the longitudinal direction (cm/cm);
D = diameter of the cylindrical zone segment (cm);
D_o = diameter of the unstrained cylindrical zone segment (cm);
L = length of the cylindrical zone segment (cm);
L_o = length of the unstrained cylindrical zone segment (cm).

The calculations of tensions for the circumferential and longitudinal directions were based on the relationships derived in the introduction, describing the physics of a cylinder under both external loading along the cylinder axis and internal pressure. It was shown that a pressure gradient across the retraction zone membrane results in both a longitudinal and a circumferential component of tension in the membrane material, designated as T_p and T_s respectively, where T_s is equal to twice T_p. Under the present conditions, the pressure component T_s represents the only deforming force acting in the circumferential direction. However, there are two tension components acting parallel to the fiber axis, that due to the

longitudinal pressure component T_p, and that due to the external force acting on the fiber, designated T_L. The tension T_L is calculated as the external force acting on the fiber per unit circumference of retraction zone membrane, and therefore

$$T_p = PD/4 = T_s/2 \qquad T_L = F_L/\pi D$$

$$T_x = T_p + T_L \qquad T_s = PD/2$$

where . . .

- D = diameter of the cylindrical zone segment (cm);
- P = hydrostatic pressure gradient across the zone membrane (dynes/cm^2);
- F_L = external force borne by the fiber along its longitudinal axis (dynes);
- T_p = longitudinal tension component in the membrane due to the pressure P (dynes/cm);
- T_L = longitudinal tension component in the membrane due to external force F (dynes/cm);
- T_x = total longitudinal tension in the membrane (dynes/cm);
- T_s^x = total circumferential tension in the membrane (dynes/cm).

The above analysis results in the reduction of an original PDT data set (P, F_L, D, L), obtained for a particular membrane state, to an equivalent "tension-strain" data set, composed of a longitudinal tension and strain (T_x and e_x) and a circumferential tension and strain (T_s and e_s).

The observed mechanical behavior of a retraction zone membrane was reported in the form of tension-strain plots, one plot for each direction through the membrane material. The figure for the circumferential direction was constructed by plotting all of the

tension-strain pairs (T_s - e_s values) observed at a particular value of longitudinal strain (e_x), and repeating the procedure for different values of e_x. Thus a family of tension-strain curves was constructed for the circumferential direction, the form of a particular curve being dictated by the value of longitudinal strain at which the circumferential quantities were evaluated. Similarly, a tension-strain plot was constructed for the longitudinal direction, showing a family of (T_x - e_x) curves at constant values of circumferential strain. The (T_s - e_s) plot could be drawn directly from the list of "tension-strain" data sets for a particular experiment, as experimental "pressure runs" were conducted at constant e_x. Construction of the complementary (T_x - e_x) plot was more difficult, because the (T_x - e_x) quantity pairs at constant values of e_s could not be read directly from "tension-strain" data sets, but rather had to be graphically interpolated from a family of (T_x - e_s) lines drawn at constant values of e_x. The latter lines could be obtained directly from the "tension-strain" data.

In addition to tension-strain plots, the PDT data obtained from a given membrane was organized in a fashion indicative of the "stiffness" of the membrane material. Stiffness was defined as the slope of a tension-strain curve. Since the tension-strain characteristics were evaluated in two directions, and because individual tension-strain curves for a given direction were found to be curvilinear,

values of membrane stiffness were specified for selected points on the tension-strain curves for each direction in the membrane. Stiffness values therefore represent instantaneous slopes at a particular location on a specific tension-strain curve, and hence are mathematically defined as

$$S_s = (\partial T_s / \partial e_s) e_x \qquad \text{and} \qquad S_x = (\partial T_x / \partial e_x) e_s$$

where S_s is a stiffness evaluated in the circumferential direction and S_x is a stiffness evaluated in the longitudinal direction, both quantities being assessed at a unique membrane configuration specified by the longitudinal and circumferential strain respectively. Stiffness values so defined, are referred to as "Tension-Strain slopes", or simply "T-S slopes", in later discussions.

RESULTS

Retraction Zone Formation

Retraction zones are the center of attention in the present work. Their formation and morphology were observed in hundreds of instances following accidental or induced fiber damage under either the dissecting (20-120X) or experimental (200, 720X) microscopes. A remarkably repeatable series of events ensues in response to fiber damage, ultimately leading in most cases to separation of the muscle contents, and leaving a cylindrical sheath of sarcolemma as the sole mechanical connection between fiber halves. A detailed portrayal of zone formation follows, including several features recorded in the present study that have not been previously described.

Figures 17 and 18 present a series of diagrams that illustrate particular stages of the zone formation sequence. The initially undamaged fiber (figure 17-A) gives rise to two clots or rigid areas of extreme disorganization (figures 17-B, C, D) bracketing the site of damage. The fiber diameter at the level of these "primary clots" is increased 50-100%, and is also exaggerated for several hundred microns on either side of an isolated region of damage, tapering gently until the normal diameter is reached. This area of exaggerated diameter is occupied predominantly by seemingly normal

Figure 17. Diagramatic representation of retraction zone formation. A, undamaged fiber. B, swelling of fiber and loss of striation immediately following damage. C, disorganized material begins to coagulate at two points lying on opposite sides of the damage site. D, continued coagulation results in the formation of two "primary clots" straddling the damage site. The three "disorganized regions", two straddling and one lying between the primary clots, can all potentially divide to form retraction zones, the resultant zones being depicted in E, F and G. In reality, more than one zone may form. In E, F, and G ellipsoidal clots represent "primary clots" formed just following the initial damage, and circular clots depict disorganized material, separated from the primary clots after division of a disorganized region, that subsequently clotted. The latter are called "secondary clots."

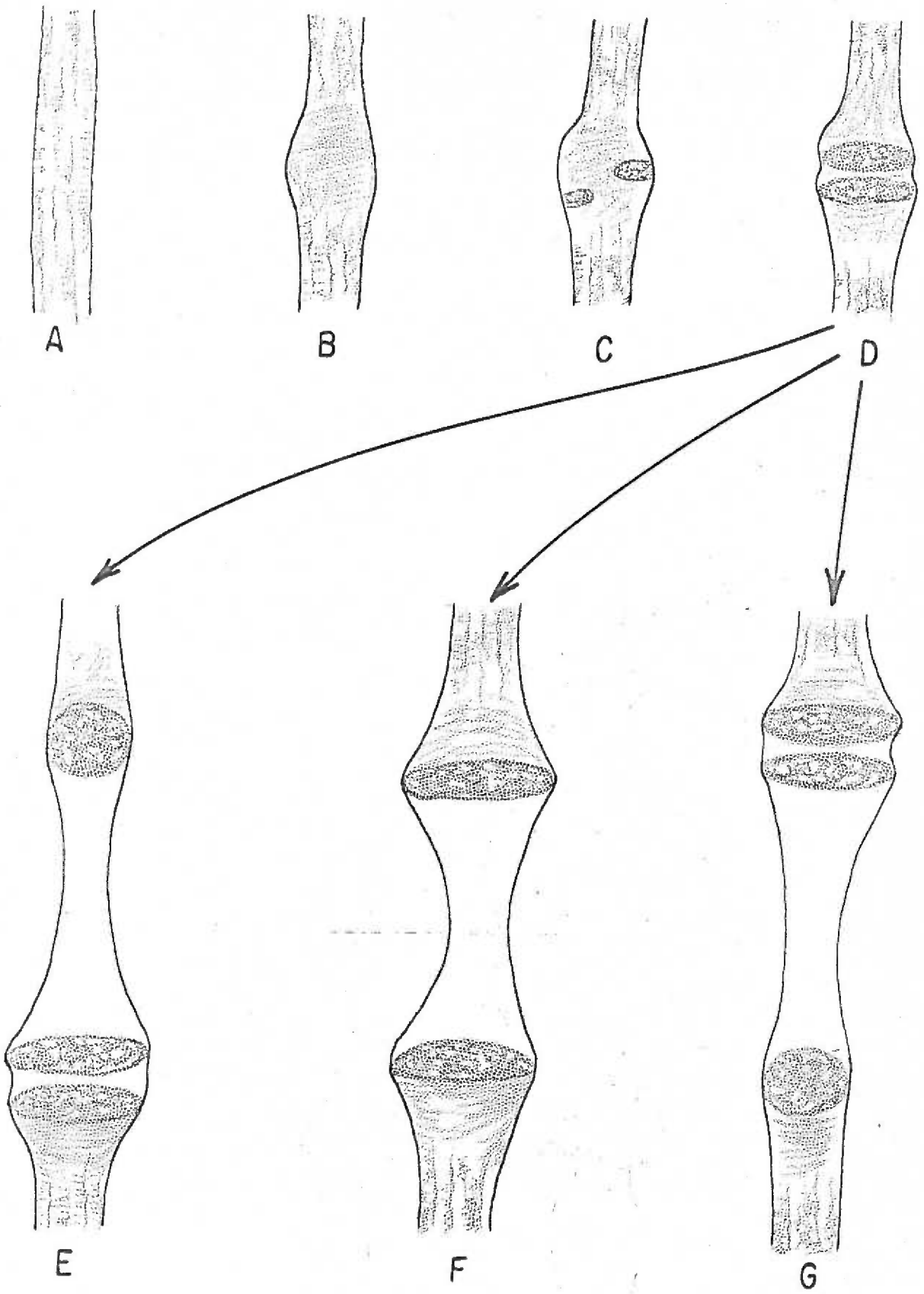
A
B
C
D
E
F
G

Figure 18. Drawings of early morphology (A) seen following fiber damage and later morphological stages (B) in damage development. Immediately following damage, the cell contents become cloudy and marked swelling occurs at the site of the insult. The cloudy region progressively transforms into the morphological pattern seen in A, where two primary retraction clots with associated disorganized regions appear, straddling the original site of damage. B shows later stages of damage development chronologically from below. Incorporation of sarcomeres into a growing disorganized region is accompanied by separation of the membrane from the disorganized muscle substance. The membrane separates as a bubble initially, but continues until it is free as a ring around the entire fiber, being separated from underlying substance by an apparent fluid layer. The disorganized region becomes longer and narrower with time, and eventually separates in a stringy manner resulting in the formation of a retraction zone.

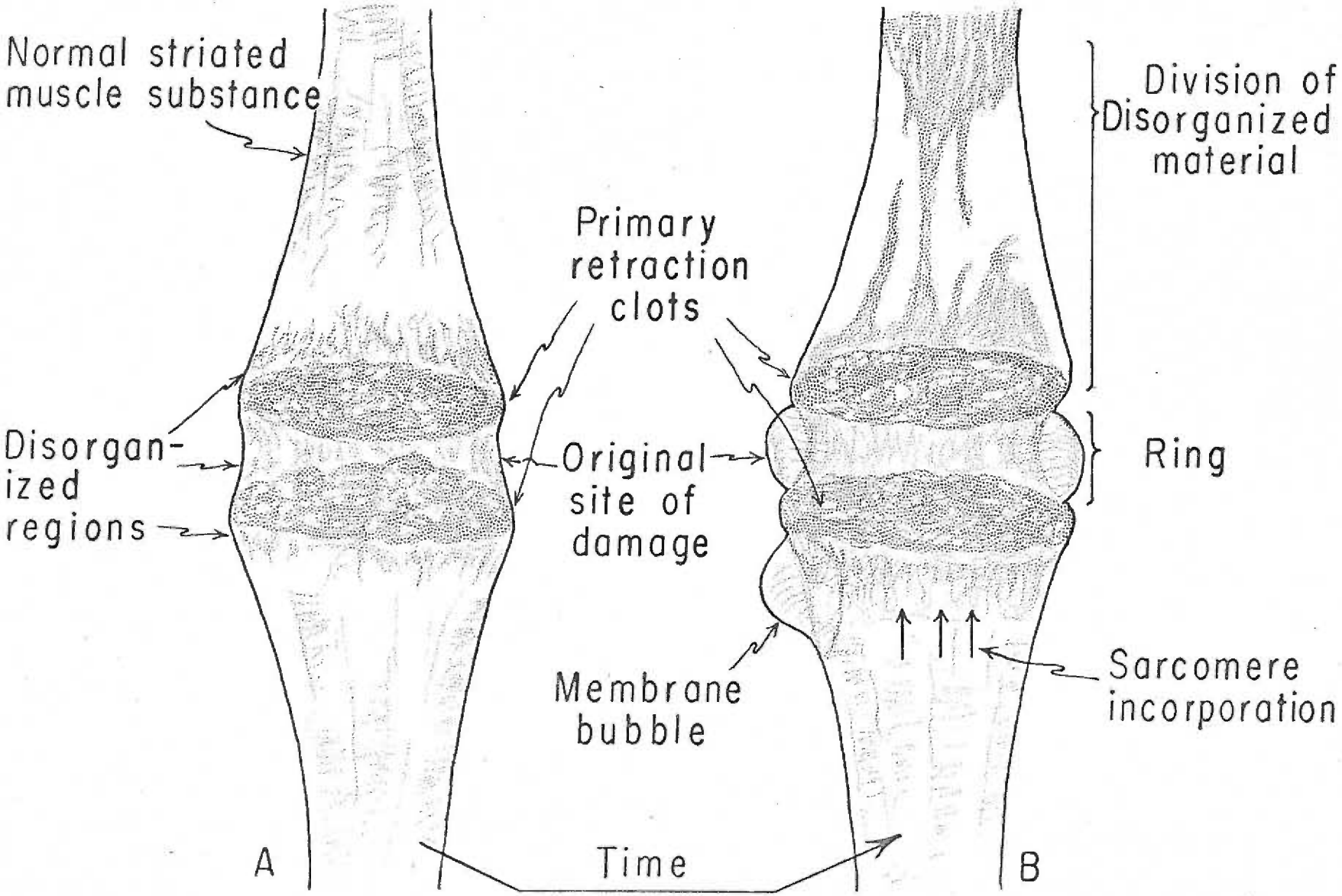
Normal striated muscle substance
Primary retraction clots
Division of Disorganized material
Disorgan-ized regions
Original site of damage
Ring
Membrane bubble
Sarcomere incorporation
A
Time
B

appearing cross-striated muscle substance, although a "disorganized region", characterized by loss of cross-striation, is encountered near the clots. A similar region of disorganization is also found between the primary clots (figure 18).

As time progresses, the two disorganized regions straddling the "primary clots" tend to engulf adjacent sarcomeres (figure 18-B). This continued accumulation of cross-striated muscle substance results in a volumetric growth of the disorganized region, and is accompanied by a tendency for the disorganized material to reorganize its geometry slowly, becoming long and narrow rather than retaining its initial short and wide configuration. Simultaneously, the sarcolemma becomes disassociated from the underlying disorganized material, generally as a small bubble at first, but continuing until the entire expanse of membrane overlying the disorganized region bulges free around the entire fiber (figure 18-B). The space between the disorganized cell contents and the outwardly bulging sarcolemma is occupied by a clear structureless medium appearing to be a fluid.

The reorganization of disorganized material to the long, narrow geometry eventually culminates in its division into two halves, resulting in a complete discontinuity of the muscle substance, (figures 17:E-G, 18-B). The diameter of the disorganized substance during the terminal phases of reorganization decreases to the

original diameter of the undamaged fiber, or, more commonly, to an even smaller diameter. As this process occurs the ends of the disorganized region move apart at an increasing rate, and the membrane contour progressively reverts to the cylindrical geometry. Separation of the disorganized contents is stringy in nature, involving the abrupt rupture of individual strands in random order (figure 18). As the separation becomes complete the two halves of disorganized muscle contents snap to a new position some distance apart. The intervening space is occupied by a clear, structureless material appearing to be fluid in nature and retained by the remaining sarcolemma. The tube of membrane is now seen to be concave in longitudinal outline, having inverted its contour as material separation became complete.

Once disorganized material has separated, both halves tend to coagulate, forming a rigid clot at either end of the tube segment (see figure 7). The consistency and diameter of such clots vary widely between individual zones. Any of the three initial disorganized regions can potentially form a retraction zone (figure 17), and zones forming from any site universally evolve at variable rates through the same sequential stages. There is no obvious indication of any disruption of membrane structure nor of interruption of connections to intracellular contents during separation of the sarcolemma from the underlying cell material. Retraction zone

Figure 19. A, Photomicrograph of an intact single muscle fiber. Notice the distinctive striation pattern and the lack of any morphological signs of damage. 280X. B, Photomicrograph of two primary clots formed at the site of damage. The disorganized material on either side of the clots occasionally exhibits local areas of coagulum. Same fiber as A; compare diameter relationships. 420X. C, Photomicrograph showing the transition from a local area of damage to normal fiber. Normal fiber segment at the bottom of the photo gives way to a region of disorganized material seen centrally characterized by loss of striation and transitional diameters. The texture of the disorganized region as seen here is more typical than that shown in B. Disorganized region is bordered by a rigid clot at the top. Same fiber as A. 325X. D, Photomicrograph of membrane separation from the cell contents of a disorganized region. Three bubbles are seen where membrane has separated from the underlying disorganized region. Same fiber as A. 420X. E, Photomicrograph of retraction zone formation. Cell material of a disorganized region has just separated seconds before, leaving an empty tube region in the lower portion of photo. Disorganized material at top has not yet coagulated into a rigid clot. Notice diameter relationships. Same fiber as A. 210X.

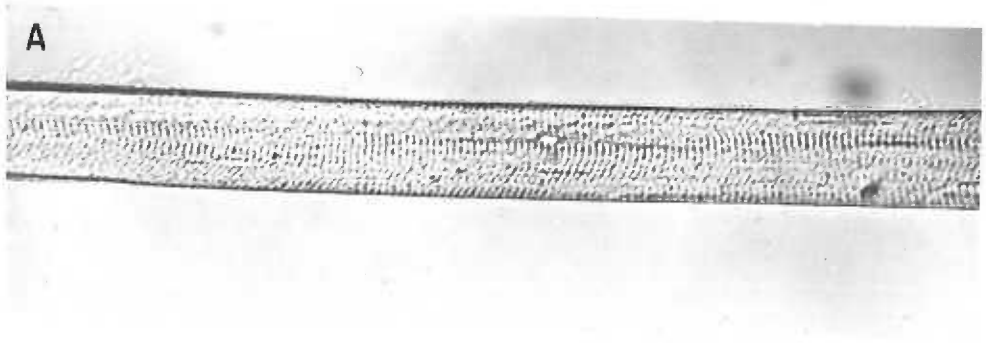
A

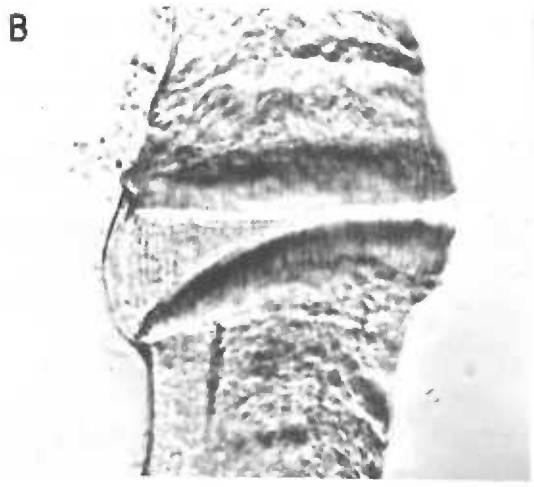
B

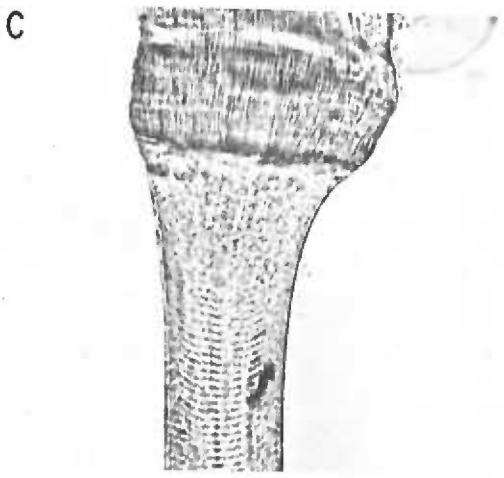
C

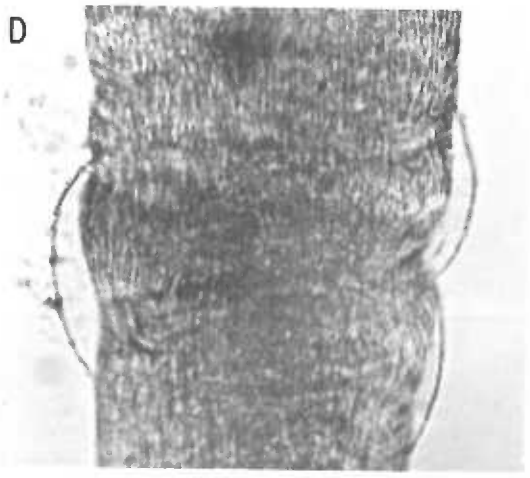
D

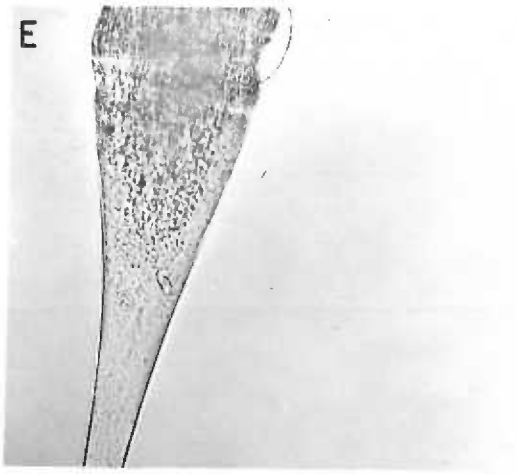
E

Figure 20. Diagram indicating morphological features of "short" and "long" retraction zones. Fiber continuity is maintained solely by the sarcolemma, as the muscle substance is discontinuous. The membrane contour is tapered in the empty tube region, having a minimum diameter centrally. Short zone tube regions show a curvilinear longitudinal contour throughout, while long zones are distinguished by having a central tube region of cylindrical geometry.

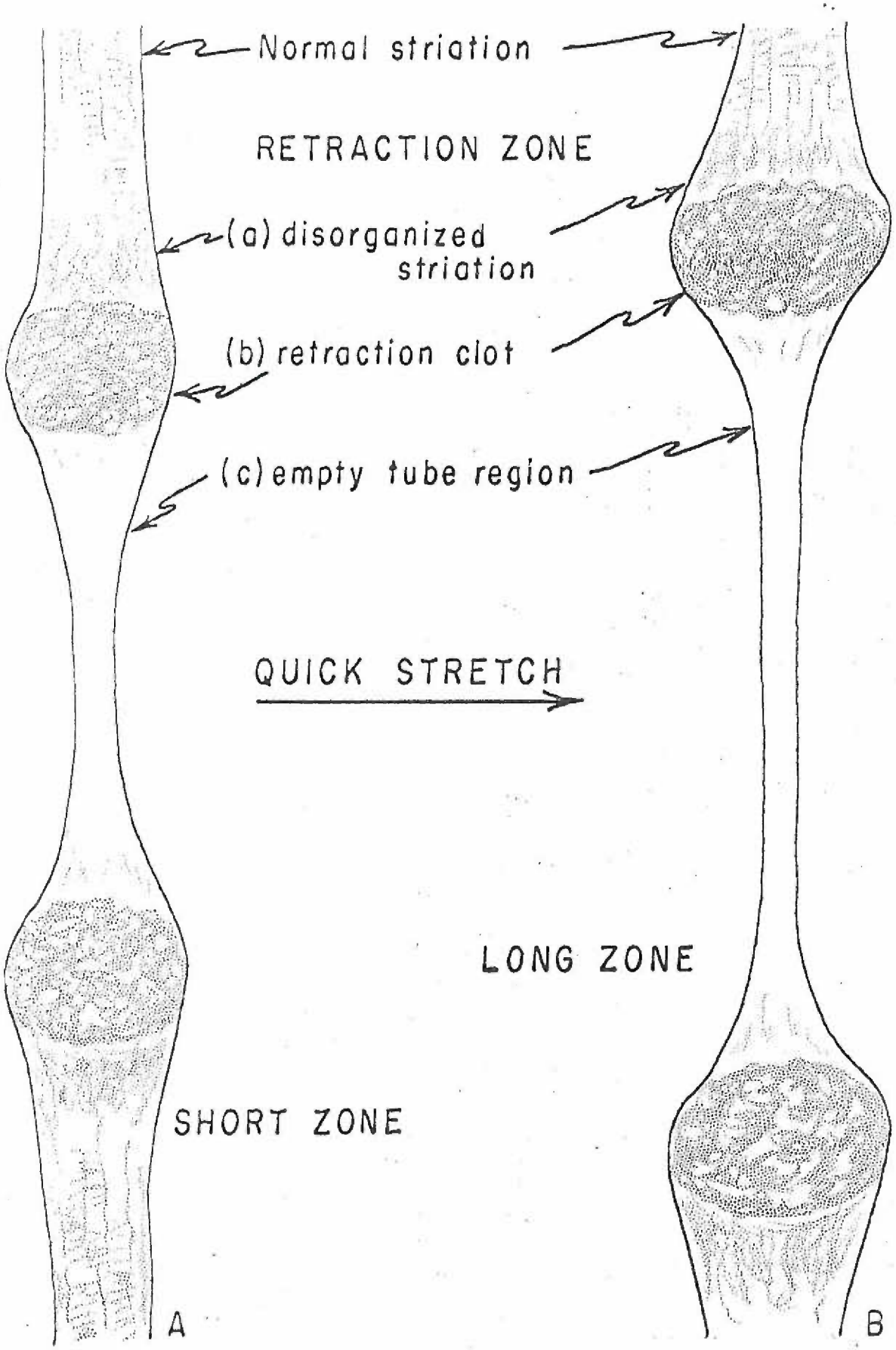
Normal striation
RETRACTION ZONE
(a) disorganized striation
(b) retraction clot
(c) empty tube region
QUICK STRETCH
LONG ZONE
SHORT ZONE
A
B

even when associated with the smallest clots observed. Furthermore, membrane encompassing a clot tends to mold itself over irregularities with curvilinear indentations, and to reversibly form a sharp conical indentation when nudged with a micropipette. Such behavior suggests that an elastic sarcolemma is being stretched circumferentially by the clots, with progressive decay of the induced geometrical distortions toward the center of the tube region.

The clots are bordered opposite the tube region by areas of disrupted muscle substance characterized primarily by loss of cross-striations. These regions are identical in appearance to the "disorganized regions" seen to form adjacent to primary clots shortly following damage (see figure 19), and can also potentially lead to the formation of additional retraction zones. Thus damage may or may not continue to spread along the fiber with the formation of new retraction zones from distally positioned disorganized regions. Consequently, disorganized regions may be bordered distally by normal cross-striation or by additional retraction zones or clots, and tend to show diameters and cross-sectional contours transitional between neighboring fiber regions.

The sarcolemma shows no obvious internal structure in normal or disrupted regions of the fiber. Membrane regions separated from cell contents as rings or empty tube regions exhibit a variable texture, ranging from a clear and structureless appearance to one

having irregular grains, blotches, or marks. These features seem to represent variable amounts of debris remaining in the aftermath of violent muscle substance separation or fiber isolation, rather than being indicative of internal membrane structure. The material can occur on either side of the membrane, but appears to be predominantly localized to the inner surface, as seen by turning the fiber on its axis. Debris is always found external to the membrane in fiber segments showing normal cross-striation. The sarcolemma is seen as a delicate, structureless sheath when devoid of other material, with no structural alterations appearing as a particular membrane region progresses from its normal state in the undamaged fiber through the various stages of disruption of the cell contents.

Two morphological classes of zones can be distinguished, designated with respect to length as "long" and "short" (figure 20). They differ only in the longitudinal contour of the tube region, as all other structural features are similar. Retraction zones of great length do not show a tapered tube contour throughout, but rather exhibit a central region where the walls are parallel for some distance and thus have infinite longitudinal curvature. Tubes of shorter length are tapered along their entire outline. If a particular short zone is made into a long zone or long zones are made longer (by procedures to be discussed presently), all regions of the retraction zone tend to retain the same geometry with the exception of the

central tube region. The latter narrows as the zone gets longer until a critical length is reached, past which further lengthening is accompanied by the growth of a cylindrical segment of membrane at constant diameter. It appears that the cylindrical portion of long zones is merely a membrane region far enough removed from the clots to be free of associated geometrical distortions.

The formation of long zones was investigated in more detail in expt. #44. An intact Semitendinosus muscle was spread out into a thin rectangular sheet in the dissection chamber, and fiber membranes were marked by injecting aluminum dust into the bathing medium. Damage was subsequently induced in individual fibers by mechanical compression, and the ensuing sequence of events observed at various magnifications (20-120X) through a dissecting microscope equipped with a zoom lens. Particular note was taken of the relative motion of cell contents and membrane as damage developed. The observations indicated that the sarcolemma in a region of muscle substance disruption is capable of independent motion with respect to underlying material. The direct formation of long zones is not a resultant of damage produced by higher degrees of fiber stretch, as might be expected, but rather follows as a consequence of membrane sliding over the clots and into the empty tube region. This process results in more membrane substance being positioned between the clots. An identical process allows

conversion of short zones into long zones, the transformation being most efficiently induced by subjecting the fiber to quick stretches. Such membrane movement was documented photomicrographically in expt. #68 (figure 21). These findings imply that membrane must also be sliding over undamaged fiber regions adjacent to the areas of disruption.

In expt. #50 a particular zone was observed to be spontaneously increasing in length. The growth was occurring from one end only, as tube membrane was stationary with respect to one clot, but was sliding smoothly over the other and into the zone from positions overlying normal striated muscle substance. This zone was first observed as a "short" retraction zone, with a length of 160 μ. As it grew, the long zone morphology developed at a length of approximately 370μ. Growth continued at a uniform rate until the tube region had a length in excess of 1100μ at which time the process ceased. Once the long zone morphology was reached no changes in central tube diameter were noted, even though the length subsequently increased by several hundred percent.

Distribution of End Effects

Lengths can be associated with the regions of tapered membrane contour (regions of "end effects") bracketing the cylindrical tube segment of long retraction zones. Geometrical distortions

Figure 21. Photomicrographs indicating the position of membrane marks relative to cell contents before, A, and after, B, subjecting the fiber to a quick stretch. Marks in B are shifted to the left approximately 1 1/2" on the photomicrographs relative to the same marks as seen in A. The same mark on each photomicrograph can be more easily identified by realizing that the fiber in B has rotated on its axis through a small angle, resulting in the membrane markers being positioned slightly closer to the viewer. Both A and B 420X.

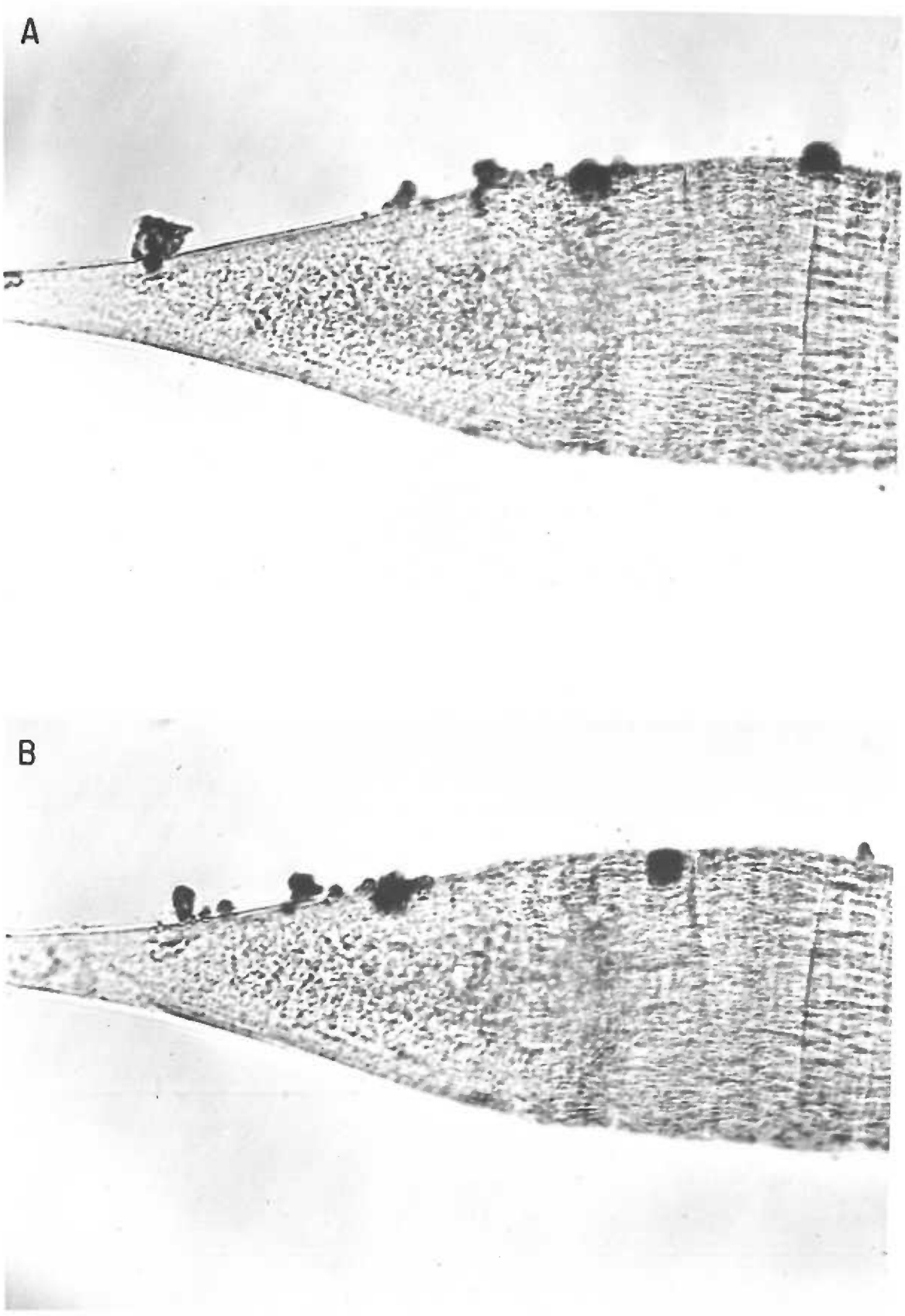
A
B

extending away from the site of edge loads are predicted by thin shell theory, and a decay length can be defined relating the extent of such disturbances to properties of the shell material. For a homogeneous, isotropic, thin elastic shell of dimensions similar to retraction zones, the theory predicts a decay length of well under 10μ. More extensive disturbances are suggestive of mechanical anisotropicity of the shell material, with the longitudinal stiffness greatly exceeding that in the circumferential direction. Retraction zone end effects persist for distances exceeding 100μ, suggesting qualitatively that the sarcolemma is grossly anisotrophic in favor of greater longitudinal stiffness. This conclusion is in support of quantitative measurements to be reported in another section.

Circumferential Membrane Strain in Normal Muscle Fibers

Previous description alludes to the fact that "short" retraction zones decrease their central diameter with increasing length at constant longitudinal tension. Eventually a point is reached where further lengthening is no longer associated with decreasing diameters. This phenomenon is quantitatively demonstrated by a plot of the normalized zone shape variables (D_Z/D_N) versus (L_Z/D_N) described in the "Materials and Methods" chapter, for repeated measures on the same zone at different length and for different zones of various shapes. Figure 22 summarizes 148 measurements recorded

Figure 22. Graphical representation of "normalized zone shape variable" data. Each point represents the central (minimum) diameter (D_Z) and length (L_Z) of a retraction zone tube region, after both dimensions were divided by the diameter of the undamaged cell for interfiber normalization. All measurements were recorded at resting fiber length.

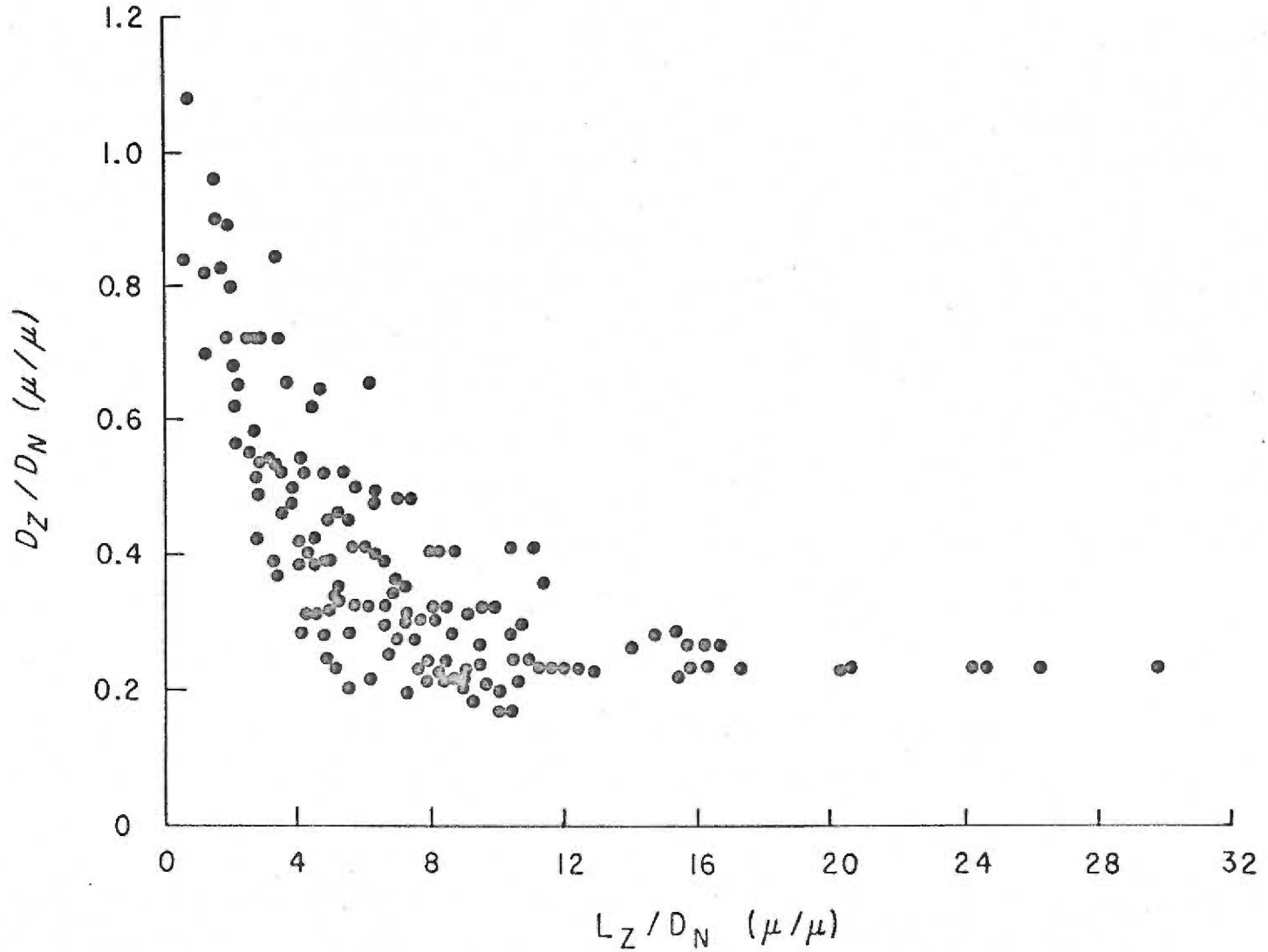
1.2
1.0
0.8
0.6
0.4
0.2
0
D_Z / D_N (μ/μ)
0
4
8
12
16
20
24
28
32
L_Z / D_N (μ/μ)

from 39 zones illustrating that as retraction zone shape becomes longer a state is reached where diameter changes become independent of changes in zone length.

In many experiments, it was possible to obtain repetitive measurements of retraction zone length and diameter from the same zone in various configurations, including representatives of both the "short" and "long" zone morphology. The final values of normalized diameter (D_Z/D_N) found for these fibers in the long zone configuration are indicated in table II. The mean value for the normalized long zone diameter was found to be remarkably constant, being $0.22\mu \pm 0.03\mu$ S.D. for 15 fibers.

As described in the Introduction, the geometry of the central cylindrical region of retraction zone membrane is dependent solely on two distributed deforming forces, the excess hydrostatis pressure inside the zone and the external force acting on the fiber. The "unstrained" dimensions of the zone segment are represented by the length and diameter found when both deforming forces are zero. The final values of normalized zone diameter reported in table II were measured at rest length of the fiber, and therefore the external force acting on the fiber was negligible. Furthermore, there is no consistent and usually no detectable difference in central zone diameter before and after impalement of a long retraction zone with an unpressurized pipette. This finding indicates that the

TABLE II

Final values found for the "normalized zone diameter" (D_Z/D_N) in retraction zones of the "long" morphological class. (D_N) is the diameter of the intact fiber and (D_Z) the diameter of the central cylindrical segment of a long retraction zone in the same cell, both diameters measured at rest length of the cell.

Expt. Number	$D_N(\mu)$	$D_Z(\mu)$	$D_Z/D_N(\mu/\mu)$
47	45	10	0.22
49	67	14	0.21
50	39	9	0.23
50	39	9	0.23
51	76	15	0.20
51	76	17	0.22
51	76	16	0.21
52	79	15	0.19
54	77	18	0.23
58	58	15	0.26
60	71	15	0.21
61	74	18	0.24
63	78	16	0.21
64	74	21	0.28
66	113	18	0.16

transmembrane hydrostatic pressure gradient in retraction zone tube regions is zero or very nearly so, since it is shown in a later section that alterations in the membrane pressure gradient by a few millimeters of mercury, which are negligible in terms of the range of pressures employed experimentally, produce large changes in zone diameter. The central cylindrical segment of the empty tube region of long retraction zones is therefore representative of "unstrained" zone membrane.

The data of table II shows that the "unstrained" membrane, on the average, has only 22% of the diameter of normal fiber regions, when both are compared at rest length of the fiber. It follows that if zone membrane is representative of normal sarcolemma from a mechanical standpoint, as the morphological data indicates, then the membrane of normal muscle fibers at rest length have a mean circumferential elongation of (1/0.22) x 100 or 450%. A circumferential elongation of 450% corresponds to a circumferential strain e_s, as defined in the "Materials and Methods" chapter, of 3.50 cm/cm.

Longitudinal Membrane Strain in Normal Muscle Fibers

Quantitative information is also available regarding the longitudinal membrane strain present in the intact muscle fiber at rest length. This information was collected in same manner as the data for the circumferential direction, that is the relative elongation of

sarcolemma in the intact fiber was determined with respect to the length of "unstrained" retraction zone membrane. However, because the membrane of the intact muscle cell is festooned in longitudinal contour while festooning is lost during retraction zone formation (see the Introduction), the above measurement represents an underestimate of the true relative elongation of the membrane material. The amount of data collected was therefore limited, because the quantitative measurements are relegated by the above considerations to qualitative conclusions.

In expt. #67 the separation of two marks (bits of debris) adhering to the membrane was noted with the fiber held at rest length. Damage was subsequently induced nearby, and movements of the membrane markers relative to each other were quantitatively recorded. As the two primary clots formed, the diameter of the fiber near the marks began to increase gradually, and the marks began to migrate slowly toward the clots. Eventually, the marks reached the nearest clot, which had originally been more than 100μ away. In doing so the mark separation decreased from an initial value of 29μ to 11μ, as the diameter of the fiber increased by 70%. The separation then increased to 25μ as continued motion allowed the leading mark to move over the clot and arrive at a region of smaller fiber diameter. Finally, the markers returned along their original path over the clot, as the disorganized region lying between the clot and

the striated muscle substance over which the markers had been positioned originally separated and formed a retraction zone. The marks again showed a minimum separation as they passed over the point of maximum clot diameter.

Table III summarizes quantitative data from three experiments in which the relative motion of membrane marks straddling sites of damage was recorded. Observations recorded during expt. #67 showed two marks to decrease their separation by 20% as two primary clots formed and grew between the markers over a period of 10 minutes. Their separation then increased as zones began to form in disorganized regions adjacent to the clots. Qualitatively similar decreases in mark separation were noted during fiber diameter increases accompanying primary clot formation in expt. #49. In the latter case, however, the formation of primary clots occurred much more rapidly, and the mark separation reached a minimum in three minutes. Fiber diameters were not measured in the above experiments but were noted to be moderate (50-100% increase). Diameter changes were recorded in expt. #57 and eventually were seen to exceed 200% of the initial fiber diameter.

The above results were observed in local fiber areas where the membrane was visibly in contact with obvious cell contents (type I membrane). In contrast to the above results, local membrane regions which were separated from structural cell contents

TABLE III

Measurements of the change in separation of marks adherent to the sarcolemma during the development of fiber damage. Data from experiments #67 and #49 show the change in mark separation with time, and data from experiment #57 illustrates the change in mark separation with change in the fiber diameter at the site of damage.

Expt. #67		Expt. #49		Expt. #57	
Time (min)	Separation (μ)	Time (min)	Separation (μ)	Diameter (μ)	Separation (μ)
1	190	0.5	83	23	100
1.5	165	1.0	80	45	55
2	160	1.5	75	47	47
10	152	2.0	71	50	40
15	160	3.0	67	57	36
20	170	5.0	70		
25	180				

by an apparent fluid space (type II membrane) did not show changes in elongation in response to alterations in diameter, (expts. #53, 65, and 67). Type II membrane is seen when the sarcolemma separates from disorganized muscle substance as a bubble or annular ring, and in retraction zones. Present and forthcoming evidence implies the distinguishing feature between type I and II membranes is the nature of the pressure causing circumferential elongation, being hydrostatic[1] in type II membrane and nonhydrostatic in type I.

Longitudinal Elongation Within Runs

The procedure employed for PDT data reduction, discussed under "Materials and Methods", presumed that the longitudinal elongation during a pressure run at constant external load, F_L, was independent of circumferential tension or strain. During such runs in which hydrostatic deformations were introduced, it was found that, in fact, both the longitudinal elongation and external load tended to remain unchanged. Table IV contains raw data from several experiments indicating the mean length and the range of lengths of membrane tube segments observed for runs at indicated external

[1] A hydrostatic pressure is one in which the magnitude of the force vector is independent of direction, whereas the force per unit area varies with direction in a nonhydrostatic pressure.

TABLE IV

Longitudinal membrane elongations recorded during "pressure runs" at constant external fiber loads. The observed mean length and range of lengths are indicated for pressure runs consisting of the indicated number of PDT data sets collected for the stated fiber force and range of pressure.

Exp. /Run	Force (dynes)	Maximum Pressure (mmHg)	Number PDT Data Sets	Mean Length (μ)	Length Range (μ)
55/1	3	5900	12	101	101-102
2	6	6000	10	133	133-135
3	9	6000	14	119	118-122
4	11	6000	8	91	91
5	16	7500	8	155	153-156
6	25	6000	4	106	106
60/1	0	5600	17	58	56-60
2	4	5700	10	124	122-127
3	7	6000	18	123	122-124
4	9	6100	11	123	122-124
5	13	6000	14	168	168
6	14	5800	8	168	168
7	16	6200	10	83	83
8	18	5800	6	100	100
64/1	3	5700	14	122	122-124
2	4	5600	11	127	125-127
3	6	5600	10	112	112-114
4	8	5000	8	83	83
5	10	6200	9	150	148-150
6	11	4800	10	154	154
7	14	5800	6	156	156
8	20	5700	8	124	124
66/1	0	6100	16	156	152-156
2	7	6200	9	172	172
3	13	6800	8	176	173-176
4	16	6600	5	180	180

loads. These experiments were selected from those in which multiple runs were made. The greatest variabilities were observed in experiments #60 and #66. The remaining examples are more typical, and in general it is concluded that of all the membranes studied, there is essentially no change in the length of zone segments during pressure-deformation runs at constant F_L, within the limits of experimental measurement.

Tension-Strain Relationships

Twenty-two experiments were completed in which the hydrostatic pressure within retraction zones was altered and consequent elastic membrane deformation observed. Certain qualitative observations, typical of all fibers studied, establish some important conclusions. Sudden alterations of transmembrane pressure result within one to five seconds in the zone membrane assuming a new stable geometrical configuration. The lag time between pressure and geometry changes is related to pipette tip diameter, and therefore probably to the time required for sufficient fluid to pass through the pipette lumen to introduce the required zone volume change. A small additional increase in zone diameter following very rapid deformations can also be seen, and may represent a component of volume change lag time due to viscous relaxation of the membrane. Viscous phenomena are discussed in a later section.

Pressure-deformation-tension (PDT) measurements were made on 14 fibers, including expt. #1 discussed in a later section dealing with membrane viscosity. The remaining 13 experiments were concerned with a characterization of the elastic behavior of the membrane and involved 519 PDT data sets.

The circumferential strains recorded at near zero external load on the fiber ($F_L \approx 0$) and at high circumferential tensions (T_s), about 10,000 dynes/cm, are recorded in table V for the 13 experiments directed toward characterization of elastic properties of the sarcolemma. Expt. #5, listed last in the table, differed from the other experiments in that the retraction zone studied was of the "short" zone morphology, and showed results suggesting "stiffer" membrane behavior. The remaining experiments were conducted on "long" retraction zones, where it was found that the mechanical behavior was in comparative agreement between individual membranes.

Although the mechanical behavior of long zone membranes were found to be similar, considerable scatter in the data from individual fibers was apparent. Such interfiber behavior differences may be due to disproportionate removal of portions of the connective tissue investments of individual fibers during isolation (25). For this reason, unique membrane segments examined in retraction zones may not be comparable from a mechanical standpoint, either in thickness or in internal structure, depending on the depth and nature

TABLE V

Circumferential strains (e_s) found in 13 experiments at high values of circumferential tension (T_s) under conditions in which the external fiber load (F_L) was near zero. Expt. #5, listed at the bottom of the table, was conducted on a "short" retraction zone, whereas the remaining data is from zones of "long" morphology.

Expt. Number	F_L (dynes)	T_s (dynes/cm)	e_s (cm/cm)
4	0	11900	1.33
11	0	9800	1.89
54	3	10400	1.12
55	3	11000	1.25
58	0	10400	2.04
60	0	8500	1.50
62	0	7300	0.89
63	0	15600	1.22
64	3	9000	2.36
65	1	11000	1.40
66	0	10300	1.40
67	0	9600	2.43
5	0	9800	0.07

of connective tissue separation during fiber isolation. All retraction zones were therefore treated as separate entities for analysis.

Figures 23 through 26 illustrate the tension-strain plots for both the circumferential (s) and longitudinal (x) directions, constructed as described in "Materials and Methods", for two experiments. The behavior is typical of all membranes studied, and indicates that at constant longitudinal strain, a plot of strain versus tension in the circumferential direction is non-linear, being concave to the tension axis. The circumferential tension-strain behavior becomes markedly "stiffer" as higher values of longitudinal strain are imposed. Analogous results were found for membrane behavior in the longitudinal direction at constant circumferential strains. Within each experiment, the range of tensions applied in the circumferential and longitudinal directions were similar. Nevertheless, for both experiments illustrated, the range of circumferential strains exceed those in the longitudinal direction by roughly an order of magnitude. Similar results were found in all other fibers examined, and it is concluded that the membrane shows different mechanical properties in the direction of the two principal axes through the material, i. e., the membrane is anisotropic. The same conclusion was reached from examination of the distribution of "end effect" distortions found near the clots, in studies of retraction zone morphology described in a previous section.

Figure 23. Tension-Strain plot of experiment #60 for the circumferential direction. The complementary plot for the longitudinal direction is shown in figure 24.

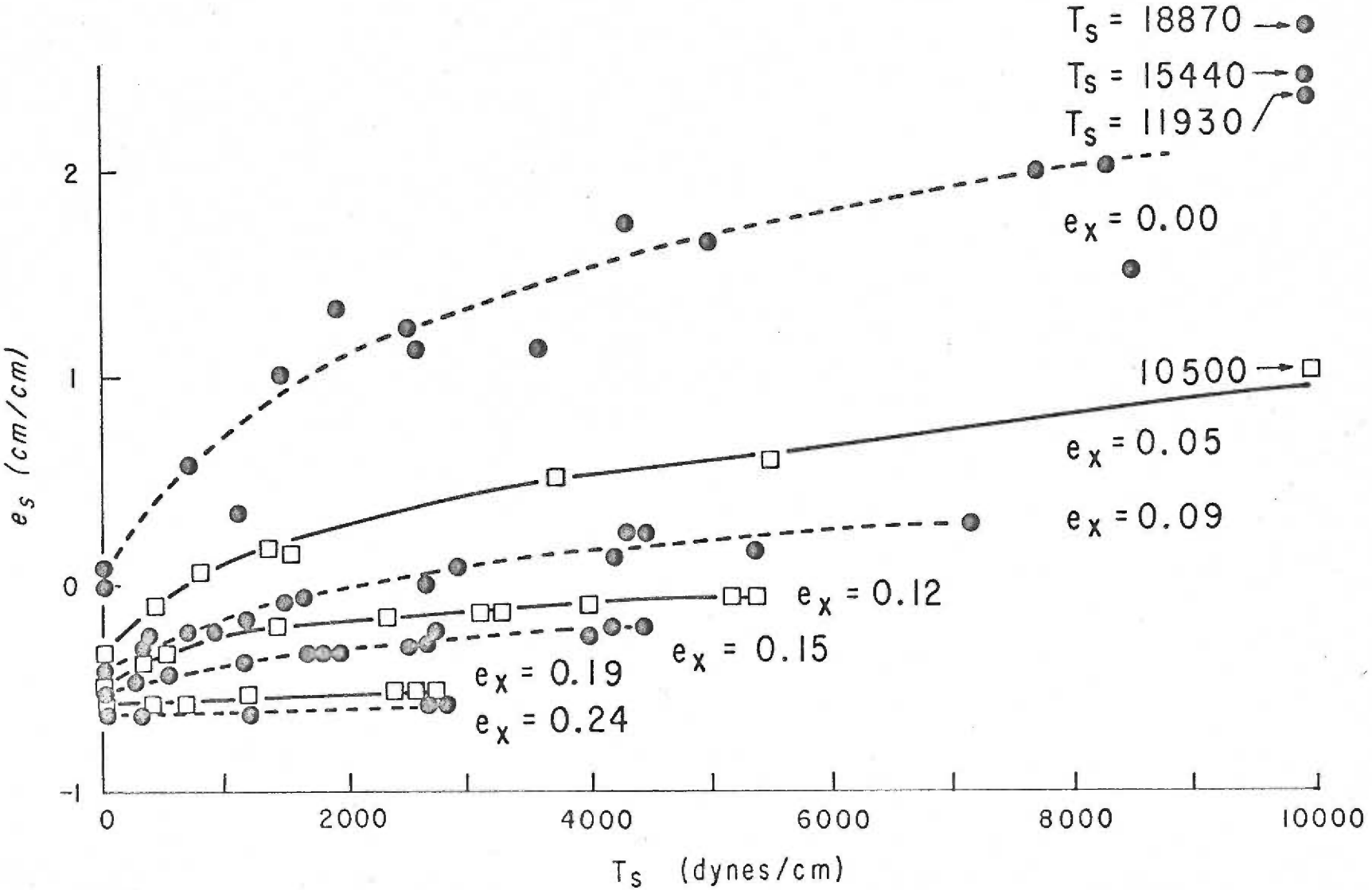
T_s = 18870
T_s = 15440
T_s = 11930
e_x = 0.00
10500
e_x = 0.05
e_x = 0.09
e_x = 0.12
e_x = 0.15
e_x = 0.19
e_x = 0.24
e_s (cm/cm)
2
1
0
-1
0
2000
4000
6000
8000
10000
T_s (dynes/cm)

Figure 24. Tension-Strain plot of experiment #60 for the longitudinal direction. The complementary plot for the circumferential direction is shown in figure 23.

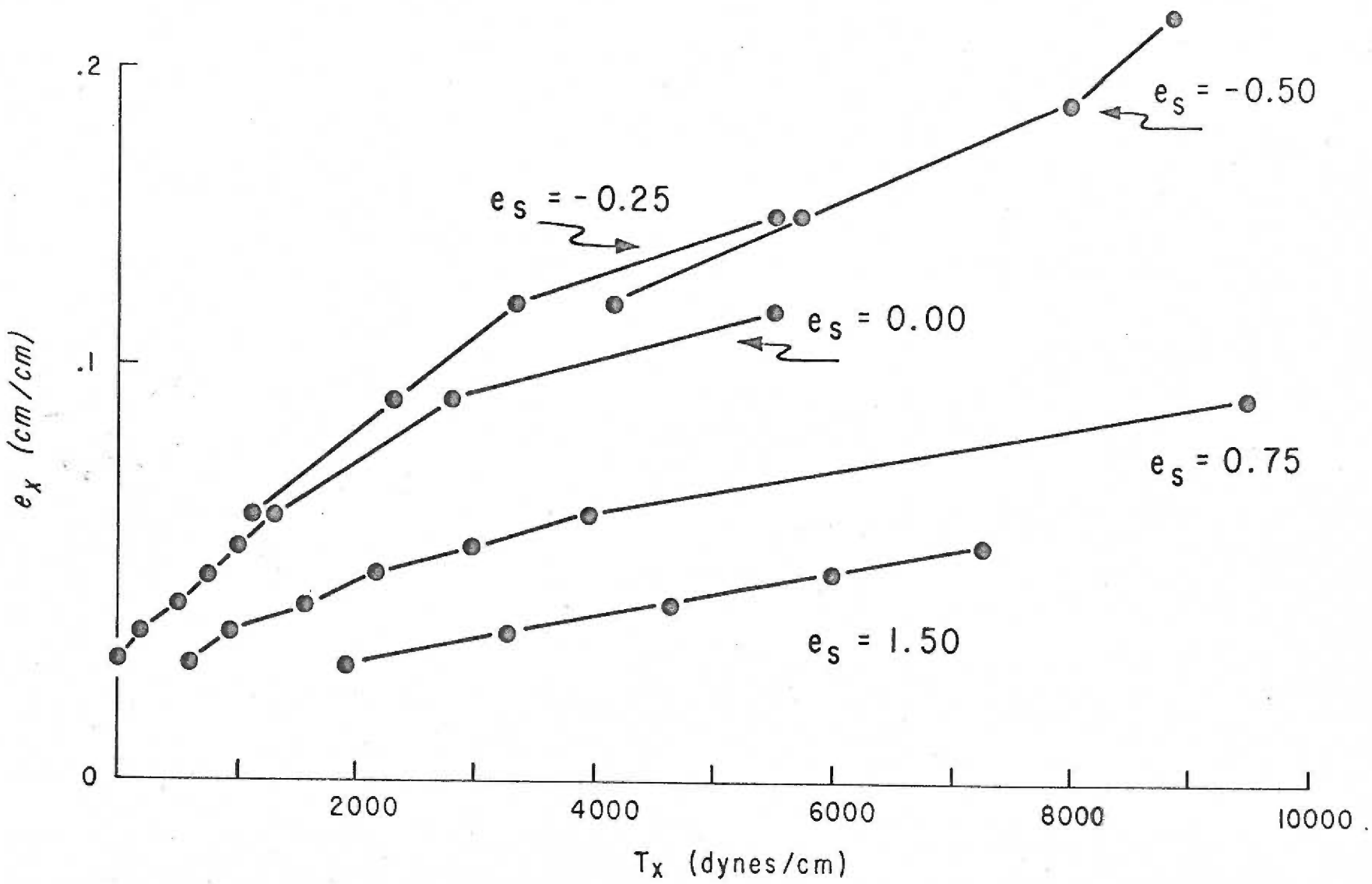
.2
.1
0
e_x (cm/cm)
e_s = -0.50
e_s = -0.25
e_s = 0.00
e_s = 0.75
e_s = 1.50
2000
4000
6000
8000
10000
T_x (dynes/cm)

Figure 25. Tension-Strain plot of experiment #65 for the circumferential direction. The complementary plot for the longitudinal direction is shown in figure 26.

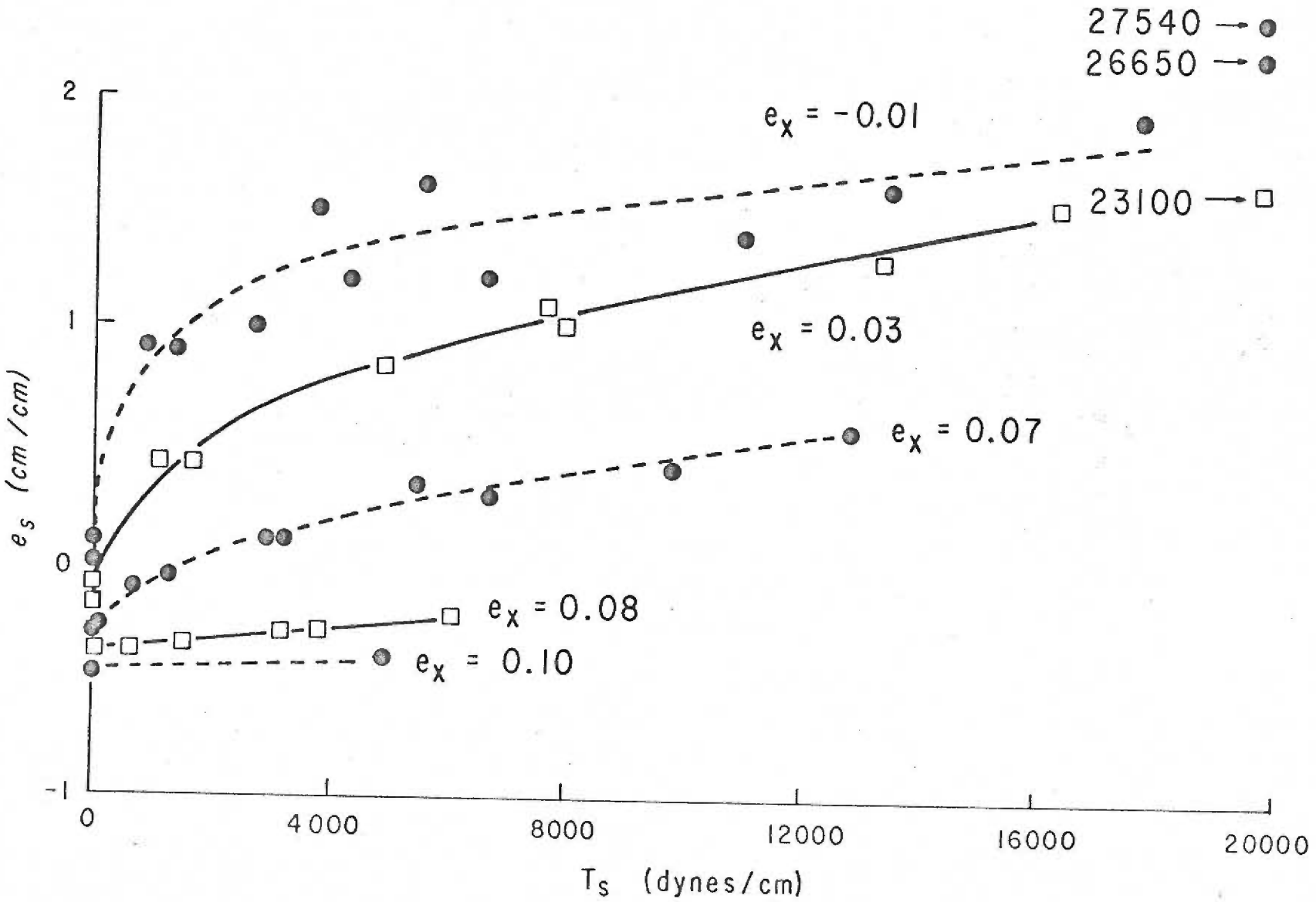
27540
26650
23100
e_x = -0.01
e_x = 0.03
e_x = 0.07
e_x = 0.08
e_x = 0.10
2
1
0
-1
e_s (cm/cm)
0
4000
8000
12000
16000
20000
T_s (dynes/cm)

Figure 26. Tension-Strain plot for experiment #65 for the longitudinal direction. The complementary plot for the circumferential direction is shown in figure 25.

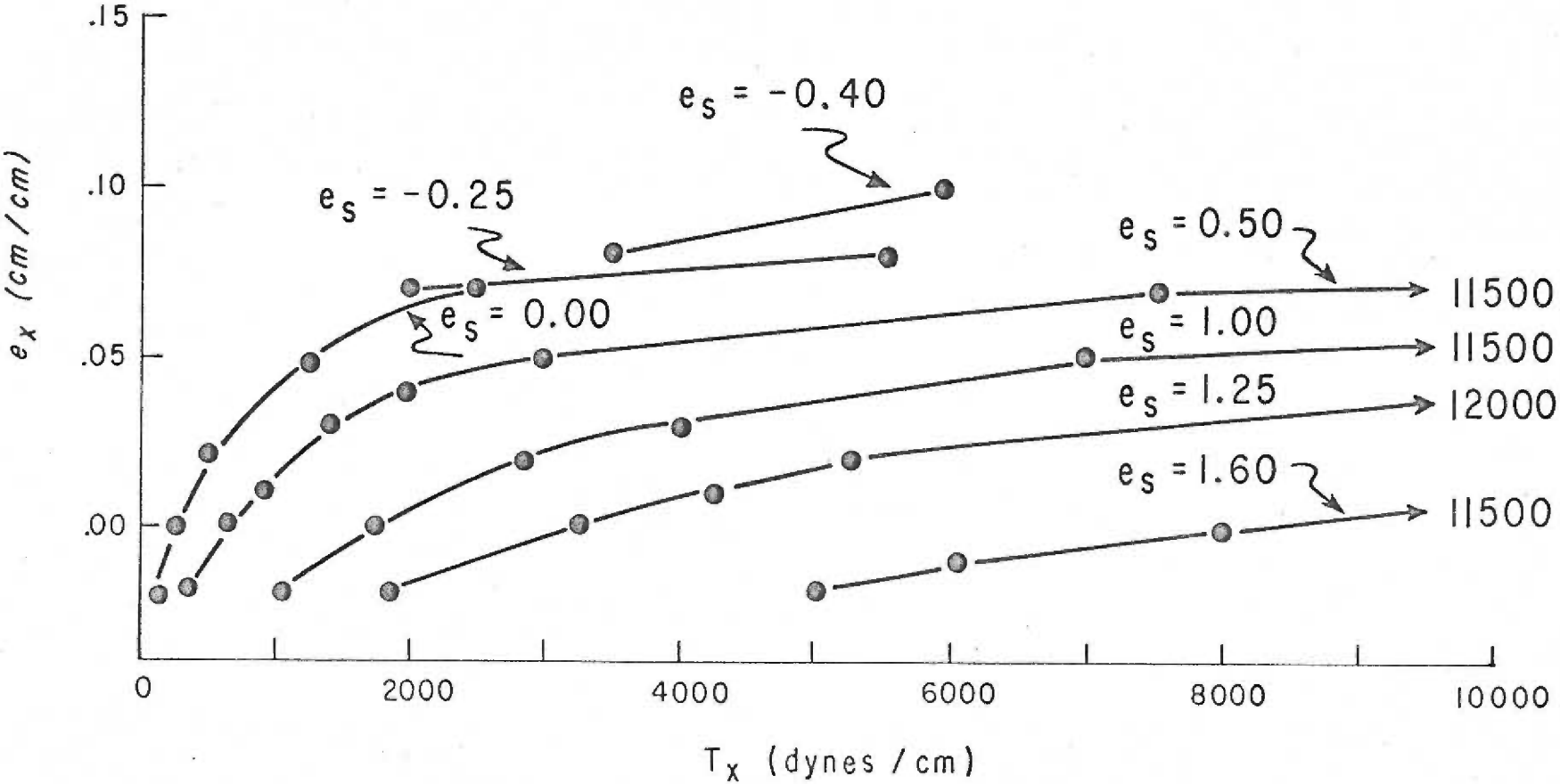
.15
.10
.05
.00
e_x (cm / cm)
e_s = -0.40
e_s = -0.25
e_s = 0.00
e_s = 0.50
e_s = 1.00
e_s = 1.25
e_s = 1.60
11500
11500
12000
11500
0
2000
4000
6000
8000
10000
T_x (dynes / cm)

Membrane "Stiffness"

The pressure-deformation-tension (PDT) results are summarized in the form of Tension-Strain slopes (T-S slopes), infinitesimal (Δ tension/Δstrain) ratios at specified values of circumferential and longitudinal strain, for both principal directions in the membrane (see "Materials and Methods"). The marked non-linearity of the Tension-Strain relationships and the interaction between tensions and strains in the two directions requires the computation of T-S slopes for a series of specified conditions (see tables VI and VII). The longitudinal T-S slopes are computed at "low", "moderate", and "high" circumferential strains, being -0.25, 0.00, and 0.50 cm/cm respectively. Circumferential T-S slopes are similarly reported for "low", "moderate", and "high" longitudinal strains. "High" longitudinal strains refer to values at which circumferential strains changed only slightly under maximum circumferential tension; this value varied for different experiments over the range 0.12-0.20 cm/cm. The "low" longitudinal strain specification refers to near zero strain, and the "moderate" designation refers to strains approximately midway between the low and high strains used in the analysis of that particular experiment.

At each of the specified elongations, the T-S slopes were grouped according to the tension at which they were measured. The

TABLE VI

Circumferential T-S slopes (dynes/cm) as a function of circumferential tension (T_s) at constant longitudinal strain (e_x), and as a function of longitudinal strain at constant circumferential tension. The "high" value of e_x, depending on the experiment, was taken to be a value in the range 0.16 ± 0.04 cm/cm. The "low" e_x values were zero or nearly so, and the "moderate" values were midway between "high" and "low".

	e_x (cm/cm)	Low		Moderate		High
Expt.			T_s (dynes/cm)			
Number	1000	5000	9000	1000	5000	1000
54	4000	11000	---	---	---	32000
55	5500	10500	20500	15000	23000	>50000
60	2000	7500	12500	6500	21000	32000
64	2000	8700	12000	14500	38000	---
65	2700	18000	34000	8500	21000	>50000
66	2600	16500	30000	16500	34000	>50000
67	1500	14000	26000	7000	21000	36000

TABLE VII

Longitudinal T-S slopes (dynes/cm) as functions of longitudinal tension (T_x) at constant circumferential strain (e_s), and of circumferential strain at constant longitudinal tension. The "high, medium, and low" values of e_s used in the analysis are shown in brackets. T-S slopes were taken for low values of T_x where the T-S curves bend sharply ($T_x < 2000$) and for higher values ($T_x > 2000$) where the curves are approximately linear (see figures 24 and 26).

Expt. Number	e_s (cm/cm) Low (-0.25)		Moderate (0.00)		High (0.50)	
	T_x (dynes/cm)					
	< 2000	>2000	< 2000	>2000	< 2000	>2000
54	28000	164000	16000	116000	41000	100000
55	26000	88000	18000	83000	61000	122000
60	30000	75000	20000	91000	33000	138000
64	---	68000	6000	60000	21000	158000
65	---	226000	9000	---	14000	225000
66	47000	122000	41000	180000	45000	150000
67	23000	60000	33000	50000	51000	205000

available values of tension were limited by the experimental design of these studies and the behavior of the membrane.

Estimates of the T-S slopes involved interpolation of graphical data, and reliable estimates could be made in only 7 of the 13 experiments in which elastic parameters were quantitatively measured. Even so, the tables VI and VII could not be entirely completed. The visual estimates of T-S slopes from Tension-Strain plots were deemed reliable to within 10%. As the purpose of such estimates is to permit comparisons of mechanical properties of the membranes with each other and with known structural materials, the combination of analytical and experimental errors offer negligible obstruction to careful interpretation.

The results of table VI indicate that circumferential T-S slopes increase (the membrane becomes "stiffer") with increasing circumferential tension (T_s) at constant longitudinal strain (e_x), and also increase with increasing longitudinal strain at constant circumferential tension. For the data of expt. #67, the T-S slopes evaluated for "low" (near zero) longitudinal strain were found to be 1,500, 14,000, and 26,000 dynes/cm for circumferential tensions of 1,000, 5,000, and 9,000 dynes/cm respectively. Alternatively, for a constant circumferential tension of 1,000 dynes/cm, the T-S slopes were found to be 1,500, 7,000, and 36,000 dynes/cm for "low", "moderate", and "high" values of longitudinal strain respectively.

Analogous behavior was found for the six other fibers. Thus, for a given membrane configuration, attempting to increase membrane dimensions either circumferentially by applying circumferential tension or longitudinally by increasing the longitudinal strain results in increased membrane "stiffness" in the circumferential direction. A similar analysis applied to the data of table VII shows that the membrane "stiffness" in the longitudinal direction is also increased in most instances by increasing either membrane dimension.

In situations where high strains are present in both directions, circumferential T-S slopes tend to approach values determined for the longitudinal direction. For the data of expt. #67 at the highest tension and strain value assessed for each direction, tables VI and VII show the circumferential and longitudinal T-S slopes to be 36,000 and 60,000 dynes/cm respectively. This is in marked contrast to the circumferential and longitudinal T-S slopes determined for the same fiber at the lowest tension and strain combination for each direction, being 1,500 dynes/cm circumferentially and 51,000 dynes/cm for the longitudinal direction. Thus the marked anisotropicity seen in membrane "stiffness" under low deformations is largely negated when high strains are manifest in the membrane material.

Reversibility of Experimental Manipulations

The pressure-deformation-tension (PDT) data sets for a given experiment were collected experimentally as a series of "pressure runs" conducted at constant values of fiber length, as described in "Materials and Methods". The first and last PDT data set in each pressure run involved measurement of the dimensions of the retraction zone segment when the transmembrane pressure gradient was zero. The reproducibility of experimental manipulations was assessed for individual runs and for series of runs by comparing these initial and final PDT data sets.

Individual runs were carried out under conditions in which longitudinal tension and strain were essentially constant. Since the initial and final PDT data sets for a particular run are measured at the same pressure, the deforming forces acting on the membrane are identical for these two measurements. A comparison of zone diameters in the initial and final PDT data sets for a given run therefore permits a test of the reproducibility of circumferential deformations. Data of this nature is summarized in table VIII for three experiments, illustrating examples were the zone diameter at the termination of a run was found to be less than, equal to, or greater than the diameter of the zone before the run began. These results are typical of all fibers examined in this respect, and if any

TABLE VIII

Initial and final values of retraction zone diameter taken from the first and last PDT data sets of individual pressure runs. The runs were recorded at constant zone length and external fiber load. The number of PDT data sets obtained and the maximum diameter recorded during each run are indicated.

Expt. /Run	# PDT data sets	Maximum Diameter (μ)	Initial Diameter (μ)	Final Diameter (μ)
55/1	12	44	18.0	18.0
2	10	18	11.5	-
3	14	17	9.2	9.2
4	8	11	9.2	9.2
5	8	9	8.0	8.0
6	4	8	7.6	7.6
64/1	14	85	21.8	21.8
2	11	37	18.4	18.4
3	10	34	16.1	18.4
4	8	23	16.1	16.1
5	9	17	12.6	13.3
6	10	18	11.5	11.5
7	6	14	10.8	11.5
8	8	11	9.9	9.9
66/1	16	64	23	23
2	9	16	9.2	9.0
3	8	11	8.0	8.0
4	5	8	7.6	7.4

trend was evident, it was toward a slight increase in diameter following a run.

Quantitative measurements obtained in expt. #1 demonstrated that a slow viscous relaxation can be seen in the circumferential

direction, following the immediate elastic adjustment in zone diameter occurring in response to a step change in the transmembrane pressure gradient. The viscous relaxation was seen as a further increase in zone diameter occurring over a period of a few seconds, and eventually resulting in the deformation due to the elastic response being increased by 5-10%. The presence of viscous behavior in the circumferential direction through the membrane material is in agreement with the fact, noted above, that there may be a tendency for diameters to be slightly increased following the circumferential deformation imposed in pressure runs.

Series of runs were conducted at successively longer zone lengths, without being returned to the unstressed condition once longitudinal stresses were imposed. In expts. #12-15, "long" zones in fibers stretched slowly to roughly 200% of rest length over a period of several minutes showed a slight reduction of approximately 10% in their central diameters when returned to resting length. A similar measurement recorded after expt. #67 showed the diameter at rest length to be 14.3μ as compared to a value of 16.1μ recorded before the experiment began. However, the diameter returned to 16.1μ after the transmembrane hydrostatic pressure was raised to 5000 mmHg ten times for intervals of ten seconds. Thus there appears to be a small amount of viscous behavior manifest in the longitudinal direction through the membrane material, analogous to a

similar phenomenon seen to accompany circumferential deformations. All diameter and length measurements were recorded under conditions in which these viscous changes were substantially complete.

Transzone Pressure and Micropipette Radius

Fluid leakage from retraction zones may become significant as the transmembrane pressure is elevated to high values. If such leakage exists, fluid must continually enter through the pipette to maintain constant zone volume. Thus there would exist two resistances to flow arranged in series, each with an accompanying drop in pressure, at the pipette tip and membrane respectively. Therefore, the pressure measured in the external pressure system might not be representative to intrazone pressure. This situation is schematized in figure 27.

It was assumed for PTD data analysis that the external pressure P_1 is equal to intrazone pressure P_2. Direct measurement of flows and resistances through the pipette and zone membrane was not possible. However, the validity of the assumed pressure equivalence on either side of the pipette tip can be partially assessed by comparing PTD data collected in the same or different zones using pipettes of different radius. The pressure drop across the pipette tip is proportional to the reciprocal of the fourth power of the tip diameter, and would therefore differ by 625 : 1 in pipettes of relative diameter

Figure 27. Diagramatic representation of hypothetical resistances to flow through the pressure system and experimental preparation. Resistance to flow through pipette (R_p) is in series with the parallel combination of leakage through the membrane (R_m) and around the site of impalement (R_s).

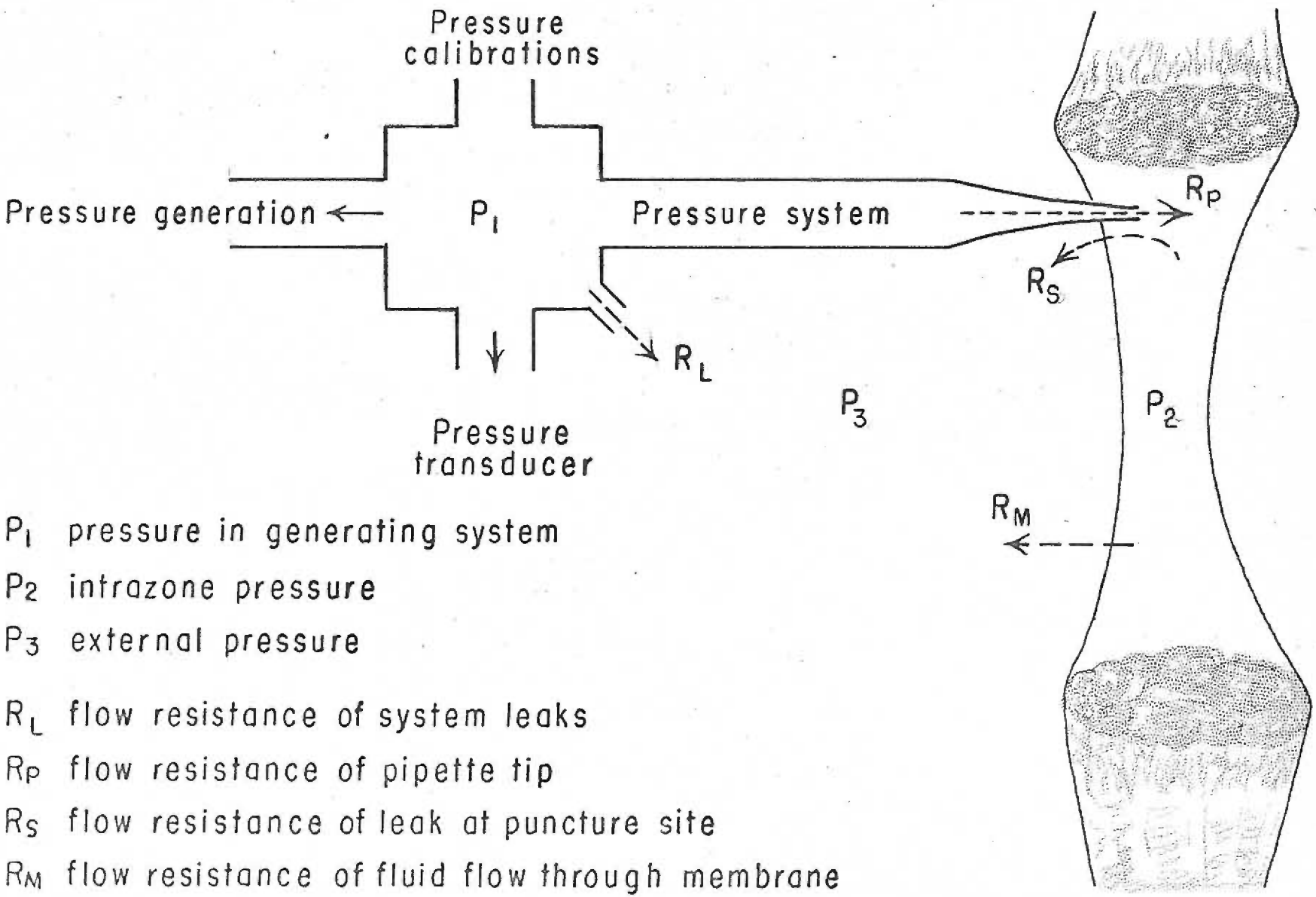

P_1 pressure in generating system

P_2 intrazone pressure

P_3 external pressure

R_L flow resistance of system leaks

R_P flow resistance of pipette tip

R_S flow resistance of leak at puncture site

R_M flow resistance of fluid flow through membrane

1 : 5. The Tension-Strain slopes of tables VI and VII were determined from data acquired using pipettes with inside diameters ranging from less than 0. 2μ (the theoretical limit of resolution of the microscope) to greater than 1. 0μ. If a significant flow resistance existed across pipette tips, the tabulated data from different fibers should differ by several orders of magnitude. This is obviously not the case.

Sarcomere Spacing

Sarcomere spacings were measured at an external fiber load of 4 mg in a population of fibers to provide an independent check of the tension recording system and to furnish a preliminary appraisal of the preparation before damage. The spacings were computed from counts of the number of sarcomeres lying between 20 eyepiece divisions, a single measurement being recorded for each fiber. The measurements were made at a point as far removed as possible from the tendon end of the isolated fiber segment, to avoid nonuniformities in sarcomere length that occur near fiber ends (101). The mean striation spacing was found to be 3. 34μ ±0. 17μ S. D. for 26 fibers varying in radius over the range 18-56μ (mean 33μ ± 8μ S. D.), and is in general agreement with values recently reported by Gordon et al. (102) for isolated fibers from the semitendinosus muscles of Rana temporaria.

Breaking Stress and Breaking Tension

The breaking stress of damaged fibers has been reported in the literature (70). Similar measurements were made in this study for comparative purposes and as a further assessment of preparation credibility. After determining the fiber radius at an external load of 4 mg, the fiber was stretched at a uniform rate, so that fiber length was doubled in approximately one minute. The external force exerted just prior to break was recorded and reduced to the Breaking Stress (force per unit cross-sectional area of the fiber) and the Breaking Tension (force per unit circumference). The cross-sectional area and circumference of the fiber were calculated using the radius of the undamaged fiber at an external load of 4 mg. Table IX summarizes the data for nine experiments indicating that both the Breaking Stress and Breaking Tensions were reasonably reproducible for these fibers, being 1640 ± 270 dynes/cm^2 and 2.75 ± 0.58 dynes/cm respectively.

TABLE IX

Breaking Stress and Breaking Tension determinations for nine fibers containing retraction zones. These values were calculated from the indicated measurements of the force at which the fiber broke under slow uniform stretch, and the radius of the undamaged fiber with an external load of 4 mg.

Expt. Number	Fiber Radius (μ)	Breaking Force (dynes)	Breaking Stress (dynes/cm^2)	Breaking Tension (dynes/cm)
29	33	70	2050	3.38
35	34	58	1590	2.71
36	34	56	1540	2.61
38	34	48	1320	2.24
39	43	74	1270	2.74
42	29	44	1670	2.42
43	38	92	2030	3.85
47	23	28	1690	1.94
65	37	67	1560	2.89

DISCUSSION

Structural Basis of the Observed Mechanical Properties

Retraction zone membrane probably is representative of sarcolemma without its plasma membrane component (24). The plasma membrane and associated layers in the red blood cell have mechanical properties which are insignificant compared to those observed in the present work for muscle (103-105), and there is no reason to suppose the plasma membrane and overlying amorphous layer in muscle subserve mechanical functions. The latter generalization is speculative, but it is not believed to be grossly in error, as it will presently be shown that some particular properties observed in membrane mechanical behavior are best explained as arising from a fibrous network, composed of stiff fibers arranged parallel to one another and in a helical array around the cell, with only minor contributions from other components.

Inspection of figures 23-26, the tension-strain plots for the two principal directions in the membranes observed in expts. #60 and 65, leads to a number of intuitive conclusions suggesting the presence and nature of the proposed fiber network. First, in the plots of longitudinal tensions (T_x) versus longitudinal extensions (e_x) at constant circumference (e_s) (figures 24 and 26), there is obviously a profound interaction between longitudinal and circumferential

elongation, that is circumferential elongation (increasing e_s) at constant longitudinal tension (T_x) results in longitudinal contraction (decreasing e_x). This interaction cannot be explained by membrane fibers oriented parallel and/or perpendicular to the muscle cell axis, because longitudinally directed forces would not exert component forces in the circumferential direction. The directional interaction can be easily explained if fibers were oriented at an angle to both principal axes. A similar directional interaction is seen in the complementary T_s - e_s plots at constant values of e_x (figures 23 and 25).

Secondly, the T - e plots reveal that the membrane is much stiffer longitudinally than circumferentially and, furthermore, the curves for both directions show markedly nonlinear tension-strain characteristics at low elongations which approach linearity at high elongations. Such behavior is difficult to explain in terms of continuous materials showing either very extensible (rubber) or rigid (steel) force-extension characteristics, but is easily explained in terms of a fibrous net possessing the proper architectural arrangement of component fibers (106). It is as if the fibers are predominantly oriented in the longitudinal direction giving rise to higher longitudinal stiffness, and are either markedly nonlinear at low elongations or possess a certain amount of slack that must be taken out before their full (and linear) elasticity becomes apparent. It is also possible that two membrane components are present, a weak

component responsible for behavior at low membrane strains which is overwhelmed by a stiff component, initially slack, but predominating at high strains. It is noteworthy that the initial "slack" can be removed either by stretching the membrane circumferentially or by stretching it longitudinally.

It is difficult to distinguish between the above hypotheses of fiber arrangement. Figure 28-A indicates the mechanical behavior of a fiber with linear force-extension properties and possessing some initial slack. As the length is increased, no force is required until the slack is removed at length L_s, past which further elongation bears a linear relationship to the required force. The addition of a second fiber component of much weaker elastic properties but having no initial slack alters the force-extension diagram to that shown in figure 28-B, where the weak component dictates behavior for lengths less than L_s, and both components are additive for greater lengths (106). A single fiber component having the proper nonlinear force-extension characteristics can exhibit a very similar plot as indicated in figure 28-C, as can a system containing linear fibers with variable initial slack (figure 28-D). Thus force-extension data alone is insufficient to distinguish between these possibilities.

The present treatment describes a fiber network composed of individual fibers with initial slack and linear force-extension characteristics, because this is the simplest hypothesis consistent with

Figure 28. Force- length diagrams of selected one- and two-component fibrous networks. The length axis in each plot is assumed to begin from some reference length not equal to zero. A, one component system where all fibers are parallel, have the same initial slack, and show linear force-length characteristics once the slack has been removed at a legnth L_s. B, same system as A with an additional weak fiber component having no initial slack. C, one component system composed of fibers showing non-linear force extension characteristics and having no initial slack. D, one component system identical to A except that individual fibers have variable amounts of initial slack.

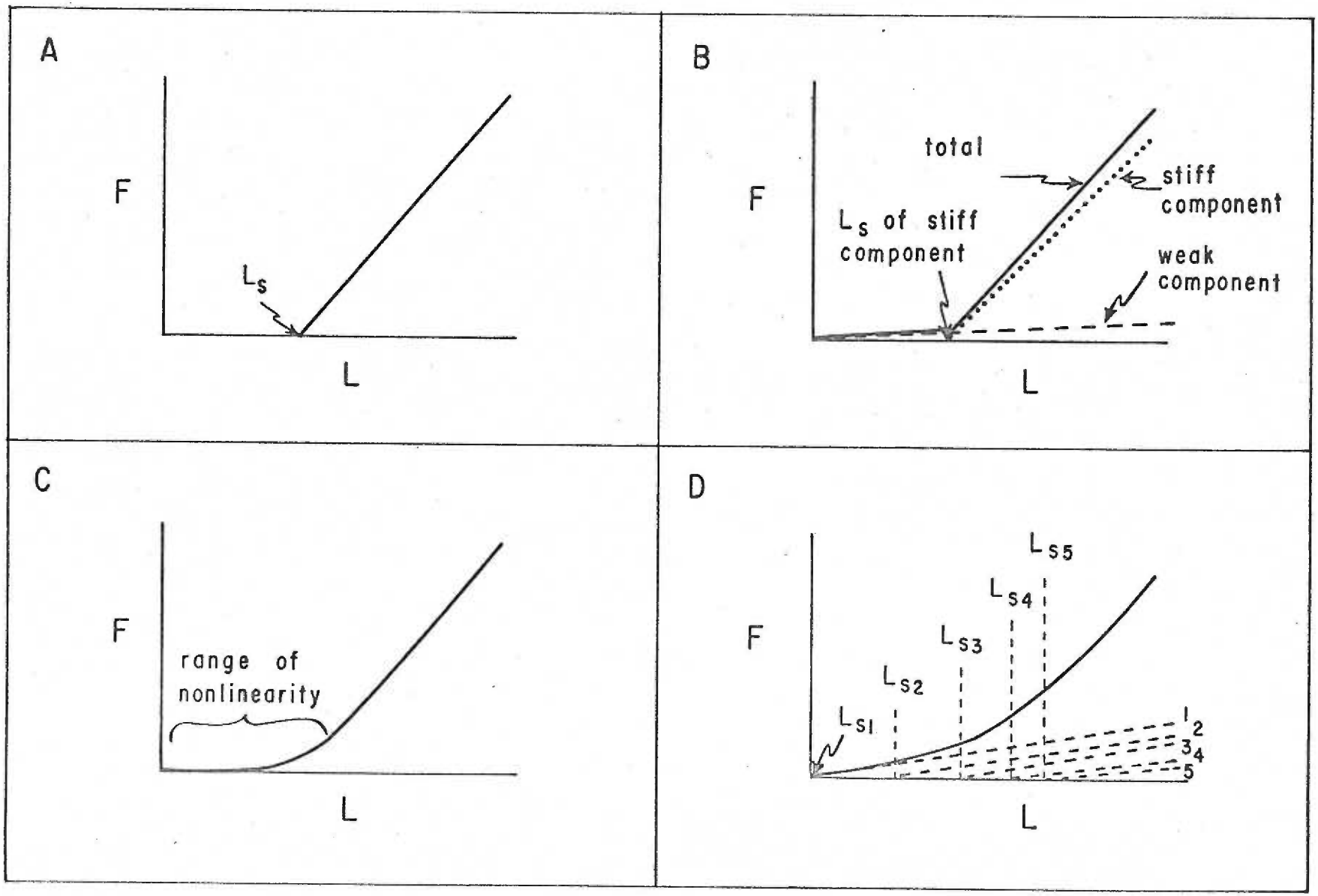
A
F
L_s
L
B
F
total
stiff component
L_s of stiff component
weak component
L
C
F
range of nonlinearity
L
D
F
L_{s5}
L_{s4}
L_{s3}
L_{s2}
L_{s1}
1
2
3
4
5
L

the observed characteristics and the anatomical architecture of the sarcolemma. It must be realized, however, that the analysis will not distinguish between the above hypothetical arrangements. With this reservation, the subsequent treatment describes the required relationships between the initial angle and the degree of slack of the proposed helical fibers and the experimentally observed membrane strains.

Consider the membrane to be composed of two sets of fibers wound in helical fashion around the cell in opposite directions. For simplicity, it is assumed that fibers in each set are parallel and the two sets are at the same angle to the fiber axis at any one time. All membrane deformations are referred to the "unstrained" configuration of the retraction zone. The data is highly suggestive of slack, but note that its presence requires postulating another weaker membrane component, fibrous or nonfibrous, which is responsible for maintaining the unstrained membrane configuration and dictates behavior within the range of slack in the stiffer angular component. An expression is now derived relating the amount of slack and the fiber angle in the unstrained membrane to the longitudinal and circumferential strains under conditions of deformation.

Figure 29 illustrates a "unit square" of "unstrained" retraction zone membrane with longitudinal dimension $x = x_o = 1$ (cm) and circumferential dimension $s = s_o = 1$ (cm). A representative fiber

Figure 29. Geometry of the "unit square". A "unit square" of membrane is indicated as having longitudinal and circumferential dimensions of x and s respectively. In the "unstrained" membrane, the unit square has dimensions $x_o = s_o = 1$ (cm). The portion of a helical fiber associated with the "unstrained" unit square is indicated as having some initial slack, an end-to-end length (neglecting slack) of ℓ_o, and being oriented at an angle θ_o to the x-axis. Membrane deformation results in a deformation of the unit square to dimensions (x, s) from its undeformed dimensions of (x_o, s_o), and is accompanied by a change of coordinates of the end of the helical fiber from (x_o, a) to $(x_o + c, b)$. Following unit square deformation, the helical fiber has some new length ℓ and angle θ_2. Any membrane deformation may be represented as having a circumferential and a longitudinal component, and the strains of the membrane (e_x and e_s) are related to quantities in the unit square by the indicated relationships.

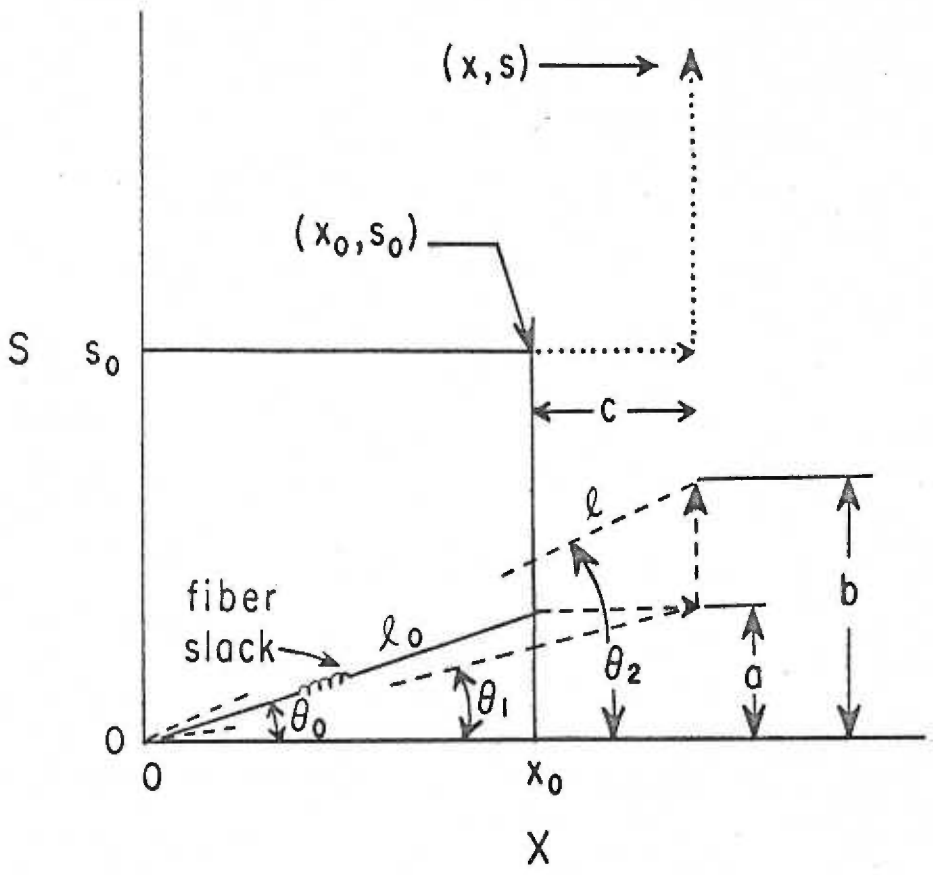

$$e_x = \frac{(x_0 + c) - x_0}{x_0} = \frac{c}{x_0} = \frac{x - x_0}{x_0}$$

$$e_s = \frac{b - a}{a} = \frac{s - s_0}{s_0}$$

component of magnitude ℓ_o in the "unstrained" unit square is depicted having some initial slack and being oriented at an angle θ_o. As the membrane is deformed the corner of the unit square is displaced from an initial position (x_o, s_o) to some new point (x, s). Simultaneously, one end of the helical fiber is displaced from x_o, a) to (x, b), indicated by dashed lines as two component displacements, (x_o, a) to (x, a) and (x, a) to (x, b). The fiber exists at different angles to the fiber axis after each component displacement, indicated as θ_1 and θ_2 respectively. The geometry of the deformation process in terms of the indicated quantities is

$$\tan\theta_o = a/x_o, \tag{1}$$

$$\tan\theta_1 = a/x = (a/x)(x_o/x_o) = (a/x_o)(x_o/x) = (x_o/x)(\tan\theta_o), \tag{2}$$

$$\tan\theta_2 = b/x = (b/x)(a/a) = (b/a)(a/x) = (b/a)(\tan\theta_1). \tag{3}$$

From symmetry considerations

$$(b/a) = (s/s_o) \tag{4}$$

and, therefore

$$\tan\theta_2 = (s/s_o)(\tan\theta_1) = (s/s_o)(x_o/x)(\tan\theta_o); \tag{5}$$

$$\tan\theta_2 = (\tan\theta_o)(s/s_o)/(x/x_o) \tag{6}$$

From the definitions of membrane strains presented in the "Introduction", it can be seen that

$$s/s_o = 1 + e_s \qquad\qquad x/x_o = 1 + e_x, \tag{7}$$

strain plots for the circumferential direction (figures 23 and 25). At constant e_x, the individual curves become stiffer and tend to linearity at high T_s. It is assumed that any slack present in the membrane at low T_s has been removed where the curve is linear. Extrapolation of the curve at high T_s to $T_s = 0$ then gives the value of e_s at which slack was just removed (see figure 28-B) for that particular curve (that particular e_x). Extrapolation of each curve on a particular $(e_s - T_s)$ plot thus gives a set of e_s and e_x values where slack has just been removed. Individual lines on the complementary plot $(e_x - T_x)$ plot can also be extrapolated to the e_x axis for each curve of constant e_s. It is therefore possible to obtain (e_x, e_s) pairs for situations in which $\ell = \ell_s$ from both the $(e_s - T_s)$ and $(e_x - T_x)$ plots for an individual fiber. Plotting $(1 + e_x)_s^2$ versus $(1 + e_s)_s^2$ for data pairs from each plot should, according to equations (14-16), result in a straight line if the proposed structure is truly the basis of the observed behavior. Furthermore, the set of data pairs derived from the $(e_x - T_x)$ plot and the set derived from the complementary $(e_s - T_s)$ plot must predict the same line.

Figure 30 is a plot of the $(x_s/x_o)^2$, $(s_s/s_o)^2$ pairs so obtained from the tension-strain plots of expt. #65, shown in figures 25 and 26 respectively. The line predicted by a linear regression analysis of $(x_s/x_o)^2$ on $(s_s/s_o)^2$ is also shown. The regression line of the figure is analyzed in terms of equation (14) to evaluate the constants

Figure 30. Plot of $(x_s/x_o)^2$ versus $(s_s/s_o)^2$ for the data of expt. #65. See the text for details of the analysis theory. The data of expt. #65 is plotted in terms of equation (14); the solid line represents the linear regression line for $(x_s/x_o)^2$ on $(s_s/s_o)^2$ by the method of least squares. Data points derived from the circumferential tension-strain plot (figure 25) are indicated as a circle (O), those derived from the longitudinal tension-strain plot (figure 26) by dots (●). The present plot is analyzed in terms of the $(x_s/x_o)^2$ intercept (equal to ℓ_s^2) and the slope ($\tan^2 \theta_o$) of the regression line. ℓ_s represents the predicted length at which slack is just removed from the helical fibers, in relation to the abscissa of the "unstrained" unit square (x_o). θ_o represents the angle between the helical fibers and the longitudinal direction of the muscle cell in the "unstrained" unit square.

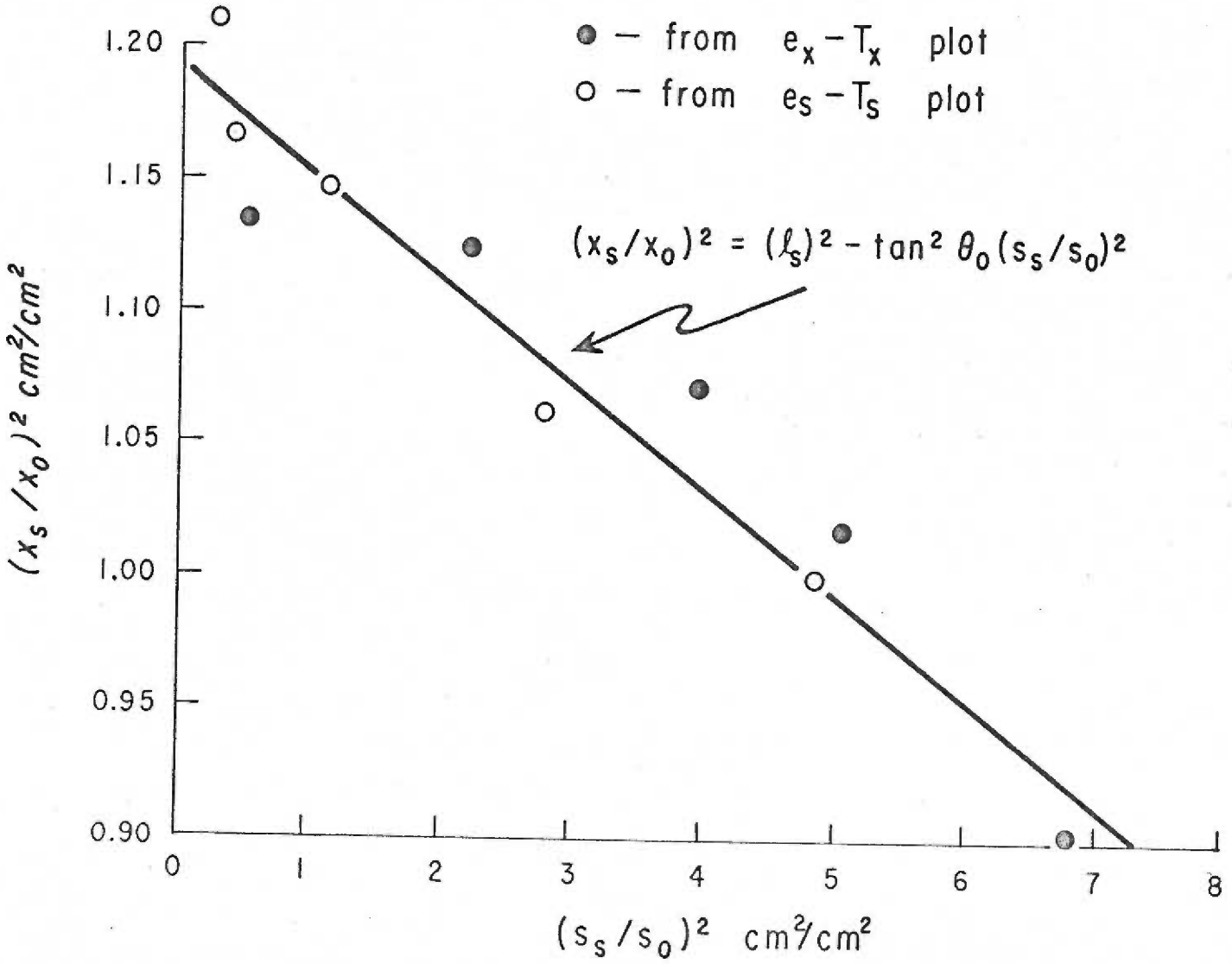
● — from $e_x - T_x$ plot
○ — from $e_s - T_s$ plot
$(x_s/x_0)^2 = (\ell_s)^2 - \tan^2\theta_0 (s_s/s_0)^2$
$(x_s/x_0)^2$ cm²/cm²
$(s_s/s_0)^2$ cm²/cm²
1.20
1.15
1.10
1.05
1.00
0.95
0.90
0
1
2
3
4
5
6
7
8

ℓ_s and θ_o describing properties of the helical fibers of this particular membrane. The $(x_s/x_o)^2$ intercept defines the constant $(\ell_s)^2$, from which ℓ_s is found. The constant ℓ_s (cm/cm) represents the length of the helical fibers at which the slack is just removed, relative to the length of the abscissa of the "unstrained" unit square, x_o. The slope of the line of figure 30 represents $-\tan^2\theta_o$, where is the angle between the helical fibers and the longitudinal direction in the "unstrained" unit square. By this procedure, it is found that ℓ_s = 1.10 and θ_o = 11° for the data of expt. #65. Further analysis indicated that the predicted value of 11° for θ_o could range from only 10° to 12° for ±1 SEM of $\tan^2\theta_o$. Thus there is sufficient agreement indicated between the helical fiber hypothesis and the experimental data.

Once θ_o is known, the length of the helical fibers in the unstrained unit square, ℓ_o, can be determined, since $\cos\theta_o = (x_o/\ell_o)$ (see figure 29). Furthermore, the amount of extension of the helical fibers required to remove the initial slack $(\ell_s - \ell_o)$ can be evaluated. The latter quantity is designated as the "percent slack" and is calculated as $100(\ell_s - \ell_o)/(\ell_o)$. For the data of expt. #65, it is found that ℓ_o equals 1.02 and the percent slack equals 7.9.

Similar results were obtained from the data of seven experiments in which enough "pressure runs" were recorded to allow a sufficient number of (x_s, s_s) pairs to be calculated. The data of

each experiment was subjected to two regression analyses, $(x_s/x_o)^2$ on $(s_s/s_o)^2$ and vice versa, and the standard error of the regression coefficient was evaluated in each case. These results are summarized in table X. The low values found for the standard errors of the regression slopes provide satisfactory support for the contention that the $(x_s/x_o)^2$, $(s_s/s_o)^2$ data pairs show a linear relationship for a given experiment, as predicted by the proposed helical fiber architecture of membrane structure.

The slopes predicted by the two regression analyses applied to the data of a given experiment were evaluated to determine θ_o, and from the regression intercepts two values of ℓ_s were obtained. A singular value for ℓ_s and for θ_o for a particular experiment was then obtained by averaging the respective quantities found from the two regression calculations. The average ℓ_s and θ_o found for seven experiments are summarized in table XI, as are the quantities ℓ_o and percent slack evaluated therefrom.

Force-Extension Properties of the Helical Fibers

The proposed structural hypothesis assumes that the individual helical fibers in the membrane exhibit a linear force-extension relationship if stretched sufficiently to remove their initial slack. Since the angle θ between the helical fibers and the longitudinal direction in the membrane can be calculated for all membrane configurations

TABLE X

Summary of $(x_s/x_o)^2$ versus $(s_s/s_o)^2$ linear regression analysis. The values found for the angle between the helical fibers and the cell axis in the unstrained membrane (θ_o) and the length at which the initial slack in the helical fibers is just removed (ℓ_s) relative to the abscissa of the unstrained unit square are indicated for the regressions of $(x_s/x_o)^2$ on $(s_s/s_o)^2$ and vice versa. The range of θ_o for ±1 SEM of the regression slope are shown in parentheses.

	$(x_s/x_o)^2$ on $(s_s/s_o)^2$		$(s_s/s_o)^2$ on $(x_s/x_o)^2$	
Expt.	θ_o(degrees)	ℓ_s(cm/cm)	θ_o(degrees)	ℓ_s(cm/cm)
54	13 (11-15)	1.07	15 (13-17)	1.09
55	13 (11-14)	1.05	13 (12-15)	1.06
60	10 (9-12)	1.08	11 (10-12)	1.09
64	8 (6- 9)	1.04	8 (7- 9)	1.05
65	11 (11-12)	1.09	12 (11-12)	1.10
66	9 (7-10)	1.06	11 (10-11)	1.06
67	6 (3- 8)	1.04	7 (6-11)	1.05

TABLE XI

Summary of the slack: Angle analysis of the proposed helical fibers. The slope and intercept of the two regression analyses conducted on each experiment, $(x_s/x_o)^2$ on $(s_s/s_o)^2$ and vice versa, were evaluated to predict ℓ_s and θ_o. The two ℓ_s values predicted for a given experiment were then averaged as were the two values for θ_o, and these average values are reported below. The quantities ℓ_o and percent slack, obtained from the average ℓ_s and θ_o, are also indicated. See text for details of calculation.

Expt.	θ_o (degrees)	ℓ_s (cm/cm)	ℓ_o (cm/cm)	% slack
54	14	1.08	1.03	5
55	13	1.06	1.03	3
60	11	1.09	1.02	7
64	8	1.04	1.01	3
65	11	1.10	1.02	8
66	10	1.06	1.02	4
67	7	1.05	1.01	4

(see the previous section) and the force-extension properties of the membrane have been determined, sufficient data is on hand to determine the forces and extensions parallel to the helical fibers for various states of membrane deformation. It is therefore possible to evaluate the force-extension properties of the helical membrane fibers, and to verify that the experimental data is compatible with the assumption that the elastic behavior of the helical fibers is linear. The following treatment develops the relationships describing the force-extension properties of the helical membrane fibers in terms of tensions and strains in the retraction zone membrane.

If all helical fibers at a particular zone cross-section are considered at once, then the total force F acting parallel to the membrane fibers is

$$F = F_x/\cos\theta = T_x(\pi D)/\cos\theta \qquad (17)$$

where, from equation (8)

$$\theta = \arctan\left[\tan\theta_o(1 + e_s)/(1 + e_x)\right] \qquad (18)$$

and

F = force parallel to the membrane fibers (dynes),
F_x = force in the longitudinal direction in the membrane (dynes),
T_x = tension in the longitudinal direction in the membrane (dynes/cm),
D = diameter of the cylindrical retraction zone segment (cm),
e_s = circumferential strain of retraction zone membrane (cm/cm),
e_x = longitudinal strain of retraction zone membrane (cm/cm).

From equation (9), the length ℓ of the helical membrane fibers associated with a unit square of membrane is

$$\ell = [(x/x_o)^2 + (x/x_o)^2(\tan^2\theta)]^{\frac{1}{2}} \quad (19)$$

where, from equation (15),

$$(x/x_o) = (1 + e_x) \quad (20)$$

and, from equation (8),

$$\tan\theta = \tan\theta_o(1 + e_s)/(1 + e_x). \quad (21)$$

In the unstrained membrane, the helical fibers are somewhat slack, and do not resist extension until their length ℓ (cm/cm) in the unit square rises from its initial value of ℓ_o to the length at which slack is just removed, ℓ_s. For lengths ℓ greater than ℓ_s, we have

$$F = K(\ell - \ell_s) \quad (22)$$

where K is the proportionality constant relating force and extension along the axis of the helical fibers, considering all such fibers around the cell at a particular cross-section collectively. Therefore, a plot of the experimental data in terms of total fiber force (F, equation 17) versus extension (ℓ, equation 19) should, according to equation (22), yield a straight line with slope K and an ℓ-intercept of ℓ_s.

Figure 31 presents a force-extension plot of the experimental data from expt. #65, using the values of ℓ_s and θ_o obtained from the $(x_s/x_o)^2$ versus $(s_s/s_o)^2$ plot (figure 30). A straight line has been drawn through the predicted length at which slack is removed from the helical fibers (ℓ_s = 1.10, table XI) and the scatter of data points

Figure 31. Force-extension curve of the helical membrane fibers for the zone segment of expt. #65. Ordinate; the total force (dynes) exerted for all helical fibers, considered collectively at a given cross-section of the muscle fiber. Abscissa; the length of the helical fibers relative to the abscissa of the unstrained "unit square". The data points were calculated as described in the text. A distinctive symbol is used to designate all of the data points arising from a particular "pressure run". The solid line represents the predicted linear force-extension relationship of the helical fibers. The line was drawn through the calculated abscissa length ℓ_s at which the slack in the helical fibers is just removed, (table XII, expt. #65), and through the scattered data points at high values of force. The value of ℓ_o represents the length of the helical fibers in the unstrained "unit square", where $x_o = 1.00$.

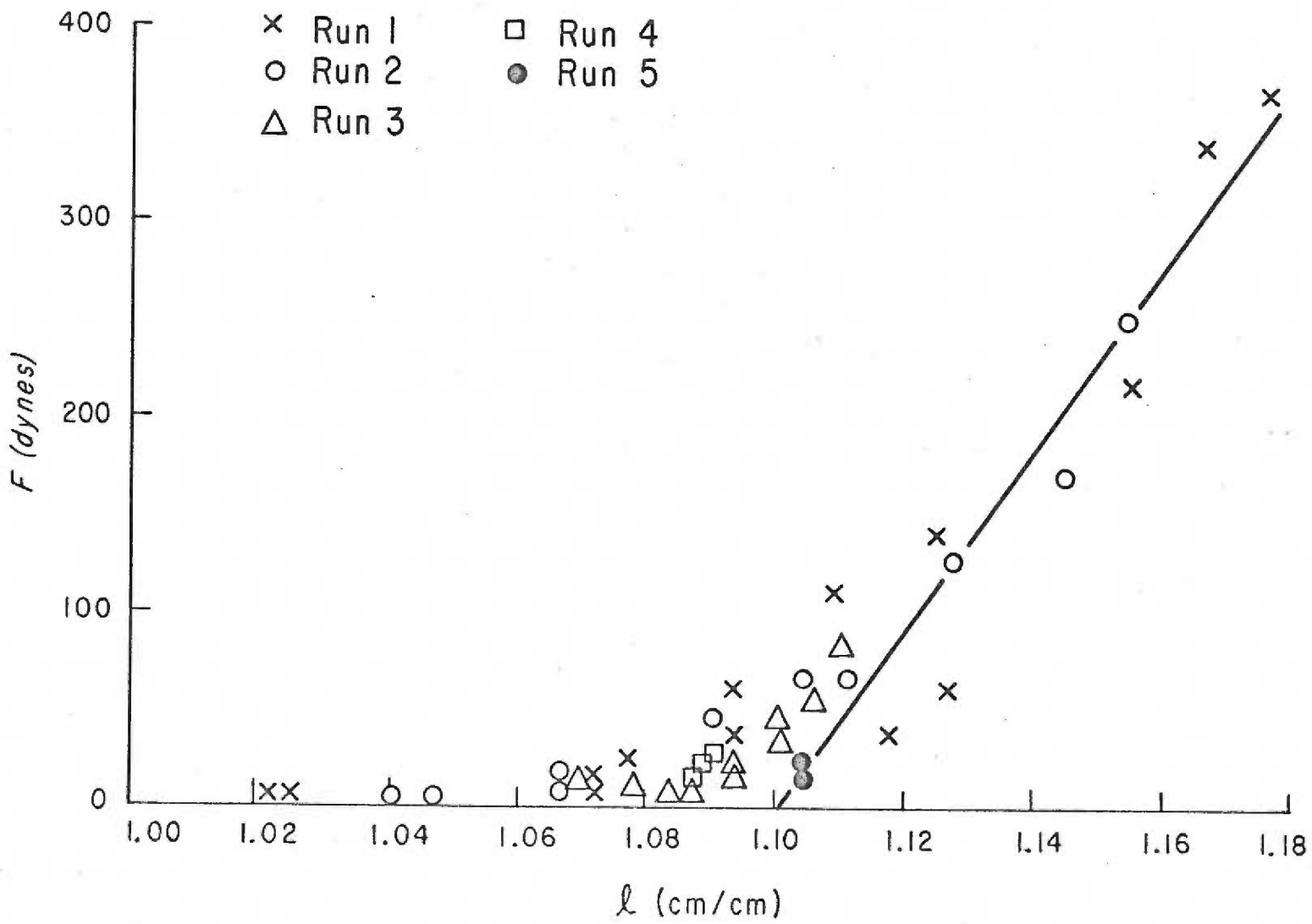
Run 1
Run 2
Run 3
Run 4
Run 5
400
300
200
100
0
F (dynes)
1.00
1.02
1.04
1.06
1.08
1.10
1.12
1.14
1.16
1.18
ℓ (cm/cm)

for helical fiber lengths greater than ℓ_s. The results shown in figure 30 are compatible with the predictions, as the data points are in reasonable agreement with the straight line force-extension hypothesis for lengths ℓ greater than ℓ_s. Similar results were found for the six other experiments in which $(x_s/x_o)^2$ versus $(s_s/s_o)^2$ data could be obtained. It is important to note that similar points on the force-extension curve were derived from data collected at widely different membrane configurations ("pressure runs" 1-5).

The data in figure 31 indicates that the helical membrane fibers can withstand forces of several hundred dynes. These values were obtained for membrane configurations in which the angle θ between the helical fibers and the longitudinal direction in the membrane was large (runs 1 and 2). The hypothesis of helical fiber structure postulates that these helical fibers are responsible for the principal membrane rigidity and therefore carry the burden of membrane loads. It is paradoxical that in highly stretched muscle cells containing retraction zones, where the angle θ of the helical fibers is small, cell rupture occurs in zone regions with external forces on the muscle cell of less than 100 dynes (see Results). It is improbable that the breaking strength of the fibers depends on their orientation in the membrane. It is possible that the helical fiber strands do not run the entire length of the muscle cell, but instead shorter

fiber strands are periodically interconnected. If this is the true arrangement, it would appear that the breaking stress of the molecular bonds responsible for helical fiber interconnection depends on the angle θ between the helical fibers and the cell axis.

The force-extension data points indicated in figure 31 for lengths approximately equal to or less than ℓ_s show deviations from the estimated force-extension line. The departure from force-extension linearity at low values of force was anticipated in the previous section, and was attributed to either helical fiber nonlinearity or variable slack, or as being due to the contribution of a second mechanical component of the membrane (see figure 28). Nonlinearity of the force-extension properties of the helical fibers or variations in helical fiber slack should result in a unique force-extension relationship for low forces as well as for high forces, as shown in figure 28. Thus, the large scatter of the data points seen in figure 31 for expt. #65 and in force-extension data from other experiments cannot be explained in terms of the nonlinear elasticity or variable slack hypotheses. In contrast, the force-extension data for a given "pressure run" does tend to indicate a unique force-extension curve even at low forces. This result can be explained by contributions of a second membrane component. It therefore appears that the hypothesis of a linearly elastic fiber with a fixed amount of initial slack in undeformed membrane, chosen for mathematical simplicity,

represents the most logical choice in light of the experimental data.

Constraint of Cell Volume

The treatment applied to the simple assumption of a helical arrangement of restraining fibers in the sarcolemma has resulted in a reasonably complete description of the geometry and elastic properties of these fibers. Their lengths and angular position have been calculated for the unstrained retraction zone and general equations were derived that specify these magnitudes in any other membrane configuration. The "slack" of the fibers in the unstrained retraction zone was calculated, and it can be shown that the elastic properties of the fibers are like those of collagen (see Appendix II).
It must now be shown that the proposed geometry adequately accounts for the passive behavior of intact muscle cells and whole muscle.

The proposed structural arrangement requires presence in the membrane of a weak elastic component (not necessarily fibrous) in addition to a stiff helical component. Deformations in the range of membrane configurations for which the helical component is slack ($\ell \leqslant \ell_s$) requires very low forces (see figure 31), whereas once the helical fibers become taut, rather stiff stress-strain behavior is manifest. Thus for weak forces, an area constraint is imposed on a "unit square" of membrane, the possible configurations limited to values for which the helical fiber length ℓ is less than or equal to ℓ_s.

An area constraint imposed on retraction zone membrane implies a volume constraint on cylinder volume. The implications of this latter phenomenon are presently considered.

We assume that deformation of a unit square of membrane is limited under low stresses by the inextensibility of the helical fibers, that is, a fiber of length ℓ_o in the unit square is limited to a length of ℓ_s. If we define L_o and R_o as the unstrained length and radius of the cylindrical membrane segment of a long retraction zone, and L and R as any deformed zone dimensions, then

$$L/L_o = x/x_o \qquad L = (L_o)(x/x_o) \tag{23}$$

$$R/R_o = s/s_o \qquad R = (R_o)(s/s_o) \tag{24}$$

From equation (13), remembering that ℓ is dimensionless (cm/cm), it is found that

$$\ell^2 = (x/x_o)^2 + (s/s_o)^2(\tan^2\theta_o) \tag{25}$$

for any ℓ, or substituting equations (23) and (24), we find

$$\ell_s^2 \geqslant \ell^2 = (L/L_o)^2 + (R/R_o)^2(\tan^2\theta_o) \tag{26}$$

for any ℓ within the constrained region of fiber length, $\ell \leqslant \ell_s$.

The volume V of a cylindrical segment of retraction zone is given by

$$V = \pi R^2 L \tag{27}$$

or

$$R^2 = V/(\pi L) \tag{28}$$

Substitution of equation (28) into equation (27) yields

$$\ell_s^2 \geq \ell^2 = (L/L_o)^2 + (V/\pi L)(\tan^2\theta_o)/(R_o^2) \tag{29}$$

and rearranging, remembering that $(\pi R_o^2 L)/(\tan^2\theta_o) > 0$, we find

$$[\ell_s^2 - (L/L_o)^2](\pi R_o^2 L)/(\tan^2\theta_o) \geq V \tag{30}$$

or $$V \leq (\pi R_o^2 L)(\ell_s^2)/(\tan^2\theta_o) - (R_o^2 L^3/L_o^2)(\pi)/(\tan^2\theta_o). \tag{31}$$

The latter expression specifies the range of volumes that are possible without stretching the helical fibers.

The maximum volume of the cylinder permitted by the condition $\ell \leq \ell_s$ can be found by differentiating equation (31) with respect to L and setting the results equal to zero.

Thus

$$\frac{dV}{dL} = \frac{d}{dL}\left[\frac{(\pi R_o^2 L)(\ell_s^2)}{\tan^2\theta_o} - \frac{(R_o^2 L^3/L_o^2)(\pi)}{\tan^2\theta_o}\right] \tag{32}$$

or $$0 = (\pi R_o^2)(\ell_s^2)/(\tan^2\theta_o) - (R_o^2)(L/L_o)^2(3\pi)/(\tan^2\theta_o). \tag{33}$$

Solving for (L/L_o) and recalling equation (23), we find

$$(\ell_s^2/3) = (L/L_o)^2 = (x/x_o)^2, \tag{34}$$

and $$(x/x_o) = (L/L_o) = 0.58\,(\ell_s). \tag{35}$$

Equation (35) states that the relative elongation of a given segment of retraction zone at maximum volume is a unique function of the degree of slack in the helical fibers, and occurs when the angle between the longitudinal direction and the helical fibers is equal to 55 degrees ($\cos\theta = 0.58$).

By an analogous procedure, the corresponding expression for (R/R_o) can be derived by solving equation (27) for L and substituting the results into equation (26). By this method, it is found that

$$(R/R_o) = 0.82\,(\ell_s)/(\tan\theta_o) \qquad (36)$$

which relates the cylinder radius at maximum volume relative to the radius at rest length to the degree of slack and initial angle of the helical fibers in the unstrained membrane.

The values of ℓ_s and $\tan\theta_o$ for seven fibers, obtained from table XI, are listed in table XII with the corresponding relative zone segment lengths and radii predicted for maximum retraction zone segment volume by equations (35) and (36). It is extremely interesting to realize that the (L/L_o) values found, ranging from 0.60 - 0.64 cm/cm, are in good agreement with the relative lengths of normal fiber regions as compared to retraction zone regions reported by Buchthal (69) to be 0.3 - 0.5 if allowance is also made for the breakdown of membrane festooning. Also, the average value for the ratio of the radius at rest length to that at maximum zone segment volume, the reciprocal of (R/R_o), is found to be 0.21 ± 0.05 cm/cm S.D. for the seven fibers in table XII. This finding is in remarkable agreement with the value found in the present work for the ratio of the diameter of the unstrained retraction zone to the normal fiber diameter at rest length, reported in the Results section to be 0.22 ± 0.03 cm/cm S.D. The present treatment suggests that the normal fiber

TABLE XII

Lengths (L) and Radii (R) of cylindrical retraction zone segments relative to their dimensions in the "unstrained" zone (L_o and R_o respectively) for the condition of maximum segment volume. The length of a representative helical fiber in a "unit square" of membrane at which its slack is just removed (ℓ_s) and the tangent of its angle in the unstrained membrane ($\tan\theta_o$), found from table XI, are also indicated.

Expt. #	ℓ_s(cm/cm)	$\tan\theta_o$	L/L_o(cm/cm)	R/R_o(cm/cm)
54	1.08	0.25	0.63	3.5
55	1.06	0.23	0.61	3.8
60	1.09	0.19	0.63	4.7
64	1.04	0.14	0.60	6.1
65	1.10	0.19	0.64	4.7
66	1.06	0.18	0.61	4.8
67	1.05	0.12	0.61	7.2

at rest length is residing at a diameter which maximizes the volume permitted without stretching of the helical membrane fiber components.

The Role of the Helical Fibers in the Growth and Function of Muscle

Our interpretation of the experimental results indicated that in intact muscle cells at rest length the angle between the helical fibers and the longitudinal direction of the cells is the angle which permits the maximal cylindrical volume for a given length of helical fiber. It is logical to assume that this is not a fortuitous coincidence, but is a natural result of embryological development of muscle and a necessity for its normal function.

The skeletal musculature of the limbs is derived from the mesenchyme of the limb buds. The first evidence of differentiation is the elongation of the cell nuclei and cell bodies to form myoblasts, the precursors of muscle fibers (107). As the myoblast develops, growth in the longitudinal direction occurs, and cross-striated myofibrils appear in the sarcoplasm. (The same phenomenon accompanies regeneration of sarcoplasm with the old sarcolemma following damage). The ultimate increase in diameter seen during the maturation of a fiber, following the appearance of typical muscle fiber histology, is three times or more (45). It seems reasonable to speculate that in the increase in cell volume is at least partially accommodated by a rearrangement of the surrounding helical fibers before these fibers themselves are required to grow, and before the growth process of the cell in inhibited by the elastic tension

generated when the helical fibers are stretched. The helical fibers would thus be compelled to assume an angle which permits maximum volume as a consequence of normal development. The alternative hypothesis, that the helical fibers are deposited after cell growth has ceased at an angle which happens to permit maximal internal volume, seems much less plausible.

The hypothesis of helical fiber structure follows from our interpretation of the data. In addition, Draper and Hodge (3) observed a system of helically arranged collagen fibrils in electron micrographs of frog leg muscles, and a similar system can be seen in the electron micrograph of figure 1-B taken from the work of Reed and Rudall (31). The present demonstration that this structural arrangement can be explained by a simple embryological mechanism is not yet sufficient justification for the acceptance of the proposed mechanical interpretations of membrane fibril architecture. It is obvious from the preceding chapters that the muscle component under investigation is the element which is commonly referred to as the "parallel elastic component" of striated muscle (7), or is at least a significant portion thereof. It remains to be shown, therefore, that the interpretation given to the data leads to predictions regarding the passive behavior of muscle which are consistent with generally accepted facts.

It was noted in the preceding section that the radius of a

cylindrical segment of retraction zone membrane at the maximum volume permitted without straining the helical fibers was equal to the radius of intact muscle cells at rest length, within the limits of experimental error. The length of the retraction zone membrane at which maximum volume occurred was, if anything, a little too long compared to the length of resting muscle cells, judged by the data of Buchthal (69) relating retraction zone and intact fiber segment lengths. In the following pages, the mathematical relationships between volume, length, and radius of the retraction zone will be shown to explain these results and to define the passive behavior of striated muscle.

Figure 32 shows a plot of the "volume constraint" curve, derived from equation (29) in the preceding section, for the retraction zone segment investigated in expt. #65. This curve defines the maximum volume V that the zone segment can occupy for a given relative length (L/L_o) without requiring stretch of the helical fiber component of the membrane. The equation defining this "volume constraint" curve is derived as follows. From equation (29), the length of a helical fiber associated with a "unit square" of membrane ℓ was shown to be related to the volume of the retraction zone segment by the following expression:

$$\ell^2 = (L/L_o)^2 + (\tan^2 \theta_o / R_o^2)(V)/(\pi L), \qquad (37)$$

where all quantities have been previously defined. Solving for V, we

Figure 32. Volume constraint curve for the retraction zone segment of expt. #65. The solid line shows the maximum relative volume (V/V_o) that the zone segment of expt. #65 can occupy without stretching the helical membrane fibers as a function of the relative length (L/L_o) of the zone segment. The curve is a plot of equation (42) derived in the text. The dashed line indicates the maximum zone volume permitted by the volume constraint consideration, which occurs at (L/L_o) = 0.64 cm/cm. Vertical dashed lines bracket the "functional range" of muscle fiber behavior (see text). The dotted line is drawn through the average volume predicted by intercepts of the "functional range" limits and the volume constraint curve, and represents the "actual" cell volume V_c. Sarcomere lengths are indicated on the abscissa, determined by taking the longest sarcomere length at which maximum myofilament overlap occurs in single sarcomeres, 2.25μ, as the rest length of the cell predicted by the volume constraint consideration (L/L_o = 0.64 cm/cm).

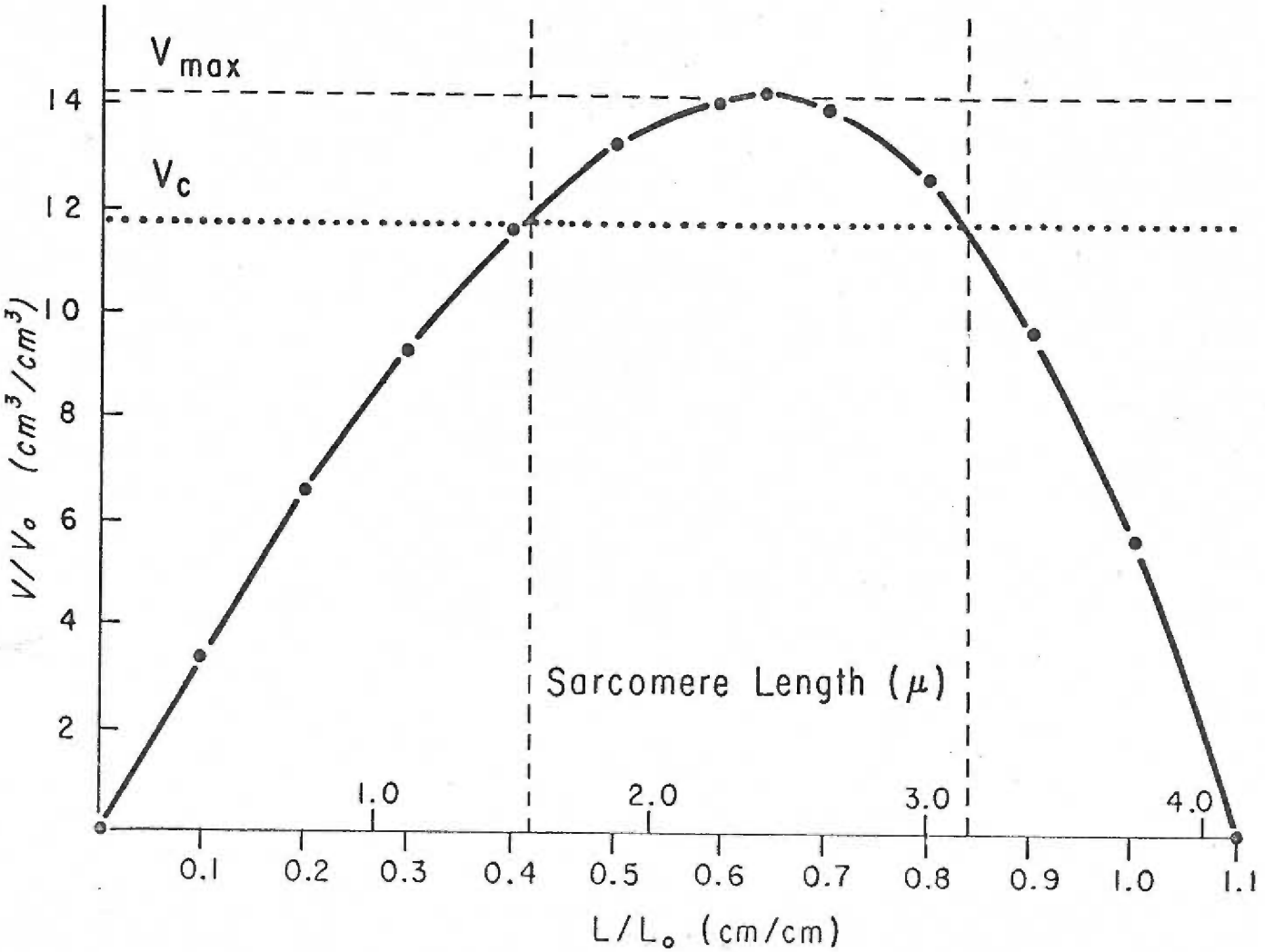
V_{max}
V_c
14
12
10
8
6
4
2
V/V_o (cm^3/cm^3)
Sarcomere Length (μ)
1.0
2.0
3.0
4.0
0.1
0.2
0.3
0.4
0.5
0.6
0.7
0.8
0.9
1.0
1.1
L/L_o (cm/cm)

find that

$$V = [\ell^2 - (L/L_o)^2] (\pi R_o^2 L)/(\tan^2 \theta_o). \quad (38)$$

Since R_o and L_o represent the radius and length of the "unstrained" retraction zone segment, V_o will be defined as the volume of the "unstrained" zone, and

$$V_o = \pi R_o^2 L_o . \quad (39)$$

The volume of the zone relative to the volume of the "unstrained" zone is then found by dividing equation (38) by equation (39):

$$V/V_o = [\ell^2 - (L/L_o)^2] (L/L_o)(\ell/\tan^2 \theta_o). \quad (40)$$

To define the zone volume for any zone configuration in which the slack in the helical fibers (ℓ_s) has just been removed, the substitutions $V = V_s$ and $L = L_s$ are made, where V_s is any zone volume in which the helical fiber length is ℓ_s:

$$V_s/V_o = [\ell_s^2 - (L/L_o)^2] (L/L_o)(\ell_s/\tan^2 \theta_o). \quad (41)$$

For the fiber of experiment #65, it is found from table XII that $\ell_s = 1.10$ cm/cm and $\tan^2 \theta_o = 0.036$. Substituting these quantities into equation (41) defines the "volume constraint" curve for the zone segment of expt. #65, which after simplification is given by

$$V_s/V_o = 33.6(L/L_o) - 27.7(L/L_o)^3. \quad (42)$$

The "volume constraint" curve of figure 32 is a plot of the dimensionless variables (V_s/V_o) versus (L/L_o) in terms of equation (42).

The figure shows that the membrane investigated in expt. #65 shows a maximum volume at a relative zone segment length (L/L_o) of 0.64 cm/cm, the value reported in table XII.

Ramsey and Street (25) found that there was complete reversibility of both active and passive tensions and a constant value for the amount of work done per unit of fiber shortening in single muscle fibers, for cell lengths between 70% and 140% of the resting length. These limits are therefore chosen as the "functional range" of the muscle fiber for the present discussion. This range is indicated in figure 32 by the vertical dashed lines, taking rest length of the intact muscle fiber as the length of maximum segment volume. The volume constraint curve for the helical fibers has a rather sharp peak, and drops to considerably lower values at the lower and upper limits of the "functional range".

The "lattice" volume occupied by the array of myofilaments making up the myofibrils of striated muscle remains constant for sarcomere lengths over the "functional range" (108). It therefore seems reasonable to assume that the volume of the muscle fiber as a whole also remains constant over this range of cell lengths. The preceding analysis shows that the cell at rest length exists at a radius which maximizes the volume permitted by the unstrained helical membrane fibers. As a consequence, this volume can only be accommodated by a stretch of the helical fibers when the length of

the cell deviates from rest length in either direction. It is therefore necessary to calculate the approximate forces in the helical fibers at either end of the functional range.

The amount of stretch in the helical fibers required for the cell volume to remain constant over the "functional range" of cell lengths can be estimated from equation (41), which after expansion of the terms is given by

$$V/V_o = (\ell^2)(L/L_o)(\ell/\tan^2\theta_o) - (L/L_o)^3(\ell/\tan^2\theta_o). \quad (43)$$

Solving for ℓ^2, we find that

$$\ell^2 = [(V/V_o) + (L/L_o)^3(\ell/\tan^2\theta_o)](L_o/L)(\tan^2\theta_o) \quad (44)$$

or

$$\ell^2 = (V/V_o)(L/L_o)(\tan^2\theta_o) + (L/L_o)^2. \quad (45)$$

Equation (45) shows the relationship between the length (ℓ) of the helical fibers associated with a "unit square" of membrane and the length and volume of the retraction zone segment for any zone configuration. To find the length of the helical fibers at the upper and lower limits of the "functional range" for a constant cell volume of $(V/V_o) = 14.2$ (V_{max} in figure 32), we substitute the corresponding values for (L/L_o) into equation (45) and solve for ℓ, recalling that $\tan^2\theta_o = 0.036$ for expt. #65 (table XII). By this procedure, it is found that ℓ is equal to 1.18 and 1.15 when (L/L_o) is 0.42 and 0.84 respectively, compared to a helical fiber length at which slack is just removed of 1.10 (ℓ_s for expt. #65).

The force-extension plot of the helical fibers for expt. #65, shown in figure 31, indicates that forces of 365 and 225 dynes are required to extend the helical fibers to relative lengths of 1.18 and 1.15 (cm/cm) respectively. Even though the helical fibers are oriented at a large angle to the cell axis in the "functional range" of cell lengths (55° at rest length), the longitudinal components of the above forces are much too large to be compatible with the known longitudinal extensional properties of single muscle fibers reported in the literature. The length-tension properties of single muscle fibers indicate that forces of only a few dynes are required for cell extension within the "functional range" (68). The requirement for helical fiber stretch within the functional range of muscle cell lengths is therefore incompatible with experimental results.

The apparent conflict indicated by the above considerations can be reconciled if the membrane of the intact muscle fiber is allowed to be "festooned" in longitudinal contour over the "functional range" of cell lengths, permitting the actual length of membrane material in the longitudinal direction to be greater than the length of the muscle fiber axis. The introduction of the proper amount of festooning in the membrane of the cell at rest length allows the muscle fiber to operate over the functional range of lengths at constant volume, with a simple variation in the amplitude of festooning accommodating length changes up to the limits of the functional range

of operation. Notice that if a given cylindrical membrane segment is festooned, its length is reduced relative to the length of the same portion of membrane without festooning, while its average diameter may remain the same. The introduction of festooning therefore requires a reduction in volume as well as in length of the cell segment under consideration.

In terms of the volume constraint curve, the cell at rest length would exist at some lower volume (i.e., V_c, the dotted line in figure 32) than that predicted by V_{max}, the festooning tending to flatten the peak of the curve over the functional range of operation. Due to the angular orientation of the helical fibers, for muscle lengths shorter than those of the functional range stiff lateral constraints would be present opposing the required increases in fiber diameter. Such lateral constraints at short fiber lengths have been proposed in the literature (102) but never proven. At fiber lengths longer than those of the functional range, the helical fibers would be oriented so as to impose stiff longitudinal length-tension behavior as seen in the passive length-tension diagram of striated muscle (see figure 6).

It was previously mentioned that Buchthal (69) found the length of intact segments to be 30-50% of the length of retraction zones in the same fiber. The volume constraint curve predicts a relative length (L/L_o) of 0.64 cm/cm for the intact cell at rest length in the absence of festooning. The "actual" cell volume (V_c) approximated

by the present treatment from the volume constraint curve (dotted lines in figure 32) was roughly 80% of the cell volume predicted in the absence of festooning, V_{max}. Since the volume of a cylinder is directly proportional to its length, the introduction of festooning reduces (L/L_o) at rest length to approximately 80% of the value predicted for the unfestooned membrane, or from 0.64 to 0.51 cm/cm. The latter value is in much better agreement with the measurements of Buchthal.

The electron micrograph of figure 5-B, taken from the work of Street et al. (47), shows that the membrane in the intact muscle fiber at a length within the functional range (sarcomere length of 2.5 microns) is definitely not linear in longitudinal contour. Rather an irregular contour of the cell is indicated, and the actual length of the membrane material is therefore somewhat longer than the axis length of the cell. The present treatment indicates that folds running circumferentially around the muscle fiber membrane, seen in sections taken parallel to the fiber axis as a festooned longitudinal contour, may not be an inconsequential result of weak connections to the cell interior (48), but may be an absolute necessity for muscle to function free of rigid constraint by the cell membrane over the "functional range" of muscle cell lengths.

SUMMARY AND CONCLUSIONS

The viscoelastic properties of cylindrical segments of sarcolemma were studied after removal of the cell contents by forming a retraction zone. Membrane geometry was studied as a function of internal hydrostatic pressure and external longitudinal tension to permit calculation of the longitudinal and circumferential tension-deformation diagrams. The membranes had nonlinear elastic properties in both directions and were much stiffer longitudinally than circumferentially.

The principal rigidity of the membrane is best explained by a system of helical fibers which have some slack in the undeformed membrane. The degree of slack, the angle, and the force-length properties of these fibers were calculated for all membrane configurations. Their stiffness, being similar to that of collagen, made it unlikely that they can be strained under physiological conditions.

The sarcolemma of intact muscle cells at rest length is about four times wider and two-thirds as long as the undeformed membrane. This configuration is just possible without stretching the helical fibers, as the cell diameter at rest length permits maximal cell volume for a given length of helical fiber. The proposed explanation is in complete agreement with the known ultrastructural and physiological properties of single muscle cells.

BIBLIOGRAPHY

1. Simpson, G.G., Pittendrigh, C.S., & Tiffany, L.H. Life: An introduction to biology. New York: Harcourt, Brace and Company, 1957. (pages 221-228)

2. Arey, L.B. Developmental anatomy. (7th Ed.) Philadelphia: W.B. Saunders Company, 1965. (page 429)

3. Draper, M.H., & Hodge, A.J. Studies on muscle with the electron microscope, 1. The ultrastructure of toad striated muscle. Australian J. Exper. Biol. Med. Sci., 1949. 27, 465-503.

4. Maximow, A.A., & Bloom, W. A textbook of histology. (3rd Ed.) Philadelphia: W.B. Saunders Company, 1940. (pages 154-156)

5. Woodbury, J.W., Gordon, A.M., & Conrad, J.T. Muscle. In T.C. Ruch and H.D. Patton (Ed.) Medical physiology and biophysics. (19th Ed.) Philadelphia: W.B. Saunders Company, 1965. pp. 113-152

6. Aubert, X., Roquet, M.L., & Van Der Elst, J. Tension-length diagram of frog's sartorius muscle. Arch. Internat. Physiol., 1951. 59, 239-241.

7. Hill, A.V. The heat of shortening and the dynamic constants of muscle. Proc. Roy. Soc. London (Ser. B), 1938. 126: 136-195.

8. Jewell, B.R., & Wilkie, D.R. An analysis of the mechanical components in frog's striated muscle. J. Physiol. (London), 1958. 143, 515-540.

9. Hill, A.V. The thermodynamics of elasticity in resting muscle. Proc. Roy. Soc. London (Ser. B), 1952. 139: 464-497.

10. Abbott, B.C., & Brady, A.J. Amphibian muscle. In J.A. Moore (Ed.) Physiology of the amphibia. New York: Academic Press, 1964. pp. 329-370

11. Wilkie, D.R. Muscle. Ann. Rev. Physiol., 1966. 28, 17-38.

12. Fung, Y. C. B. Elasticity of soft tissues in simple elongation. Amer. J. Physiol., 1967. 213, 1532-1544.

13. Buchthal, F., & Weis-Fogh, T. Contribution of the sarcolemma to the force exerted by resting muscle of insects. Acta Physiol. Scand., 1956. 35, 345-364.

14. Huxley, H. E., & Hanson, J. Changes in the cross-striations of muscle during contraction and stretch and their structural interpretation. Nature (London), 1954. 173, 973-976.

15. Huxley, A. F., & Niedergerke, R. Structural changes in muscle during contraction. Nature (London), 1954. 173, 971-973.

16. Garamvölgyi, N. The arrangement of the myofilaments in the insect flight muscle. I. J. Ultrastructure Res., 1965. 13, 409-424.

17. Garamvölgyi, N. The arrangement of the myofilaments in the insect flight muscle. II. J. Ultrastructure Res., 1965. 13, 425-434.

18. Barer, R. Observations on muscle-fibre structure. The swelling of muscle fibres by acids and alkalis. J. Anat. (London), 1947. 81, 259-285.

19. Street, S. F., & Ramsey, R. W. Sarcolemma: transmitter of active tension in frog skeletal muscle. Science, 1965. 149, 1379-1380.

20. Schwann, T. Microscopical researches into the accordance in the structure and growth of animals and plants. 1839. Translated from the German by H. Smith. London: Sydenham Society, 1847.

21. Bowman, W. On the minute structure and movements of voluntary muscle. Phil. Trans. Royal Soc. (London), 1840. 130, part II, 457-501.

22. Barer, R. The structure of the striated muscle fibre. Biol. Rev. Cambridge Phil. Soc., 1948. 23, 159-200.

23. Jordan, H. E. The structural changes in striped muscle during contraction. Physiol. Rev., 1933. 13, 301-324.

24. Mauro, A., & Adams, W. R. The structure of the sarcolemma of the frog skeletal muscle fiber. J. Biophys. Biochem. Cytol., 1961. 10, 177-185.

25. Ramsey, R. W., & Street, S. F. The isometric length-tension diagram of isolated skeletal muscle fibers of the frog. J. Cell. Comp. Physiol., 1940. 15, 11-34.

26. Nagel, A. Die mechanischen Eigenschaften von Perimysium internum und Sarkolemm bei der quergestreiften Muskelfaser. Ztschr. f. Zellforsch. u. mikroskop. Anat., 1938. 22, 694-706.

27. Bairati, A. Structure e propieta fisiche del sarcolemma della fibra muscolare striata. Ztschr. f. Zellforsch. u. mikroskop. Anat., 1938. 27, 100-124. According to Ramsey, R. W., & Street, S. F. The isometric length-tension diagram of isolated skeletal muscle fibers of the frog. J. Cell. Comp. Physiol., 1940. 15, 11-34.

28. Bremer, J., & Weatherford, H. L. A textbook of histology. (6th Ed.) Philadelphia: The Blakiston Company, 1944. (pages 157-158)

29. Gutmann, E., & Young, J. Z. The reinnervation of muscle after various periods of atrophy. J. Anat. (London), 1944. 78, 15-43.

30. Long, M. E. Development of the muscle-tendon attachment in the rat. Amer. J. Anat., 1947. 81, 159-198.

31. Reed, R., & Rudall, K. M. Electron microscope studies of muscle structure. Biochim. Biophys. Acta, 1948. 2, 19-26.

32. Weinstein, H. J. An electron microscope study of cardiac muscle. Exp. Cell. Res., 1954. 7, 130-146.

33. Bennett, H. S., & Porter, K. R. An electron microscope study of sectioned breast muscle of the domestic fowl. Amer. J. Anat., 1953. 93, 61-105.

34. Rozsa, G., Szent-Gyorgyi, A., & Wyckoff, R. W. G. The fine structure of myofibrils. Exp. Cell. Res., 1950. 1, 194-205.

35. Jones, W. M., & Barer, R. Electron microscopy of the sarcolemma. Nature (London), 1948. 161, 1012.

36. Robertson, J. D. Some features of the ultrastructure of reptilian skeletal muscle. J. Biophys. Biochem. Cytol., 1956. 2, 369-379.

37. Robertson, J. D. The ultrastructure of cell membranes and their derivatives. Biochem. Soc. Sympos., 1959. 16, 3-43.

38. Birks, R., Huxley, H. E., & Miledi, R. Unpublished work. According to Birks, R., Katz, B., & Miledi, R. Dissociation of the "surface membrane complex" in atrophic muscle fibers. Nature (London), 1959. 184, 1507-1508.

39. Robertson, J. D. The ultrastructure of a reptilian myoneural junction. J. Biophys. Biochem. Cytol., 1956. 2, 381-394.

40. Birks, R., Katz, B., & Miledi, R. Dissociation of the "surface membrane complex" in atrophic muscle fibers. Nature (London), 1959. 184, 1507-1508.

41. Boyde, A., & William, J. C. P. Surface morphology of frog striated muscle as prepared for and examined in the scanning electron microscope. J. Physiol. (London), 1968. 197, 10-11P.

42. Carr, R. W. Muscle-tendon attachment in the striated muscle of the fetal pig; demonstration of the sarcolemma by electric stimulation. Amer. J. Anat., 1931. 49, 1-42.

43. Butcher, E. O. The development of striated muscle and tendon from the caudal myotomes in the albino rat, and the significance of myotomic-cell arrangement. Amer. J. Anat., 1933. 53, 177-189.

44. Goss, C. M. The attachment of skeletal muscle fibers. Amer. J. Anat., 1944. 74, 259-290.

45. Speidel, C. C. Studies on living muscles, II. Histological changes in single fibers of striated muscle during contraction and clotting. Amer. J. Anat., 1939. 65, 471-529.

46. Porter, K. R. The myo-tendon junction in larval forms of Amblystoma punctatum. Anat. Rec., 1954. 118, 342 (Abstract)

47. Street, S. F., Sheridan, M. N., & Ramsey, R. W. Some effects of extreme shortening on frog skeletal muscle. Medical College of Virginia Quarterly, 1966. 2, 90-99.

48. Garamvölgyi, N. Inter-Z bridges in the flight muscles of the bee. J. Ultrastructure Res., 1965. 13, 435-443.

49. Fenn, W. O. Muscles. In R. Höber (Ed.) Physical chemistry of cells and tissues. Philadelphia, The Blakiston Company, 1945. (pages 453-522)

50. Bennett, H. S. Modern concepts of structure of striated muscle. Amer. J. Physical Med., 1955. 34, 46-61.

51. Hibbs, R. G. Electron microscopy of developing cardiac muscle in chick embryos. Amer. J. Anat., 1956. 99, 17-51.

52. Walls, E. W. The microanatomy of muscle. In G. H. Bourne (Ed.) The structure and function of muscle. Vol. 1. New York: Academic Press, 1960. (page 44)

53. Edwards, G. A., Ruska, H., DeSouza Santos, P., & Vallejo-Freire, A. Comparative cytophysiology of striated muscle with special reference to the role of the endoplasmic reticulum. J. Biophys. Biochem. Cytol., 1956. 2, Suppl., 143-156.

54. Podolsky, R. J. The maximum sarcomere length for contraction of isolated myofibrils. J. Physiol. (London), 1964. 170, 110-123.

55. Garamvölgyi, N. Über das Z-Gebilde des quergestreiften Muskels. Acta Physiol. Acad. Sci. Hungary, 1956. 9, Suppl., 4. (Abstract)

56. Ernst, E., & Garamvölgyi, N. Intra und interfibrilläre Z-Gebilde. Acta Physiol. Acad. Sci. Hungary, 1956. 9, 41-52.

57. Ernst, E., Garamvölgyi, N., & Guba, F. Ueber die Z-Gebilde des quergestreiften Muskels. Acta Physiol. Acad. Sci. Hungary, 1958. 14, Suppl., 40. (Abstract)

58. Garamvölgyi, N., Metzger-Tőrök, G., & Tigyi-Sebes, A. The Z- and M-formations of striated muscle. Acta Physiol. Acad. Sci. Hungary, 1962. 22, 223-233.

59. Garamvölgyi, N. Interfibrilläre Z-Verbindungen im quergestreiften Muskel. Acta Physiol. Acad. Sci. Hungary, 1962. 22, 235-241.

60. Garamvölgyi, N. Observations préliminaires sur la structure de la strie Z dans le muscle alaire de l'abeille. J. Microscopie, 1963. 2, 107-112.

61. Ernst, E. Biophysics of the striated muscle. Budapest: Akadémiai Kiadó, 1963. (page 289)

62. Hodge, A. J., Huxley, H. E., & Spiro, D. Electron microscope studies on ultrathin sections of muscle. J. Exp. Med., 1954. 99, 201-206.

63. Porter, K. R., & Palade, G. E. Studies on the endoplasmic reticulum. III. Its form and distribution in striated muscle cells. J. Biophys. Biochem. Cytol., 1957. 3, 269-300.

64. Martin, A. R. The effect of change in length on conduction velocity in frog muscle. J. Physiol. (London), 1954. 124, 22P.

65. Dorn, A. Der Feinbau des Sarkolemm und seiner Invaginationen an der Skeletmuskelfaser des Meerschweinchens. Acta Anat., 1965. 61, 558-573.

66. Weber, E. Muskelbewegung. In R. Wagner's Handwörterbuch der Physiologie., 1846. Bd. 3. (s. 1-122). According to Sichel, F. J. M. The elasticity of isolated resting skeletal muscle fibers. J. Cell. Comp. Physiol., 1934. 5, 21-42.

67. Sichel, F. J. M. The elasticity of isolated resting skeletal muscle fibers. J. Cell. Comp. Physiol., 1934, 5, 21-42.

68. Sten-Knudsen, O. Torsional elasticity of the isolated cross-striated muscle fiber. Acta Physiol. Scand., 1953. 28, Suppl. 104, 1-240.

69. Buchthal, F. The mechanical properties of the single striated muscle fiber. Det. Kgl. Danske Videnskabernes Selskab. Biologiske Meddelelser, 1942. 17, 1-138. According to Sten-Knudsen, O. Torsional elasticity of the isolated cross-striated muscle fiber. Acta Physiol. Scand., 1953. 28, Suppl. 104, 1-240.

70. Casella, C. Tensile force in striated muscle, isolated fiber, and sarcolemma. Acta Physiol. Scand., 1951. 21, 380-401.

71. Mauro, A., & Sten-Knudsen, O. The role of the sarcolemma in muscle physiology. Acta Med. Scand., 1952. 142, Suppl. 266, 715-724.

72. Buchthal, F., Svensmark, O., & Rosenfalck, P. Mechanical and chemical events in muscle contraction. Physiol. Rev., 1956. 36, 503-538.

73. Carlsen, F., Knappeis, G.G., & Buchthal, F. Ultrastructure of resting and contracted striated muscle fiber at different degrees of stretch. J. Biophys. Biochem. Cytol., 1961. 11, 95-117.

74. Ramsey, R. W. Comment. In J. W. Remington (Ed.) Tissue elasticity. Washington, D. C.: American Physiological Society, 1957. pp. 94-95.

75. Buchthal, F. Comment. In J. W. Remington (Ed.) Tissue elasticity. Washington, D. C.: American Physiological Society, 1957. pp. 95-97.

76. Ramsey, R. W., & Street, S. F. Muscle function as studied in single muscle fibers. Biol. Symp., 1941. 3, 9-34.

77. Buchthal, F., Kaiser, E., & Rosenfalck, P. The rheology of the cross-striated muscle fiber with particular reference to isotonic conditions. Det. Kgl. Danske Videnskabernes Selskab. Biologiske Meddelelser, 1951. 17, 1-318. According to Buchthal, F., Svensmark, O., & Rosenfalck, P. Mechanical and chemical events in muscle contraction. Physiol. Rev., 1956. 36, 503-538.

78. Buchthal, F., & Kaiser, E. Factors determining tension development in skeletal muscle. Acta Physiol. Scand., 1944. 8, 38-74.

79. Buchthal, F., & Rosenfalck, P. Elastic properties of striated muscle. In J. W. Remington (Ed.) Tissue elasticity. Washington, D. C.: American Physiological Society, 1957. pp. 73-97.

80. Natori, R. The property and contraction process of isolated myofibrils. Jikeikai Med. J., 1954. 1, 119-126.

81. Bozler, E. Osmotic properties of amphibian muscles. J. Gen. Physiol., 1965. 49, 37-45.

82. Rieser, P. The protoplasmic viscosity of muscle and nerve. Biol. Bull., 1949. 97, 245-246. (Abstract)

83. Gonzalez-Serratos, H. Inward spread of contraction during a twitch. J. Physiol. (London), 1966. 185, 20-21P.

84. Grimm, A. F., & Whitehorn, W. V. Characteristics of resting tension of myocardium and localization of its elements. Amer. J. Physiol., 1966. 210, 1362-1368.

85. Parsons, C., & Porter, K. R. Muscle relaxation: evidence for an intrafibrillar restoring force in vertebrate striated muscle. Science, 1966. 153, 426-427.

86. Sichel, F. J. M. The relative elasticity of the sarcolemma and of the entire skeletal muscle fibre. Amer. J. Physiol., 1941. 133, 446-447P.

87. Ramsey, R. W. Muscle: physics. In O. Glasser (Ed.) Medical physics. Vol. I. Chicago: Year Book Publishers, 1944. pp. 784-798

88. Ramsey, R. W. Dynamics of single muscle fibers. Ann. N. Y. Acad. Sci., 1947. 47, 675-695.

89. Zenker, F. A. Über die Veränderungen der willkürlichen Muskeln im Typhus abdominalis. Leipzig: F. C. W. Vogel, 1964. According to Speidel, C. C. Studies on living muscles, II. Histological changes in single fibers of striated muscle during contraction and clotting. Amer. J. Anat., 1939. 65, 471-529.

90. Cohnheim, J. F. Untersuchungen über embolische Prozesse. Berlin, 1872. According to Speidel, C. C. Studies on living muscles, II. Histological changes in single fibers of striated muscle during contraction and clotting. Amer. J. Anat., 1939. 65, 471-529.

91. Forbus, W. D. Pathologic changes in voluntary muscles: I. Degeneration and regeneration of the rectus abdominus in pneumonia. Arch. Pathol., 1926. 2, 318-339.

92. Forbus, W. D. Pathologic changes in voluntary muscles: II. Experimental study of degeneration and regeneration of striated muscle with vital stains. Arch. Pathol., 1926. 2, 486-499.

93. Thoma, R. Untersuchungen über die wachsartige Umwandlung der Muskelfasern. Virchow's Arch., 1906. Bd. 186. (s. 64-96). According to Speidel, C. C. Studies on living muscles, II. Histological changes in single fibers of striated muscle during contraction and clotting. Amer. J. Anat., 1939. 65, 471-529.

94. Davenport, H. K., Ranson, S. W., & Stevens, E. Microscopic changes of muscle in myostatic contracture caused by tetanus toxin. Arch. Pathol., 1929. 7, 978-992.

95. Davenport, H. K., & Ranson, S. W. Contracture resulting from tenotomy. Arch. Surg., 1930. 21, 995-1014.

96. Cheney, R. H. Micro-structural changes in muscle fibers after caffeine. Biol. Bull., 1938. 75, 348-349.

97. Nageotte, J. Sur la contraction extrême des muscles squelettiques chez le vertébrés. Ztschr. f. Zellforsch. u. mikroskop. Anat., 1937. 26, 603-624.

98. Speidel, C. C. Studies on living muscles, I. Growth, injury and repair of striated muscle, as revealed by prolonged observations of individual fibers in living frog tadpoles. Amer. J. Anat., 1938. 62, 179-235.

99. Burton, A. C. Physical principles of circulatory phenomena: the physical equilibria of the heart and blood vessels. In W. F. Hamilton (Ed.) Handbook of physiology. Vol. I, Section 2. Washington, D. C.: American Physiological Society, 1962. (pages 85-106)

100. Kraus, H. Thin elastic shells. New York: John Wiley and Sons, 1967. (pages 1-142)

101. Huxley, A. F., & Peachey, L. D. The maximum length for contraction in vertebrate striated muscle. J. Physiol. (London), 1961. 156, 150-165.

102. Gordon, A. M., Huxley, A. F., & Julian, F. J. Tension development in highly stretched vertebrate muscle fibers. J. Physiol. (London), 1966. 184, 143-169.

103. Rand, R. P., & Burton, A. C. Mechanical properties of the red cell membrane I. Membrane stiffness and intracellular pressure. Biophys. J., 1964. 4, 115-135.

104. Rand, R. P. Mechanical properties of the red cell membrane II. Viscoelastic breakdown of the membrane. Biophys. J., 1964. 4, 303-316.

105. Rand, R. P. The structure of a model membrane in relation to the viscoelastic properties of the red cell membrane. J. Gen. Physiol., 1968. 52, 173-186s.

106. Roach, M. R., & Burton, A. C. The reason for the shape of the distensibility curves of arteries. Can. J. Biochem. Physiol., 1957. 35, 681-690.

107. Copenhaver, W. M. Bailey's textbook of histology. (15th Ed.) Baltimore: The Williams and Wilkins Company, 1964. (pages 173-174)

108. Huxley, H. E. X-ray analysis and the problem of muscle. Proc. Roy. Soc. London (Ser. B), 1953. 141, 59-62.

APPENDIX

APPENDIX

Pressure Calibration Device - see page 83

The design of the calibration device was based on the concept that when known forces are applied to a known cross-sectional area predictable pressures are generated. Figure 33 is a photograph of the device, which allows weights hung on the end of a pivoting bar (weight bar) to act through a level ratio of 2:1 on the plunger of a well oiled tuberculin syringe. The fluid contents of the syringe communicate with the main pressure system through 1/4" O. D. copper tubing running under the benchtop. When not in operation, the calibrator is disconnected from the main pressure system by a valve (not shown) and the weight bar and weight are supported by a stop. For calibration, the valve is opened and system pressure is raised until the weight bar is just lifted free of the support. The weight bar pivots around a fixed axis at the end opposite the point of weight attachment. Because the pivot junction is composed of a roller bearing, rotation of the weight bar is opposed by negligible frictional resistance.

Figure 34 schematically diagrams the system physics, showing the three principal moments acting around the pivot. Downward (counterclockwise) torques are produced by both the weight bar and weight, and these are balanced by an upward (clockwise) torque

Figure 33. Pressure calibration device. A tuberculin syringe is mounted vertically in a frame constructed of 2" x 1/4" aluminum plates. The Syringe is glued into a bulkhead fitting running through the frame and benchtop, and connecting to the main pressure system. Right vertical frame plate supports rod axle around which weight bar pivots on roller bearings. Left vertical frame plate serves as a stop, supporting weight bar just below the horizontal orientation. Pressure is applied to the syringe plunger until the bar is lifted to precisely the horizontal level. The design allows for generation of different pressures by varying the weight employed. The weight hangs from a large ring via a fishhook and leader line providing a frictionless connection to the bar.

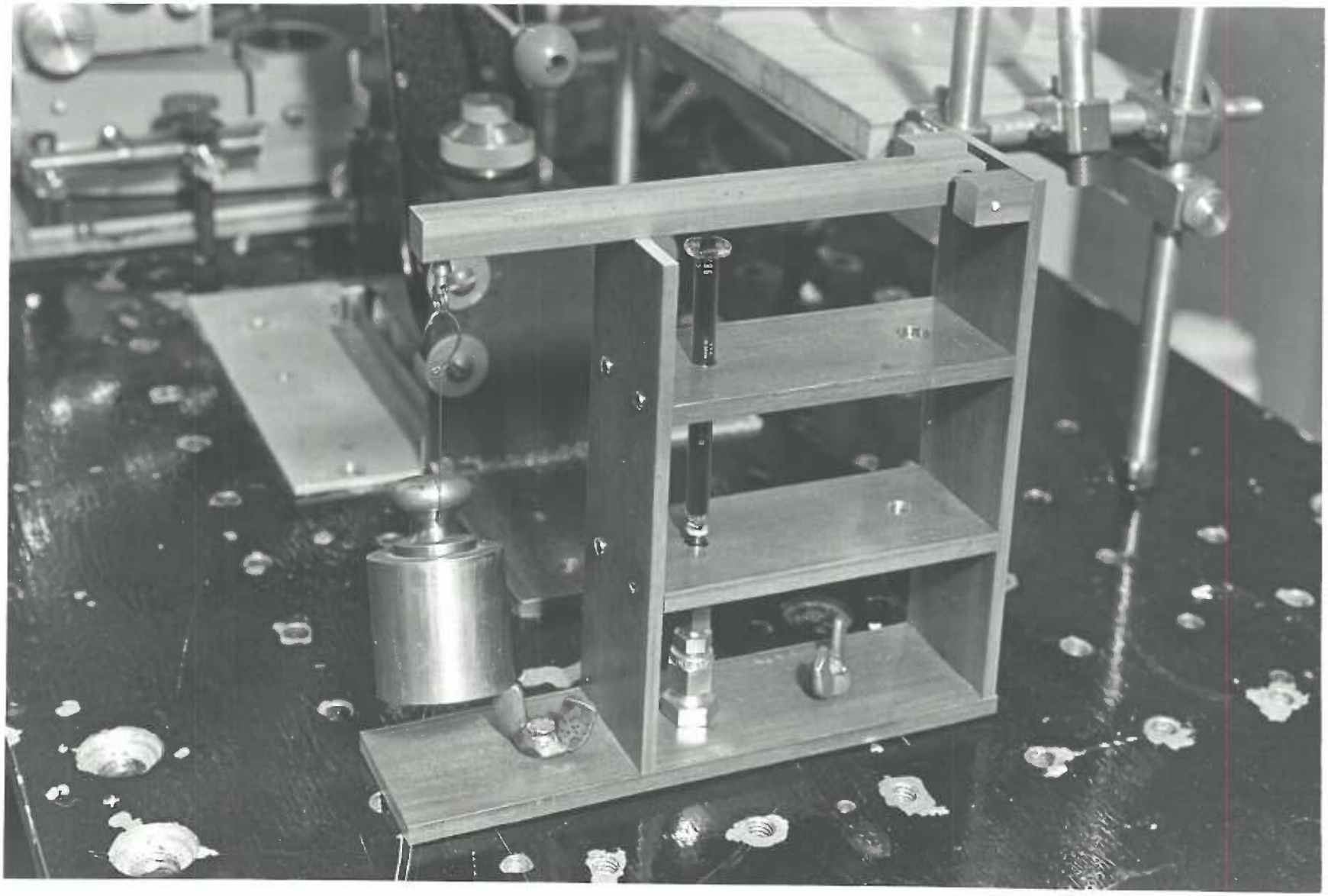

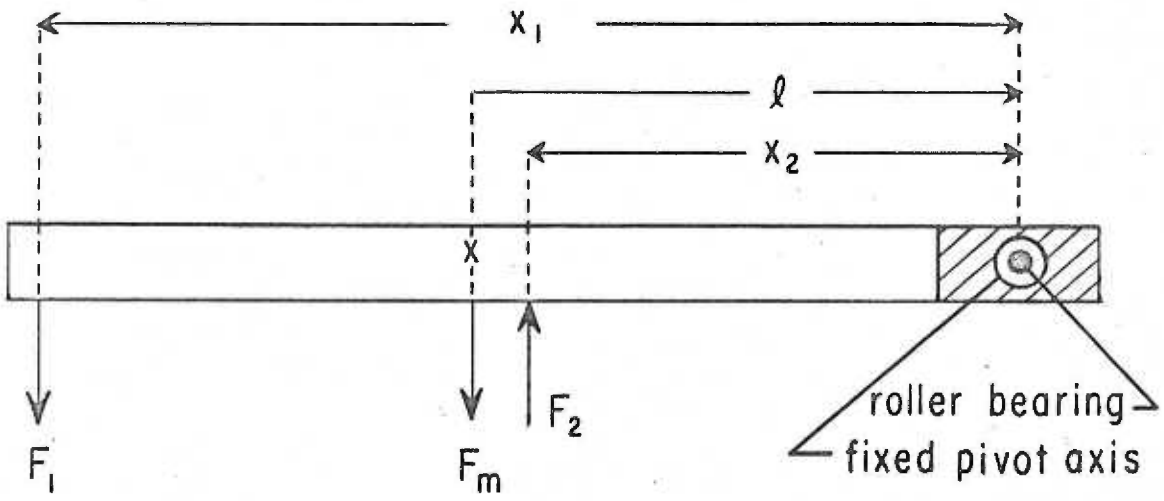

$$F_1 X_1 + F_m \ell = F_2 X_2$$

exerted by the syringe plunger. The torque of each component is represented by the product of its weight and the lever arm (the distance between the center of mass of the component and the pivot axis) through which it acts.

When the weight bar is exactly horizontal, the torque of the weight is therefore $(F_1 x_1)$, where F_1 is the force of the weight and x_1 its lever arm. Similarly, the downward torque produced by the weight bar is given by $(F_m \ell)$, where F_m is the weight of the "uncanceled" portion of the weight bar and ℓ is the distance from the pivot axis to the center of mass of the "uncanceled" length of the weight bar. The entire length of the weight bar is not considered, because the small symmetrical segment straddling the pivot axis (the hatched area in figure 34) produces equal and opposite torques and must therefore be neglected. The weight of the uncanceled portion of the weight bar was determined from the product of the weight of the bar per centimeter length (designated w) and the length of the uncanceled segment (k). The two downward torque components are balanced by the torque of the syringe plunger, given by the product of the plunger force (F_2) and the distance from the point of contact of the plunger and weight bar to the pivot axis (x_2). The plunger force is equal to the pressure (P) exerted on the plunger multiplied by the plunger cross-sectional area (a).

Based on the above considerations, the following constants

are defined:

ℓ = distance from the pivot axis to the center of mass of the "uncanceled" portion of the weight bar,
w = weight of the weight bar per cm length,
k = length of the uncanceled portion of the weight bar,
a = cross-sectional area of the syringe plunger,
x_1 = distance from the point of weight attachment to the pivot axis,
x_2 = distance from the point of contact of the syringe plunger and weight bar to the pivot axis,

and measurements recorded:

ℓ = 8.66 cm,
w = 4.47 g/cm,
k = 16.54 cm,
a = 0.165 cm^2,
x_1 = 16.60 cm,
x_2 = 8.30 cm.

The equation of equilibrium for the system is given by

$$F_m \ell + F_1 x_1 = F_2 x_2.$$

Substituting for F_m and F_2, and solving for the pressure, P, we find that

$$P = (wk\ell + F_1 x_1)/(ax_2).$$

This equation defines the theoretical pressure required to just support the weight bar and weight in the horizontal position free of the weight bar support.

An independent check of the accuracy of the above analysis and performance of the system was obtained by comparing computed values for the pressure equivalent of the torque exerted by the weight bar against values read on a mercury manometer. The readings

were taken in two sets, one measuring the manometer pressure at which fall of the bar was just prevented, and a second set noting the pressure at which bar rise ceased. The discrepancy between reading sets should bracket the calculated pressure, since frictional torque is added to pressure torque during fall of the weight bar, whereas it is subtracted from it during bar rise.

The following readings were obtained:

halt arm fall	calculated	halt arm rise
34.6 mmHg	34.4 mm Hg	34.7 mm Hg
34.2	34.4	34.3
34.3	34.4	34.5
33.0	34.4	35.3
34.8	34.4	34.6
34.2	34.4	34.1
34.1	34.4	34.9
34.3	34.4	35.5
33.2	34.4	34.8
34.0	34.4	35.0
mean error -0.31		mean error 0.37

The calculated pressures are found to be in acceptable agreement with pressures recorded by the mercury manometer, being within 1% of the calculated pressure. The discrepancy introduced by friction is of the same negligible magnitude.

Elastic Modulus of the Helical Fibers - See page 164

It is possible to make an order of magnitude approximation of the stress-strain ratio (the Young's Modulus, Y) exhibited by the helical fibers. Stress is defined as force per unit area, so that Y (dynes/cm^2) can be calculated by dividing the slope of the estimated force-strain curve of the helical fibers (solid line in figure 31) by their cross-sectional area. It is shown on page 176 that the helical fiber system in an intact cell at rest length is oriented at an angle of about 55 degrees to the cell axis. Assuming a segment of sarcolemma of 1000 $\mathring{A}$ thickness (22) and 100 μ diameter, the cross-sectional area of membrane perpendicular to the helical fibers is given by (10^{-5} cm) ($\pi \times 10^{-2}$ cm) (cos 90-55) = 2.6×10^{-7} cm^2. From figure 31, the slope of the force-strain curve of the helical fibers is found to be 300 dynes (300-0) per 0.065 cm/cm (1.165-1.100), or 4.6×10^3 dyne-cm/cm. Dividing the latter value by the estimated membrane cross-sectional area shows the Young's Modulus of the helical fibers to be 1.8×10^{10} dynes/cm^2, assuming that the helical fibril components occupy the entire cross-sectional area of the sarcolemma. This value is approximately within an order of magnitude of the published value for collagen, which is 10^9 dynes/cm^2 (105).